Stellingen

behorend bij het proefschrift

## Added Resistance due to waves of Surface Effect Ships

van

Joost Moulijn

1. Het is niet mogelijk om de toegevoegde weerstand door golven van een "Surface Effect Ship" te voorspellen op basis van louter potentiaaltheorie, dit in tegenstelling tot het voorspellen van de toegevoegde weerstand door golven van conventionele schepen.

2. De resultaten van berekeningen suggereren doorgaans een veel grotere nauwkeurigheid, dan op grond van de aannames, die aan de berekeningen ten grondslag liggen, redelijk is.

3. "Meten is weten", maar de kunst is te weten wat je meet, zodat je weet wat je weet.

4. "Even snel" leidt zelden tot het gewenste resultaat.

5. Zelfs een kussen van lucht kan hard zijn.

6. De armste kinderen op deze wereld zijn niet zondermeer gebaat bij een verbod op kinderarbeid.

7. Het verwerpen van abortus en euthanasie en tegelijkertijd steunen van de doodstraf getuigd van een sterke dubbele moraal.

8. Het leren bespelen van een muziekinstrument bestaat voor een groot deel uit afleren.

9. Bij goede muziek is het geheel altijd meer dan de som der delen.

10. Het bedenken en formuleren van stellingen is er sinds het verschijnen van het boekje "De beste stellingen zijn van hout" niet eenvoudiger op geworden.

Added Resistance due to Waves

of

Surface Effect Ships
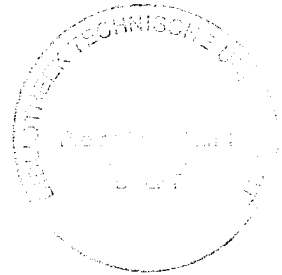
Proefschrift

ter verkrijging van de graad van doctor
aan de Technische Universiteit Delft,
op gezag van de Rector Magnificus prof. ir. K.F. Wakker,
in het openbaar te verdedigen ten overstaan van een commissie,
door het College voor Promoties aangewezen,
op maandag 10 april 2000 te 10.30 uur,

door

Joost Cornelis MOULIJN

scheepsbouwkundig ingenieur,
geboren te Leiden.

Contents

Summary

In recent years there is an increasing interest in large sea-going Surface Effect Ships (SESs). The design of these vessels requires an accurate method for the prediction of their behavior in waves. SESs are found to have a large loss of speed when they are sailing in waves, which threatens the economical feasibility of these vessels. The speed-loss is caused by an increase of the resistance due to the ambient waves that is called added resistance due to waves (or briefly added resistance). The goal of the research project that lies at the root of this thesis is to develop and to validate a computational method for the prediction of the added resistance of Surface Effect Ships.

The computational method for motions and added resistance is based on the following assumptions. The hydromechanical problem and the equations of motions can be linearized. That the excess pressure in the air cushion is constant in space. Furthermore the computational method only computes the part of the added resistance that is caused by the air cushion, because this part was expected to be the most important contribution to the added resistance.

The hydromechanic problem is solved by means of a three-dimensional Rankine panel method. The boundary conditions on the hull and the free surface are linearized around the undisturbed flow. The panel method computes the hydrodynamic forces on the hulls, the wave height inside the air cushion and the wave height and slope at the bow and stern seal. The problem is solved in the frequency domain.

Subsequently the motions of the SES and the excess pressures in the air cushion and the stern seal plenum are solved by means of a non-linear time simulation method. The equations of motion are linearized, but the non-linear form of the dynamics of the air cushion and the seals is retained. Especially the leakage of air under the seals is a highly non-linear phenomenon that cannot be linearized. The simulation method also includes a non-linear model for the bag-type stern seal.

The added resistance of the air cushion follows from the difference of the resistance of the air cushion in waves and the resistance of the air cushion in calm water. The resistance of the air cushion follows basically from the cushion excess pressure

times the difference of the wave height at the bow and stern seal times the cushion width. In addition to this there are some terms that account for the momentum of the air flows into and out of the air cushion.

The results of the computational method are compared to experimental results of MARIN. The agreement is good as far as the motions and cushion pressure are concerned. There is however a large discrepancy between computed and the measured added resistance. The computed added resistance of the air cushion is only small and in many cases even negative, while the measured added resistance is generally very large.

In order to find an explanation for the discrepancy between the computed and the measured added resistance an extensive series of experiments that was carried out at the Ship Hydromechanics Laboratory of Delft University of Technology The main goal of these experiments was to find the origin of the (large) added resistance of Surface Effect Ships. Two versions of a model were subjected to three types of experiments: forced oscillation experiments, wave force measurements and experiments were the model was free in heave and pitch. The contribution of the air cushion to the added resistance was measured separately in addition to the total added resistance. The difference yields the added resistance of the hulls. The outcome of the experiments is that the contribution of the hulls to the added resistance is large, while the contribution of the air cushion is only small. The large added resistance of the hulls is mainly caused by sinkage as a consequence of a drop of the cushion pressure caused by a larger amount of air leakage when the vessel sails in waves.

Finally the computational method is validated by means of a comparison of the results of the experiments with the results of the computational method. The correlation of the experimental and computational results is generally good, which subscribes the validity of the method. The prediction of the total added resistance however requires a calculation of the added resistance of the hulls. The added resistance of the hulls is mainly caused by sinkage due to a decrease of the cushion pressure. The computational method predicts the drop of the cushion pressure and the consequent sinkage and trim with good accuracy. It is therefore expected that the method can be very useful in the calculation of the added resistance of the hulls.

Nomenclature

Roman symbols

A	wave amplitude
A_d	deck area
$A_{jk}(\omega)$	added mas coefficients
A_l	leakage gap area
$\vec{a}$	displacement vector of a point on the hull
B	wetted hull surface; beam
$\bar{B}$	mean wetted part of the hull surface
B_c	width of the air cushion
$B_{jk}(\omega)$	damping coefficient
$B_k^{(2,2)}$	2D base function
$b^{(2)}$	1D base function
C_B	block coefficient
C_M	midship section coefficient
C_{jk}	restoring coefficient
c_l	orifice leakage coefficient
c_p	specific heat (constant pressure)
c_v	specific heat (constant volume/density)
$D_k(\omega)$	wave pumping coefficient
F_j	forcein j^{th} direction
$F_j^{(a)}$	force due to the air cushion in j^{th} direction
$F_j^{(g)}$	gravitational force in j^{th} direction
$F_j^{(h)}$	hydromechanic force in j^{th} direction
$F_j^{(p)}$	propulsive force in j^{th} direction
$F_j^{(g)}$	seal force in j^{th} direction
Fn	Froude number: $Fn = U/\sqrt{Lg}$
F_{1b}	longitudinal bow seal force
F_{3b}	vertical bow seal force

F_{1s}	longitudinal stern seal force
F_{3s}	vertical stern seal force
G	Green function
g	gravitational acceleration
h	panel dimension; height of the air cushion
h_x	longitudinal panel dimension
h_y	transverse panel dimension
i	imaginary unit
$\vec{n}$	normal vector
k	wave number
k_{yy}	pitch radius of gyration
L	ship length
M_{jk}	k^{th} element of the jth row of the generalized mass matrix
M_1	linear momentum in longitudinal direction
m_k	m-terms, $k = 1, \ldots, 6$
n_k	k^{th} component of the generalized normal vector, $k = 1, \ldots, 6$
	$(n_1, n_2, n_3)^T = \vec{n}$ and $(n_4, n_5, n_6)^T = \vec{x} \otimes \vec{n}$
p	excess pressure
$\bar{p}$	design pressure in a plenum
p_a	ambient pressure;
	excess pressure measured in the aft part of the air cushion
p_c	excess pressure in the air cushion plenum
p_f	excess pressure measured in the fore part of the air cushion
p_s	excess pressure in the stern seal plenum
$\bar{p}$	steady cushion pressure
$\tilde{p}$	unsteady cushion pressure
$Q^{(in)}$	volume flux into a plenum
$Q^{(out)}$	volume flux out of a plenum
$\bar{Q}$	design flux through a fan
R	resistance
$R^{(ac)}$	resistance of the air cushion
R_{aw}	added resistance (due to waves)
$R_{aw}^{(ac)}$	added resistance of the air cushion
$R_{aw}^{(h)}$	added resistance of the hulls
$R_{aws}^{(h)}$	added resistance of the hulls due to sinkage
S	boundary surface (of Ω); control surface
S_v	part of the control surface that is adjacent to the vessel
S_w	part of the control surface that is adjacent to the wave surface
T	thrust; draft

T_0	on-cushion draft at station 0
T_{20}	on-cushion draft at station 20
T_0^*	off-cushion draft at station 0
T_{20}^*	off-cushion draft at station 20
t	time
U	forward velocity
u_e	air escape velocity
V	volume of a plenum
V_{bc}	extra cushion volume due to the bow seal
V_c	volume of the air cushion plenum
$V^{(c)}$	air cushion volume
$V^{(d)}$	volume of the diaphragm
$\bar{V}$	design volume of a plenum
V_{sc}	the part of the cushion that is taken up by the stern seal
V_s	volume of the stern seal plenum
V_ζ	wave pumping volume
$X_j(\omega)$	wave exiting force in j^{th} direction
$\vec{x}$	position of a point on the hull
x_k	weight factor of the kth base function
$\ddot{z}_0$	vertical acceleration at station 0
$\ddot{z}_{10}$	vertical acceleration at station 10
$\ddot{z}_{20}$	vertical acceleration at station 20

Greek and other symbols

α	scale factor
Δp	pressure difference across a leakage gap
δ_{jk}	kronecker delta
ζ	wave height
ζ_b	mean wave height at the bow seal
ζ_s	mean wave height at the stern seal
η	local non-orthogonal coordinate
$\vec{\eta}$	displacement vector: $(\eta_1, \eta_2, \eta_3)^T$
η_k	displacement in k^{th} direction,
	$k = 1, \ldots, 6$ being surge, sway, heave, roll, pitch and yaw
$\hat{\eta}_k$	complex harmonic amplitude of the variation of η_k $(k = 1, \ldots, 7)$
η_7	non-dimensional unsteady cushion pressure
	$(\eta_7(t) = \tilde{p}(x, y, t)/\bar{p}(x, y))$

θ	skew angle of a panel; on-cushion trim angle (calm water)
θ_b	mean wave slope at the bow seal
θ_s	mean wave slope at the stern seal
κ	ratio of specific heats of air: $\kappa = c_p/c_v \approx 1.4$
λ	wave length
ξ	local non-orthogonal coordinate
ρ	density (sometimes of water, sometimes of air)
$\bar{\rho}$	density at the design pressure $(\bar{p})$
τ	strouhal number: $\tau = U\omega/g$
Φ	base flow potential
ϕ	steady perturbation potential
ϕ_l	potential in collocation point l
φ	unsteady perturbation potential
φ_D	diffracted wave potential
φ_I	incident wave potential
φ_k	wave potential due to harmonic motion in k^{th} direction
Ψ	total velocity potential
Ω	computational domain
$\vec{\Omega}$	rotation vector: $(\eta_4, \eta_5, \eta_6)^T$
ω	frequency of oscillation/encounter
ω^H	Helmholtz resonance frequency
ω_0	wave frequency with respect to an earth fixed coordinate system
∇	nabala operator: $\nabla = \vec{\nabla} = (\partial/\partial x, \partial/\partial y, \partial/\partial z)^T$; volume of the displaced water
$\Re$	real part of
$\Im$	imaginary part of

Coordinate systems

The following right-handed carthesian coordinate systems are used:

- an earth fixed coordinate system,

- a directionally fixed coordinate system,

- a ship bound coordinate system.

The origin of earth fixed coordinate system is located in the calm water surface. The mean water velocity with respect to this origin is zero. The x-axis points in

the same direction as the (mean) forward velocity of the SES. The z-axis point vertically upwards.

The axes of the directionally fixed coordinate system are parallel to the axes of the earth fixed system. The origin is also located in the calm water surface. This system travels with a constant velocity U in positive x-direction with respect to the earth fixed system. This velocity is the (mean) forward velocity of the SES. The hydromechanic problem is solved in this coordinate system.

The ship bound coordinate system is bound to the SES. The x-axis points in forward direction, the y-axis point to port and the z-axis points upwards. This coordinate system is used to define the geommetry of the SES. When the SES is in its (on-cushion) mean position the directionally fixed system and the ship bound system coincide. The difference between the systems are the displacement vector $\vec{\eta}$ and the rotation vector $\vec{\Omega}$.

Chapter 1

Introduction

1.1   Motivation

During the last decades there has been an increasing interest in fast sea-going Ships. This interest is due to the large speed-wise gap between aircraft and ships. An aircraft can transport light cargo at a high speed, while a ship can transport heavy cargo at a low speed. An intermediate transport facility does not really exist. Therefore several new concepts are being developed and tested on their technical and economical feasibility. One of these concepts is that of the Surface Effect Ship (SES). Section 1.2 presents a description of the SES-concept. Other concepts for fast sea transportation are that of the planing mono-hull, the catamaran, the hovercraft, the hydrofoil and the wing in ground effect vehicle. An SES is basically a hybrid of a catamaran and a hovercraft.

The behavior of a ship in waves is of great importance for its technical and economical success. When the motions and accelerations of a ship become too large, the passengers and the crew become sea-sick. In more severe conditions the cargo and even the ship itself might be damaged. Therefore the captain will reduce speed and/or change heading in order to reduce the motions and the probability of the occurrence of slamming. This speed reduction is called a voluntary loss of speed.

Ships also suffer from an involuntary loss of speed. An involuntary speed loss is directly caused by the environmental conditions in which the vessel is sailing. The actual amount of involuntary speed loss depends on the increase of the resistance of the vessel, the propulsion characteristics of the vessel, and also the (calm water) resistance characteristics of the vessel. Figure 1.1 shows an example of the resistance and propulsion characteristics of a ship. The velocity of the ship follows from the intersection point of the thrust curve and the resistance curve. When the resistance

1
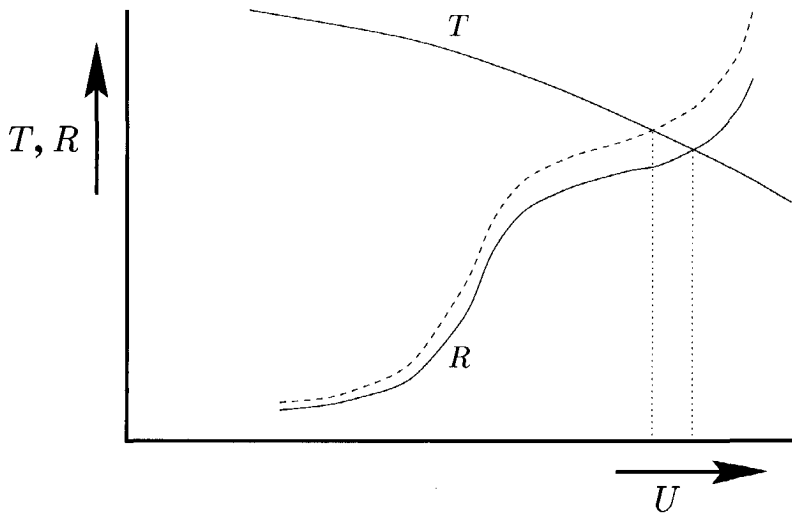
Figure 1.1: Resistance and propulsion characteristics of a ship

(R) increases the forward velocity (U) decreases. The velocity decrease depends on the increase of the resistance and on the slope of the resistance and thrust curves. A decrease of the thrust (T) can also result in a loss of speed. However the effect of waves and motions on the thrust is generally considered to be small. Therefore the involuntary speed loss of a ship is primarily caused by an increase of the resistance.

There are several phenomena such as fouling, wind and ambient waves that can cause an increase of the resistance of a ship while it is sailing at sea. The extra resistance due to the ambient of SESs waves is the subject of this thesis. This extra resistance is called *added resistance due to waves*, or briefly *added resistance*.

The high speed is of course one of the major features of a fast ship. Therefore the speed loss in waves of a fast ship should not be too large. However, the motions of fast ships are generally greater than the motions of conventional ships. This results in a large voluntary loss of speed. Usually the involuntary speed loss of fast ships is large too.

Surface Effect Ships are found to have a particularly great involuntary loss of speed when they are sailing in a seaway. This is partially due to their very flat resistance curve which enables them to attain such a high speed. On the other hand their added resistance due to waves is very large too. Kapsenberg et al.[1] measured a very large added resistance during experiments with a free sailing model. The amount

of speed loss in a seaway is of great importance for the economical feasibility of SESs. The design of SESs therefore requires an accurate prediction method for the added resistance due to waves. The development and validation of such a method was the goal of the research project that lies at the root of the present thesis.

1.2 The SES-concept

The previous section presented the motivation for the research project on added resistance of Surface Effect Ships. This section describes the SES concept. Thereafter the following section carries on with a survey of the literature on the subjects of motions and added resistance of SESs.

A Surface Effect Ship is a hybrid of a catamaran and a hovercraft. Figure 1.2 shows a sketch of an SES. An air cushion is enclosed between the side-hulls, the wet deck, the water surface and flexible seals at the bow and stern. The largest part of the vessel's weight is carried by the excess pressure inside the air cushion. The remainder is carried by the buoyancy of the hulls. Air leaks out from the cushion under the seals. Fans pump air into the cushion in order to compensate this leakage flow and to maintain an excess pressure.

Most SESs have a finger-type bow seal, which consists of a row of vertical loops of thin flexible material. Each loop represents a finger. The loops are open to the cushion side. The excess pressure automatically maintains the shape of the fingers.

The stern seal of SESs is usually of the bag-type. The bag consists of a horizontal loop of thin flexible material. The bag is open to the sides, where it is closed by the inner side of the hulls. Internal webs restrain the aft side of the bag and divide the bag in two or three lobes. The bag is pressurized by a fan at a slightly higher pressure than the air cushion. In the early days of SES-development the bow and stern seals were usually of the non-flexible planing type.

The development of the SES concept started just after the development of the hovercraft concept in the 1950s in Britain. The first SES was build as a solution to the large amount of air leakage that occurs with ACVs sailing in waves. In the early sixties the U.S. Navy started an extensive SES program as a step towards their goal of a "100 knots Navy". Eggington and Kobitz[2] and McGhee[3] presented details of this research program. After a relatively quiet period the interest in the SES concept reappeared at the end of the 1980s. The Japanese TSL-A project (see for instance the paper by Ozawa et al.[4]) and the European HYDROSES project (see for instance the paper by Kapsenberg and Blume [5]) are recent examples of this

top view

rear view

side view

front view

longitudinal cross-section

transverse cross-section
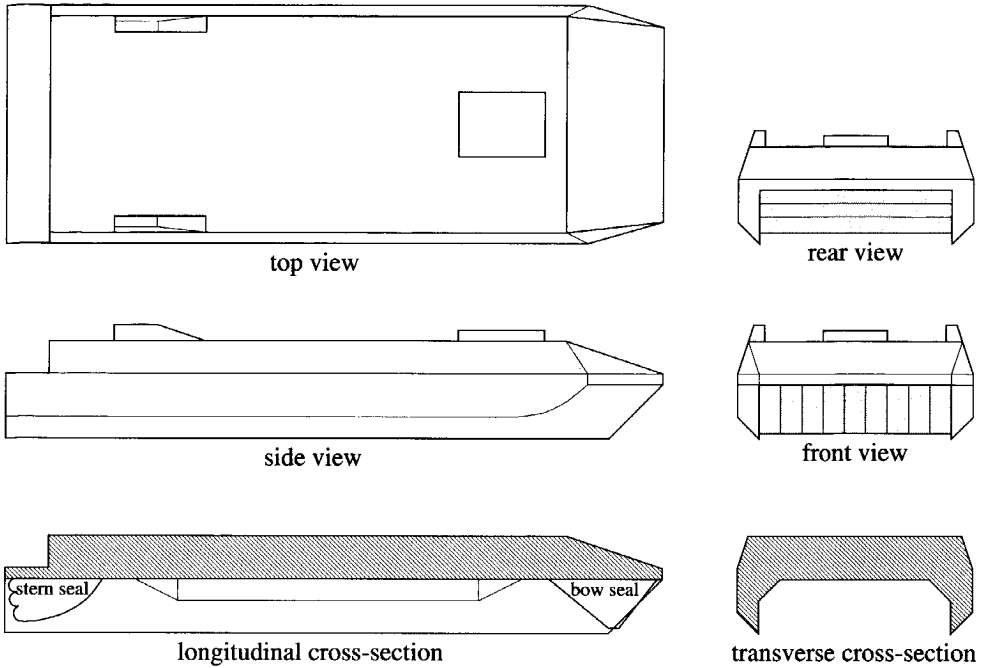
Figure 1.2: Sketch of a Surface Effect Ship

interest.

Finally this section compares the SES with its ancestors, the catamaran and the hovercraft. Compared to a catamaran an SES has a low resistance. An SES can achieve a higher speed than a similarly sized catamaran by means of a smaller amount of power, also when the additional power for the fans is taken into account. The behavior of an SES in waves is quite different from the behavior of a catamaran in waves. In the normal frequency range the motions of an SES are much smaller than the motions of a comparably sized catamaran, but in the very high frequency range SESs suffer from the so called *cobblestone effect*. The cobblestone effect is a resonant phenomenon of the air cushion that causes a high level of vertical acceleration and therewith a poor ride quality. A major disadvantage of an SES in comparison with a catamaran is the much higher level of complexity of the vessel.

A major advantage of SESs over hovercraft is that the side-hulls result in a much smaller amount of air leakage, thus reducing the power that is needed for pressurizing the air cushion. Another advantage of SESs is that the side-hulls allow water-borne propulsion like water jets or surface piercing propellers. This results in

a significant reduction of the noise production and in a higher propulsion efficiency. The side-hulls also result in very different maneuvering characteristics: an SES has a much greater course stability than a comparable hovercraft. Furthermore SESs only have seals (skirts) at the bow and stern, while hovercraft have skirts all around and also internal skirts that divide the cushion into several compartment. This is necessary for the transverse and longitudinal stability of hovercraft. In the case of SESs the stability is supplied by the hulls. The maintenance of the skirts is very expensive, which is an important drawback of the hovercraft concept. The behavior of SESs in waves also differs from the behavior of hovercraft in waves. This is mainly due the fact that the air cushion of an SES is not divided into compartments, which results in a smaller amount of pitch excitation. On the other hand the internal skirts of a hovercraft reduce acoustic resonances of the air inside the cushion to a large extent. A major advantage of hovercraft over SESs is of course that they have amphibious capabilities.

1.3 Overview of the literature

This section presents an overview of the literature on seakeeping of Surface Effect Ships. There exists only a very small amount of literature on the subject of added resistance of SESs. There is however much literature to be found on the topic of motions of SESs. The prediction of the added resistance of a vessel first requires an accurate prediction of the motions of this vessel. Therefore this section starts with a discussion of the literature on motions of Surface Effect Ships. Thereafter it goes into the literature on the subject of added resistance due to waves.

Many authors presented studies on motions of Surface Effect Ships. Kaplan and Davis[6] presented one of the first papers on the modeling of the behavior of SESs in waves. Kaplan et al.[7] developed a non-linear six degrees of freedom motion program. Doctors[8] presented an extensive overview of the literature on the dynamics of hovercraft and SESs, which contains a large amount of valuable references.

From this literature it appears that there are many aspects that are important for the seakeeping of SESs. This section subsequently pays attention to the following aspects: the cobblestone effect, the leakage of air out of the cushion, the stern and bow seal, the air supply system (fans), the interaction of the air cushion with the wave surface, and the effects of scaling.

The cobblestone effect is the collective name for high frequent oscillations of SESs due to resonant phenomena of the air inside the air cushion. The cobblestone effect

results in a high level of vertical acceleration of the SES, and therewith in a poor ride quality for the passengers and crew. At the lowest cobblestone resonance frequency the inertia of the SES is balanced by the force due to the compressibility of the air inside the cushion (Helmholtz resonance). In this case the pressure is spatially constant. The higher cobblestone frequencies are caused by acoustic resonance of the air inside the cushion. At these resonance frequencies the pressure is not spatially constant anymore.

Nakos et al.[9] were the first who addressed the importance of the spatial pressure variations. Sørensen[10], Steen[11] and Ulstein[12] presented extensive studies of the cobblestone effect. Sørensen[10] mainly concentrated on the the active control of the cobblestone oscillations by means of a ride control system. Steen[11] focused on the mathematical modeling of the cobblestone effect. He found that the bag-type stern seal and air leakage are important for the cobblestone oscillations. Ulstein[12] mainly concentrated on the (non-linear) dynamical behavior of the flexible stern seal bag.

Many authors consider air leakage out of the cushion to be very important and highly non-linear (see for instance Nakos et al.[9], McHenry et al.[13] or Masset et al.[14]). When the relative wave height at for instance the bow seal is small the seal will leave a leakage gap above the wave surface. When the relative wave height becomes larger, the leakage area decreases linearly with the relative wave height until the gap closes. A further increase of the relative wave height does of course not result in a negative leakage area. The sudden opening and closure of the seals and the consequent sudden occurrence of air leakage cannot be captured by some linear approximation. Nevertheless air leakage is often linearized or even neglected. ([9], [13]). Steen[11] showed the importance of air leakage in connection with the cobblestone effect. Ulstein[12] studied the air leakage flow by means of computations with a non-linear panel method. He found that a simple one-dimensional approach yields good results as long as the contraction of the escape air jet is taken into account.

The seals are also considered to have an important effect on the motions of SESs. The bag-type stern seal is expected to have an important effect on pitch motions in particular. Lee[15] developed a two-dimensional model for bag-type stern seals. He neglected gravitational and inertial forces as well as the dynamic pressure distribution due to air leakage under the seal. Steen[16],[11] also presented a two-dimensional bag stern seal model in which the the gravitational and inertial forces were neglected. He did however take the dynamic pressure distribution due to air leakage into account. Steen showed the importance of the stern seal where the cob-

blestone effect is concerned. Masset and Morel[17],[14] developed a very similar model. They also carried out an experimental validation of their model. Ulstein[12] developed a model that includes the inertia of the bag structure. He showed that the first eigen mode of the bag of a 28 m SES occurred at a frequency of 1.97 Hz. Therefore the inertial effects are only important for high frequency motions, i.e. the cobblestone effect.

There is not much literature to be found on finger-type bow seals. According to Masset and Morel[17] the shape of a finger-type bow seal does not deform due to pressure or air gap variations. When the seal intersects with the wave surface the part of the seal that would be located below the water surface is simply bent backwards.

The air supply system (fans) is another important aspect of SESs. All existing methods, including the method that is presented by this thesis, use steady fan characteristics to describe the behavior of the fans. Durkin and Luehr[18], Sullivan et al.[19], Masset et al.[17] and Witt[20] concluded however that fans respond in a dynamical way to oscillating pressure in the cushion plenum. Sullivan et al.[19] determined the dynamical response of a model scale air cushion lift fan. They found that the response of the fan was quite linear, but at higher frequencies the response appeared to have a considerable phase lag with respect to the varying pressure. Sullivan et al.[19] also showed that the dynamic response of the fan has a large effect on the heave response of a hovering box.

There appears to exist some difference of opinion about the importance of the interaction between the air cushion and the water surface. Waves inside the air cushion modulate the volume of the air cushion, which leads to cushion pressure variations. The cushion pressure variations cause waves again. These waves again modulate the air cushion, so it is a matter of interaction.

Kaplan et al.[6],[7] only took account of the incident waves in the air cushion. Kaplan[21] claimed that the waves induced by the vessel are small and only have a minor effect on the overall motions. Doctors[22] and Kim and Tsakonas[23] found however that the vessel-induced waves have a significant effect on the motions. McHenry et al.[13] reported only a small effect of cushion induced waves, but Nakos et al.[9] showed that including cushion induced waves damps the Helmholtz resonance of the air cushion and also shifts the Helmholtz resonance to a higher frequency. Moran[24], Kapsenberg[25] and Masset et al.[14] found from model tests that the amplitude of the incident waves is affected by the air cushion. This interaction therefore still deserves much attention.

Scale effects are very important when it comes to model testing of SESs (see for instance Lavis et al.[26]). When no special measures are taken the compressibility of the air inside the cushion is scaled erroneously, which leads to a stiffness of the air cushion that is far to great. There are several ways to reduce the stiffness of the air cushion. One is to scale the ambient pressure by the scale factor. Kapsenberg[27] carried out oscillation experiments with an SES model in the depressurized towing tank at MARIN. He found that the ambient pressure had an important effect on the added mass and damping coefficients. Another way to reduce the air cushion stiffness is to mount a flexible membrane, called diaphragm, on top of the air cushion. Kapsenberg and Blume[5] carried out model experiments for the same vessel at different scales. Both models were equipped with diaphragms that provided a correct stiffness of the air cushion. They found good agreement and concluded that the diaphragm technique is a valid way of scaling cushion dynamics. There exist, as far as the author knows, no literature on the subject of the scaling of air leakage.

Now we come to the subject of added resistance due to waves. There is only a small amount of literature to be found on the subject of added resistance due to waves of Surface Effect Ships.

Faltinsen et al.[28] presented a comparative study of the speed loss and operability of an SES and a catamaran. Their computations include the added resistance of the hulls (similar to the added resistance of conventional ships) and an increase of the frictional resistance of the hulls caused by the sinkage of the vessel due to an increased amount of air leakage. Their computations do not however include any added resistance components due to the air cushion. The outcome of the study is that the speed loss of the SES is larger than the speed loss of the catamaran. The difference is however not very large.

Kapsenberg et al.[1] measured a very large added resistance during experiments with a free sailing model. For conventional ships the added resistance is proportional the wave amplitude squared, but Kapsenberg[25],[5] showed that this relation does *not* hold for an SES.

Kapsenberg et al.[29] also presented a very simple computational model for the air cushion induced added resistance of SESs. They use a strip theory method to compute the motions of the water surface. Subsequently they use the method of Gerritsma and Beukelman [30] to calculate the added resistance. The model is however not very realistic because pitch motions, which do not have any effect on the cushion volume, also induce pitch-like motions of the water surface. Nevertheless this method leads to results that compare remarkably well to experiments.

There exists however a large amount of literature on the subject of added resistance of conventional ships. The thesis of Blok[31] presents an elaborate overview of this literature. Basically there are two approaches to computing the added resistance: the far-field approach and the near field approach.

In far-field methods conservation of momentum or conservation of energy is used to express the mean forces on the vessel in terms of the wave field at a large distance from the vessel. Maruo was one of the first to study the subject of added resistance in waves in depth. He presented many papers and articles on a simplified far-field method for predicting the added resistance in waves (see for instance [32]). Another well known and very practical far-field based method is by Gerritsma and Beukelman[30]. In this method the energy of the radiated waves is set equal to the work being done by the waves to the vessel, where the energy of the radiated waves is expressed as the sectional damping (strip theory) times the relative vertical water velocity. The method leads to very good results for head waves. The work of Newman[33] proved to be a starting point for much subsequent research on far field methods for added resistance. He derived expressions for the steady drift forces on a ship in waves at zero speed from conservation of momentum. The steady drift force is the zero speed equivalent of added resistance. Lin and Reed[34] extended Newman's method to the forward speed case. They presented however no results. The author of this thesis is not aware of a practical application of this method or any similar methods.

In near-field or pressure integration methods the added resistance follows from integration of the unsteady pressure over the wetted part of the hull. Near-field methods have the advantage that they give more detailed insight into the physical phenomena that cause the added resistance. Havelock[35] presented the first (near-field based) method for added resistance. Another relatively simple method was presented by Boese[36]. More recent studies with an increasing level of complexity were carried out by Faltinsen et al.[37] and Blok[31]. Pinkster[38] presented a pressure integration method for the mean and low frequency second order (drift) force on stationary vessels that includes all relevant terms.

The application of three-dimensional Rankine panel methods in computations of the added resistance of ships is still very limited. Sclavounos and Nakos[39] implemented a pressure integration method in their Rankine panel code. They used this method for computing the added resistance of IACC sailing yachts. They never presented results for commercial vessels. Bertram[40] also presented a 3-D Rankine panel method which uses pressure integration to compute the added resistance. He did not show any validation.

From this overview of the literature it appears that there is still a lot of work to be done on the subjects of motions and added resistance of SESs. When it comes to the mathematical modeling of the motions of SESs in waves the following aspects still require much attention: the leakage of air out of the cushion, the bow and stern seals, the air supply system of fans, and the interaction between the air cushion and the water surface. In the case of model experiments scale effects are a serious problem. There is still very little known on the subject of added resistance of SESs. For conventional ships good results for the added resistance due to waves have been achieved, but the underlying theories are only partially applicable to SESs.

1.4   The objective and outline of this thesis

The objective of this thesis is to find an answer to the following research question:

How can one calculate the added resistance due to waves of a Surface Effect Ship?

This objective is slightly less ambitious than the goal of the research project that lies at the root of this thesis that is the development and validation of a computational method for the added resistance due to waves of Surface Effect Ships. This goal has yet not been accomplished completely.

At the beginning of the research project most emphasis was laid on the mathematical modeling of the motions of SESs. This was done because the computation of the added resistance due to waves of a vessel first requires an accurate prediction of the motions of this vessel and, in the case of an SES, also of the cushion pressure variations. Furthermore, at the start of the research project, there was much credit to the hypothesis that the large added resistance of SESs is caused by the air cushion. The step from an accurate prediction of the motions and cushion excess pressure to a prediction of the added resistance of the air cushion was expected to be relatively small.

Chapter 2 treats the hydromechanical problem of the interaction between the water, the hulls and the air cushion. First it presents the translation of the physical problem into a mathematical problem. Thereafter it presents the Rankine panel method that is used to solve this mathematical problem. Subsequently Chapter 2 presents some results of the panel method.

Chapter 3 presents the non-linear simulation method for motions and added resistance of the air cushion of SESs. It presents the equations of motion. Then it treats the modeling of the dynamics of the air cushion and the seals. Thereafter it

describes how the added resistance of the air cushion is calculated. Finally Chapter 3 presents results of the non-linear simulation method.

The presentation of the results of the simulation method at the end of Chapter 3 also involves a comparison of these results to the results of experiments that were carried out by Kapsenberg et al.[1] at MARIN. The correlation of the computational and experimental results is good as far as motions and cushion pressures are concerned. There is however a huge discrepancy between the computed added resistance of the air cushion and the measured (total) added resistance. The computed added resistance of the air cushion was only small, while the measured (total) added resistance was very large. Probably the hypothesis that the large added resistance of SESs is caused by the air cushion is not valid. Therefore the next step in the research project was to investigate the origin of the added resistance of SESs by means of model experiments.

Chapter 4 describes an extensive series of model tests that was carried out at the Ship Hydromechanics Laboratory of Delft University of Technology. The aim of these experiments was to find the origin of the large added resistance of SESs. An attempt was made to measure the added resistance of the air cushion, next to the total added resistance. The difference then yields the added resistance of the hulls. After an introduction the chapter goes into the scaling of air cushion dynamics. Thereafter it describes the model and the different types of experiments to which the model was subjected. Subsequently it treats the measurement of the added resistance, the added resistance of the air cushion and the added resistance of the hulls. Finally Chapter 4 presents and discusses the results of the experiments as far as they concern the added resistance due to waves.

Chapter 5 presents a comparison of the results of the computational method to the results of the experiments that were described by Chapter 4. The objective of this comparison is to investigate the validity of the computational method. The chapter pays attention to the heave and pitch motions, the excess pressures in air cushion and stern seal plena, the seal forces, the behavior of the fans and the added resistance due to waves.

Chapter 6 concludes this thesis. It presents an answer to the question that was posed at the beginning of this section. Furthermore it presents additional conclusions concerning the motions and cushion pressure variations of SESs. These conclusions are only of indirect importance to this question. This chapter ends with recommendations for further research and extensions of the computational method.

1.5   Basic assumptions

This section describes the basic assumptions that underlie the computational method that is presented in Chapter 2 and Chapter 3.

The first basic assumption is that non-linear effects mainly occur in the dynamics of the air cushion and seals. The hydromechanics and the equations of motion are therefore linearized, while the non-linear form of the equations that represent the dynamics of the air cushion and seals is retained. The linearization of the hydrome-chanical problem also enables solving this problem in the frequency domain. This circumvents a complex time stepping algorithm and also saves a lot of computa-tional time. The equations of motion and the equations that represent the dynamics of the air cushion and seals are coupled, and must be solved simultaneously in a time simulation procedure, because the latter equations are non-linear. The fre-quency domain and the time domain are related by a Fourier transform. Appendix A discusses the interrelation of the frequency domain and the time domain.

Another basic assumption is that the cobblestone effect is *not* important for the added resistance due to waves of Surface Effect Ships. The cobblestone effect par-ticularly occurs in small sea-states when the added resistance is negligible. The air cushion excess pressure is therefore assumed to be constant in space.

The last basic assumption that underlies the computational method is that the major contribution to the added resistance of SESs is due to the air cushion. Therefore the added resistance of the hulls is neglected for the time being.

Chapter 2

Hydromechanics

This chapter presents the solution method for the hydromechanical problem. In the first section the physical problem of the (water) flow around a SES sailing in a seaway is translated into a mathematical problem. The section presents a formulation that is exact within potential flow theory. This formulation is linearized, and a frequency domain approach is introduced. The hydrodynamic forces that act on the hulls and the wave height in the air cushion are expressed in the solution of the mathematical problem.

The second section describes the solution method for the mathematical problem. The mathematical problem is solved by means of a three-dimensional Rankine panel method. First an integral equation is presented. Then the numerical solution scheme for this integral equation is treated.

Section 2.3 presents results of the panel method. First it displays some examples of computed wave patterns. Thereafter it presents a brief convergence study of the computed hydrodynamic coefficients and the wave pumping volume of the air cushion. Finally Section 2.3 presents a comparison of results of the panel method to experimental data.

2.1 The mathematical problem

First the physical problem, that has to be translated into a mathematical problem is defined. The SES is assumed to sail at a constant mean forward velocity U in deep waters. The incident waves cause the vessel to carry out oscillatory motions superimposed on the translatory forward motion. The incident waves also cause an oscillatory excess pressure in the air cushion. The oscillating hulls and air cushion

excess pressure generate waves. The flow of the water around the SES is the actual hydromechanical problem that needs to be solved.

2.1.1 Exact formulation

The mathematical problem is formulated in a right-handed coordinate system. This coordinate system moves at a constant positive velocity U in positive x-direction; the same direction as the mean forward velocity of the SES. The origin of the system is situated in the undisturbed free (wave) surface. The z-axis points upwards, and the y-axis points to the port side of the SES.

The fluid is assumed to be in-viscid and irrotational. Therefore a velocity potential $\Psi(x, y, z, t)$ can be introduced. The fluid velocity is equal to the gradient of the velocity potential: $\nabla \Psi$. Conservation of mass leads to the Laplace equation:

$$\Delta \Psi = \nabla^2 \Psi = 0 \tag{2.1}$$

This linear partial differential equation is the governing field equation for Ψ.

Two boundary conditions hold on the free surface, which is elevated a distance $\zeta(x, y, t)$ above the $z = 0$ plane:

- the kinematic free surface condition,

$$(\frac{\partial}{\partial t} + \nabla \Psi \cdot \nabla)(z - \zeta(x, y, t)) = 0 \qquad \text{on } z = \zeta \tag{2.2}$$

- the dynamic free surface condition,

$$\zeta = -\frac{1}{g}\left(\Psi_t + \frac{1}{2}(\nabla \Psi \cdot \nabla \Psi - U^2) + \frac{p(x, y, t)}{\rho}\right) \qquad \text{on } z = \zeta \tag{2.3}$$

where $p(x, y, t)$ is the excess pressure which equals zero outside the air cushion, ρ is the density of water, and a subscript denotes differentiation with respect to this quantity.

The kinematic free surface condition ensures that no water penetrates the free surface. The dynamic free surface condition follows from the Bernoulli equation. It ensures that the water pressure at the free surface is equal to the air pressure above the free surface. These conditions can be combined to:

$$g\Psi_z + \Psi_{tt} + 2\nabla \Psi \cdot \nabla \Psi_t + \frac{1}{2}\nabla \Psi \cdot \nabla(\nabla \Psi \cdot \nabla \Psi) = -\frac{1}{\rho}(p_t + \nabla \Psi \nabla p) \qquad \text{on } z = \zeta \tag{2.4}$$

This combined free surface condition is non-linear. Moreover it holds on the unknown position of the free surface.

The boundary condition on the hull surface reads:

$$\nabla \Psi \cdot \vec{n} = \frac{\partial \vec{a}}{\partial t} \cdot \vec{n} \qquad \text{on } (B) \tag{2.5}$$

where $\vec{a}$ is the local displacement vector of the hull surface, and $\vec{n}$ is the unit vector which is normal to the surface and pointing into the fluid domain. This condition ensures that no water penetrates the hull. Although this condition is linear itself, it holds on the unknown position of the hull.

Next to the boundary conditions, a radiation condition has to be imposed to ensure the uniqueness of the solution. This condition requires that energy carried by the waves, that are caused by the vessel, propagate away from the vessel. Only the energy carried by incident waves can propagate towards the vessel. The implementation of the radiation condition treated in Section 2.2.3.

The author is not aware of any solutions of the fully non-linear unsteady boundary value problem with forward speed. Up to now, always some kind of linearization was used. The development of a method that can solve the fully non-linear unsteady problem is far beyond the scope of this thesis. Therefore, the boundary conditions will be linearized.

2.1.2 Linearized formulation

Several schemes can be used to linearize the boundary conditions that were presented in the previous section. The most accurate and only fully consistent approach is to linearize the unsteady part of Ψ around the steady part of Ψ. The steady potential describes the flow around a ship sailing at a constant speed in otherwise undisturbed water. The fully non-linear steady problem has among others been solved by Raven[41]. Bunnik[42] recently examined into this linearization procedure.

Another popular approach is to linearize both the steady wave potential and/or the unsteady potential around the double body flow (i.e the flow around the hull and its mirror image in the undisturbed surface while the presence free surface is neglected). This approach was followed by Dawson[43] for the steady wave flow. Nakos[44], van't Veer[45] and others used this linearization procedure for the unsteady problem.

In this thesis the problem will be linearized around the undisturbed uniform flow. This linearization scheme is also known as Neumann-Kelvin linearization. According to Nakos[44] application of uniform flow linearization for the hull boundary condition leads to poor results. However, only a small part of the weight of an SES is carried by the buoyancy of the hulls, as most of the vessel's weight is carried by the air cushion. Therefore, as far as the motions of an SES are concerned, the hydrodynamic forces on the hulls are relatively small in comparison with the forces due to the air cushion. Moreover, the hulls of an SES are usually very slender, so approximation of the base flow by the undisturbed flow is not too crude. The main goal of this thesis is to develop a computational method which incorporates the most relevant phenomena, rather than to built a mathematical model that is as consistent as possible.

The total potential Ψ is written as the sum of the potential of a base flow Φ, a steady potential ϕ and an unsteady potential φ:

$$\Psi(x, y, z, t) = \Phi(x, y, z) + \phi(x, y, z) + \varphi(x, y, z, t) \qquad (2.6)$$

The velocity fields $\nabla\phi$ and $\nabla\varphi$ are assumed to be of comparable order and small compared to $\nabla\Phi$. Φ is chosen to be the potential of the undisturbed flow, as was argued by the previous paragraph ($\Phi = -U \cdot x$).

Free surface boundary condition

First the free surface boundary condition is linearized. When products of small quantities like $\nabla\phi\nabla\phi$, $\nabla\phi\nabla\varphi$, e.t.c. are neglected the free surface boundary condition (Equation 2.4) can be written as:

$$g(\phi_z+\varphi_z)+\varphi_{tt}-2U\varphi_{xt}+U^2(\phi_{xx}+\varphi_{xx}) = -\frac{1}{\rho}(p_t-Up_x+\nabla(\phi+\varphi)\nabla p) \quad \text{on } z = 0$$
$$(2.7)$$

The excess pressure p in the air cushion is not a small quantity. If the seals at the bow and stern seal the cushion perfectly, ∇p tends to infinity just under the seals because of the pressure jump. Therefore the term $(\nabla\phi + \nabla\varphi)\nabla p$ is not a product of small quantities like $\nabla\phi\nabla\phi$. The right hand side of Equation 2.7 acts however as the *forcing* of the problem. The term $(\nabla\phi + \nabla\varphi)\nabla p$ is small when compared to the term Up_x, so it gives only a minor contribution to the total forcing of the problem and can therefore be neglected.

Now we have arrived at a linear boundary condition. However, it still must be applied on the unknown position of the free surface. The condition is transfered
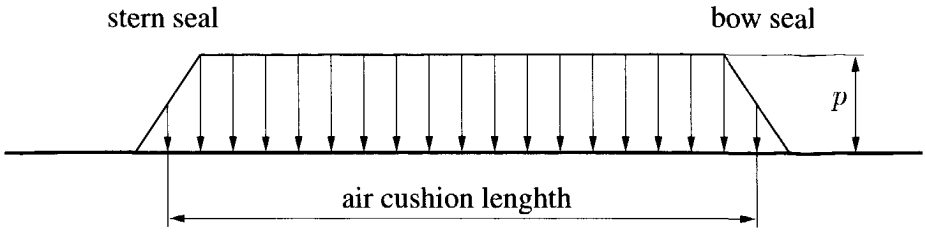
Figure 2.1: Distribution of the air cushion excess pressure

from $z = \zeta$ to $z = 0$ by means of a Taylor expansion. The linearized expression for ζ follows from the dynamic boundary condition (Equation 2.3):

$$\zeta = -\frac{1}{g}\left(\varphi_t - U(\phi_x + \varphi_x) + \frac{p(x,y,t)}{\rho}\right) \tag{2.8}$$

For normal ships without an air cushion this wave height is of the same order as $\nabla\phi$ and $\nabla\varphi$. The excess pressure in the expression for ζ results in the fact that ζ is not small anymore. This excludes a fully consistent linearization scheme. Therefore ζ is still assumed to be small and of the same order as $\nabla\phi$ and $\nabla\varphi$. Then, in the case of uniform flow linearization, the transfer of the boundary condition to $z = 0$ does not give rise to any additional terms in the free surface boundary condition.

The air cushion excess pressure is written as the sum of a steady and an unsteady part: $p(x,y,t) = \bar{p}(x,y) + \tilde{p}(x,y,t)$. This thesis does not focus on acoustic resonant phenomena of the air inside the air cushion . Therefore the excess pressure is assumed to be constant in space except for small strips under the bow and stern seal. At these strips the excess pressure drops linearly from the cushion pressure to zero, as is shown in Figure 2.1. A sudden pressure jump at the seals would cause numerical problems. Doctors[8] investigated the effect of smoothing the edges of the pressure distribution on wave resistance of air cushions. For not too low Froude numbers the effect is only small. Therefore the pressure is linearly increased and decreased at the bow and stern seals. For convenience a non-dimensional unsteady pressure is defined: $\eta_7(t) = \tilde{p}(x,y,t)/ \cdot \bar{p}(x,y)$. Now the mathematical problem can be split up into a steady and an unsteady problem. The separate linearized free surface boundary condition are:

$$g\phi_z + U^2\phi_{xx} = \frac{U}{\rho}\frac{\partial\bar{p}}{\partial x} \qquad \text{on } z = 0 \tag{2.9}$$

for the steady potential, and

$$g\varphi_z + \varphi_{tt} - 2U\varphi_{xt} + U^2\varphi_{xx} = -\frac{1}{\rho}\left(\bar{p}\frac{\partial\eta_7}{\partial t} - U\frac{\partial\bar{p}}{\partial x}\eta_7\right) \qquad \text{on } z = 0 \qquad (2.10)$$

for the unsteady potential. The separate expressions for the wave height are:

$$\zeta = \frac{1}{g}\left(U\phi_x - \frac{\bar{p}}{\rho}\right) \tag{2.11}$$

for the steady problem, and

$$\zeta = -\frac{1}{g}\left(\varphi_t - U\varphi_x + \eta_7\frac{\bar{p}}{\rho}\right) \tag{2.12}$$

for the unsteady problem.

Hull surface boundary condition

Now the hull boundary condition is linearized. In the steady case some sinkage and trim of the vessel are assumed. The position of the hull is then known on fore hand and the otherwise linear condition can be written as:

$$\nabla\phi \cdot \vec{n} = U \cdot n_1 \qquad \text{on } (\bar{B}) \tag{2.13}$$

where n_1 is the x-component of the normal vector and $\bar{B}$ denotes the assumed mean position of the hull surface. When the assumed position of the hull turns out to be incorrect, the computation can be repeated using more appropriate assumptions for sinkage and trim.

The unsteady hull boundary condition reads:

$$\nabla\varphi \cdot \vec{n} = \frac{\partial\vec{a}}{\partial t} \cdot \vec{n} - \nabla(\Phi + \phi) \cdot \vec{n} \qquad \text{on } (B) \tag{2.14}$$

This condition holds on the unknown position of the hull surface. Taylorizing and dropping terms of higher order than linear leads to (see Timman and Newman[46]):

$$\nabla\varphi \cdot \vec{n} = \frac{\partial\vec{a}}{\partial t} \cdot \vec{n} - (\vec{a} \cdot \nabla)\nabla\Phi \cdot \vec{n} + (\nabla\Phi \cdot \nabla)\vec{a} \cdot \vec{n} \qquad \text{on } (\bar{B}) \tag{2.15}$$

An alternative form of Equation 2.15 can be derived if the small displacement of the hull surface is expressed as:

$$\vec{a} = \vec{\eta} + \vec{\Omega} \otimes \vec{x}. \tag{2.16}$$

where $\vec{\eta}$ is the translation vector of the vessel and $\vec{\Omega}$ is the rotation vector of the vessel. With

$$
\begin{aligned}
(\eta_1, \eta_2, \eta_3)^T &= \vec{\eta}, \\
(\eta_4, \eta_5, \eta_6)^T &= \vec{\Omega}, \\
(n_1, n_2, n_3)^T &= \vec{n}, \\
(n_4, n_5, n_6)^T &= \vec{x} \otimes \vec{n}, \\
(m_1, m_2, m_3)^T &= -(\vec{n} \cdot \nabla)\nabla\Phi, \\
(m_4, m_5, m_6)^T &= -(\vec{n} \cdot \nabla)(\vec{x} \otimes \nabla\Phi),
\end{aligned}
$$

the boundary condition on the hull can be written as:

$$
\nabla\varphi \cdot \vec{n} = \sum_{k=1}^{6} \left(\frac{\partial\eta_k}{\partial t} n_k + \eta_k m_k \right) \qquad \text{on } (\bar{B}) \qquad (2.17)
$$

This notation was introduced by Ogilvie and Tuck[47]. The terms $\eta_k m_k$ account for the interaction between the unsteady flow and the base flow, and are usually referred to as the *m-terms*. If uniform flow linearization is applied the only non-zero m-terms are $m_5 = U \cdot n_3$ and $m_6 = -U \cdot n_2$.

2.1.3 Flow around transom sterns

This section goes into the flow around transom sterns. Fast ships usually have a transom stern because it results in a lower resistance, and because it enables easy installation of the water-jet propulsion system. The flow around a transom is very complex. Raven[41] discusses the flow around transom sterns extensively.

The flow around transoms is essentially non-linear. At sufficiently high speed the flow will separate at the sharp transom edge. The wave height just behind the transom is equal to the draft at the transom. This means that the wave height is not small compared to the draft of the hull, so the free surface boundary condition cannot be transferred to the z = 0 plane. Raven[41] solved the fully non-linear steady problem. He applies the free surface boundary conditions at the actual wave surface. His results seem to be very accurate.

Despite the non-linear behavior of the flow around transoms, it will be treated in a linear way. The method of Reed et al.[48] is largely followed. A smooth flow detachment is assumed at the transom. Therefore the following conditions must

hold on the free surface just behind the transom:

$$\zeta(x_{tr}, y) = z(x_{tr}, y)$$

$$\frac{\partial \phi}{\partial z}(x_{tr}, y, , 0) = U \frac{\partial z}{\partial x}(x_{tr}, y) \qquad (2.18)$$

for the steady potential, where $-z(x, y)$ is the local draft of the hull, and

$$\zeta(x_{tr}, y, t) = a_3(x_{tr}, y, t)$$

$$\frac{\partial \phi}{\partial z}(x_{tr}, y, , 0, t) = U \frac{\partial a_3}{\partial x}(x_{tr}, y, t) + \frac{\partial a_3}{\partial t}(x_{tr}, y, t) \qquad (2.19)$$

for the unsteady potential, where $a_3(x, y, t)$ is the local vertical displacement of the hull. $\partial \phi / \partial z$ and $\partial \varphi / \partial z$ follow from the free surface boundary conditions for ϕ (Equation 2.9) and φ (Equation 2.10).

Some confusion appears to exist about the importance of vorticity that is shed at the transom edge. Reed et al.[48] claim, referring to Tulin and Hsu[49], that vorticity is very important. Therefore they add a vortex sheet behind the transom, which is inside the fluid domain. According to Raven[41] vorticity has no physical meaning, and vorticity inside the fluid domain is fundamentally wrong. In the present method a vortex sheet was included. Later, when the results with and without a vortex sheet appeared to be very similar, it has been omitted again.

2.1.4   Formulation in the frequency domain

In the previous sections we have arrived at a linear boundary value problem. Linear problems can be solved in either the time domain or the frequency domain. Both approaches are equivalent and related by a Fourier transform. Appendix A treats the relationship of the time domain and the frequency domain.

The choice was made to solve the unsteady hydromechanical problem in the frequency domain. With this a complex and time consuming time-stepping algorithm is avoided, as differentiation to time changes to multiplication with $i\omega$. On the other hand the problem has to be solved for quite a lot of frequencies which is also time consuming. Later the motions of a SES will be calculated in a time simulation procedure, as the non-linear form of the dynamics of the air cushion will be retained. Therefore the frequency domain results must be transformed to the time domain.

This transformation is treated by Appendix A.

The unsteady potential (φ) is split up into potentials due to harmonically oscillating motion in surge, sway, heave, roll, pitch and yaw, oscillating cushion excess pressure, regular incident waves and diffractional waves:

$$\varphi = \Re\left\{[A(\varphi_I + \varphi_D) + \sum_{k=1}^{7} \hat{\eta}_k \varphi_k] e^{i\omega t}\right\} \tag{2.20}$$

where

A = the amplitude of the incident wave

φ_I = the unit incident wave potential

     = $\dfrac{ig}{\omega_0} e^{kz} e^{-ik(x\cos\beta + y\sin\beta)}$

     where $\omega = \omega_0 - kU\cos\beta$, $k = \omega_0^2/g$, and ω_0 is the incident wave frequency as viewed from a stationary frame

φ_D = the unit diffracted wave potential

$\hat{\eta}_k$ = the complex amplitude of harmonic motion in k^{th} direction, $k = 1, \ldots, 6$, being surge, sway, heave, roll, pitch and yaw respectively

φ_k = the potential due to unit harmonic motion in k^{th} direction, $k = 1, \ldots, 6$.

$\hat{\eta}_7$ = the complex amplitude of harmonic pressure oscillation

φ_7 = the potential due to unit harmonic pressure oscillation

Substitution of Equation 2.20 into the boundary conditions (2.10) and (2.17) and separately balancing each mode, leads to the following boundary value problems:

$$\Delta\varphi_k = 0$$
$$g\frac{\partial\varphi_k}{\partial z} - \omega^2\varphi_k - 2i\omega U\frac{\partial\varphi_k}{\partial x} + U^2\frac{\partial^2\varphi_k}{\partial x^2} = 0 \qquad \text{on } z = 0$$
$$\nabla\varphi_k \cdot \vec{n} = i\omega n_k + m_k \qquad \text{on } (\bar{B})$$

plus the radiation condition $\qquad\qquad\qquad$ (2.21)

for the potentials due to harmonic motion (k = 1, $\ldots$, 6),

$$\Delta\varphi_7 = 0$$
$$g\frac{\partial\varphi_7}{\partial z} - \omega^2\varphi_7 - 2i\omega U\frac{\partial\varphi_7}{\partial x} + U^2\frac{\partial^2\varphi_7}{\partial x^2} =$$

$$-\frac{1}{\rho}(i\omega - U\frac{\partial}{\partial x})\bar{p} \qquad \text{on } z = 0$$

$$\nabla\varphi_7 \cdot \vec{n} = 0 \qquad \text{on } (\bar{B})$$

plus the radiation condition $\hspace{10em}$ (2.22)

for the potential due to harmonic cushion pressure oscillation,

$$\Delta\varphi_D = 0$$

$$g\frac{\partial\varphi_D}{\partial z} - \omega^2\varphi_D - 2i\omega U\frac{\partial\varphi_D}{\partial x} + U^2\frac{\partial^2\varphi_D}{\partial x^2} =$$

$$\qquad -g\frac{\partial\varphi_I}{\partial z} + \omega^2\varphi_I + 2i\omega U\frac{\partial\varphi_I}{\partial x} - U^2\frac{\partial^2\varphi_I}{\partial x^2} \qquad \text{on } z = 0$$

$$\nabla\varphi_D \cdot \vec{n} = -\nabla\varphi_I \cdot \vec{n} \qquad \text{on } (\bar{B})$$

plus the radiation condition $\hspace{10em}$ (2.23)

for the diffracted wave potential.

These boundary value problems can be solved by a three-dimensional panel method. Section 2.2 presents such a panel method.

2.1.5   Hydrodynamic forces and wave pumping volume

This Section presents expressions for the hydrodynamic forces that act on the hull surface and for the volume modulation of the air cushion due to waves. This volume modulation will be referred to as *wave volume pumping*. The hydrodynamic forces and the wave pumping volume are expressed in terms of the solutions of the boundary value problems that were formulated in the previous sections.

The hydrodynamic forces that act on the vessel follow from pressure integration over the wetted surface of the hulls. The pressure p in the flow, which should not be mixed up with the excess pressure in the air cushion, can be expressed by means of Bernoulli's equation:

$$p = -\rho(\Psi_t + \frac{1}{2}\nabla\Psi \cdot \nabla\Psi - \frac{1}{2}U^2 + gz) \qquad (2.24)$$

This expression is transferred to the mean position of the hull surface by means of Taylor expansions. Then linearization leads to

$$p = -\rho(gz - U\phi_x) \qquad (2.25)$$

for the steady pressure, and

$$p = -\rho(\varphi_t - U\varphi_x + (\vec{a} \cdot \nabla)gz) \tag{2.26}$$

for the unsteady pressure. The hydrodynamic forces that act on the vessel follow from:

$$F_j = -\iint_{\bar{B}} pn_j dS \qquad j = 1, \ldots, 6 \tag{2.27}$$

where the subscript j denotes the direction of forcing, n_j is defined by Equation 2.17 and $\bar{B}$ is the part of the hull surface that is below the undisturbed water surface, except for the transom which is dry because of the smooth detachment of the flow at the sharp transom edge.

When the frequency Equation 2.20 is substituted into Equation 2.26 which is subsequently substituted into Equation 2.27, the unsteady hydrodynamic force can be written as:

$$F_j = \Re\left\{ \sum_{k=1}^{7} \left([\omega^2 A_{jk}(\omega) - i\omega B_{jk}(\omega) - C_{jk}]\hat{\eta}_k + AX_j(\omega) \right) e^{i\omega t} \right\} \qquad j = 1, \ldots, 6 \tag{2.28}$$

where

$$A_{jk}(\omega) = \frac{\rho}{\omega^2}\Re \iint_{\bar{B}} (i\omega\varphi_k - U\frac{\partial\varphi_k}{\partial x}) n_j \, dS,$$

$$B_{jk}(\omega) = -\frac{\rho}{\omega}\Im \iint_{\bar{B}} (i\omega\varphi_k - U\frac{\partial\varphi_k}{\partial x}) n_j \, dS,$$

$$(C_{j1}, C_{j2}, C_{j3})^T = -\rho \iint_{\bar{B}} \nabla(gz) n_j \, dS,$$

$$(C_{j4}, C_{j5}, C_{j6})^T = -\rho \iint_{\bar{B}} (\vec{x} \otimes \nabla)(gz) \, n_j \, dS,$$

$$C_{j7} = 0,$$

$$X_j(\omega) = \rho \iint_{\bar{B}} [i\omega(\varphi_I + \varphi_D) - U\frac{\partial}{\partial x}(\varphi_I + \varphi_D)] n_j \, dS.$$

$A_{jk}(\omega)$, $B_{jk}(\omega)$ and C_{jk} are the well known added mass, damping and restoring coefficients, A is the wave amplitude and $X_j(\omega)$ is the exiting force due to regular

unit amplitude incident waves. This exiting force is the sum of the Froude-Kriloff force and the force due to diffraction of the incident waves.

It can be more convenient to use a different definition of the hydrodynamic coefficients. When ω tends to zero, $\varphi_k(x, y, z, \omega)$ approaches a real non-zero function of x, y and z. Basically $\varphi_k(x, y, z, 0)$ is a correction to the steady potential $(\Phi + \phi)$ due to a constant unit displacement of the vessel ($\eta_k = 1$). Although $\varphi_k(x, y, z, 0)$ is rather small it causes A_{jk} to be infinite when $\omega = 0$. This steady part of φ_k contributes to the coefficient A_{jk} while it should contribute to C_{jk}. Therefore the following definition of the hydrodynamic coefficients is more realistic.

$$A_{jk}^*(\omega) = \frac{\rho}{\omega^2}\Re\iint_{\bar{B}}\left[i\omega\varphi_k(\omega) - U\frac{\partial}{\partial x}\big(\varphi_k(\omega) - \varphi_k(0)\big)\right]n_j\,dS,$$

$$B_{jk}^*(\omega) = -\frac{\rho}{\omega}\Im\iint_{\bar{B}}\left[i\omega\varphi_k(\omega) - U\frac{\partial}{\partial x}\big(\varphi_k(\omega) - \varphi_k(0)\big)\right]n_j\,dS,$$

$$C_{jk}^* = -\rho\iint_{\bar{B}} -U\frac{\partial}{\partial x}\varphi_k(0)\,n_j\,dS \; + \; C_{jk}.$$

Then the effect of forward speed on the restoring force is incorporated by C_{jk}^* instead of by A_{jk}. A_{jk}^*, B_{jk}^* and C_{jk}^* will be designated as the *modified* added mass, damping and restoring coefficients. Please note that $B_{jk}^* = B_{jk}$ because $\Re\varphi_k(0)$.

The wave pumping volume (V_ζ) follows from integration of the wave height over the part of the free surface that is covered by the air cushion. The unsteady wave height follows from Equation 2.12. When the frequency domain solution (Equation 2.20) is substituted into this expression the wave pumping volume can be written as:

$$V_\zeta = \Re\left\{\sum_{k=1}^{7} D_k(\omega)\hat{\eta}_k + A(D_I(\omega) + D_D(\omega))\right\} \qquad (2.29)$$

where

$$D_k = -\frac{1}{g}\iint_{FS_c}\left(i\omega\varphi_k - U\frac{\partial\varphi_k}{\partial x} + \frac{\bar{p}}{\rho}\delta_{7k}\right) \qquad (2.30)$$

and FS_c is the part of the free surface that is covered by the air cushion and δ_{7k} is the Kronecker delta.

This section presented a mathematical problem for the water flow around a Surface Effect Ship sailing in waves. The problem was linearized and a frequency domain

solution was introduced. The hydrodynamic forces which act on the hull surface and the modulation of the air cushion volume due to waves were expressed in the solution of the problem. The next section presents the solution method for this mathematical problem.

2.2 Rankine panel method

This section presents a solution method for the mathematical problem that was formulated in the previous section. The first section presents a boundary integral equation. The solution of this boundary integral equation is an alternative for directly solving the field equation (Equation 2.1) in the entire computational domain. The second subsection treats the numerical solution of the integral equation. The third subsection presents the implementation of the radiation condition.

2.2.1 Integral equation

There are several ways to cast a boundary value problem for the Laplace equation (Equation 2.1) into the form of a boundary integral equation (see for instance Sloof[50]). For the present method the so called *direct formulation* will be used.

Green's theorem is applied to the unknown potential ϕ and a Green function which is taken as the potential of the Rankine source in the point $\vec{x}$. This Green function reads:

$$G(\vec{x}, \vec{x}') = -\frac{1}{|\vec{x} - \vec{x}'|} \tag{2.31}$$

When the point $\vec{x}$ is an element of the computational domain Ω which is bounded by the surface S application of Green's theorem this leads to:

$$\phi(\vec{x}) = \frac{1}{4\pi} \iint_S \left(\frac{\partial \phi(\vec{x}')}{\partial n'} G(\vec{x}, \vec{x}') - \phi(\vec{x}') \frac{\partial}{\partial n'} G(\vec{x}, \vec{x}') \right) dS' \qquad \text{for } \vec{x} \in \Omega \quad (2.32)$$

From this it follows that the potential is determined in the entire computational domain when ϕ and it's normal derivative are prescribed on the boundary of that domain. This implies that finding ϕ and $\partial \phi / \partial n$ on the boundary surface S is equivalent to solving the unknown potential in the entire computational domain Ω.

When the point $\vec{x}$ is moved to the boundary surface Equation 2.32 becomes:

$$\phi(\vec{x}) = \frac{1}{2\pi} \iint_S \left(\frac{\partial \phi(\vec{x}')}{\partial n'} G(\vec{x}, \vec{x}') - \phi(\vec{x}') \frac{\partial}{\partial n'} G(\vec{x}, \vec{x}') \right) dS' \qquad \text{for } \vec{x} \in S \quad (2.33)$$

where the integral should be taken in a principal value sense. In the present case the boundary S consists of the hull surface, the wave surface and a control surface at infinity. The contribution of the control surface can be shown to vanish when $\vec{x}$ remains finite.

The normal derivative of the unknown potential follows from the appropriate boundary condition. The normal derivative on the hull surface is known from the hull Boundary condition. The normal derivative on the free surface can be expressed in tangential derivatives of the potential by means of the free surface boundary condition, as $\partial\phi/\partial n = -\partial\phi/\partial z$. The following section treats the solution of the integral equation.

An alternative integral equation can be obtained when the Green function is taken as the more complex potential of the Kelvin source which implicitly fulfills the Kelvin boundary condition on the free surface. Then the integration over the free surface can be reduced to a line integral along the water line of the vessel, leading to a much smaller number of unknowns. The radiation condition can also be satisfied implicitly. The evaluation of the kernel however is much more difficult and time consuming, and the air cushion cannot be included directly as it gives rise to extra terms in the free surface condition. Furthermore the code was developed jointly with van't Veer[45] who linearized the free surface condition around the double body flow. Then this alternative formulation cannot be used as the coefficients in the free surface condition are not constant anymore. Hence we choose this formulation with Rankine singularities.

2.2.2 Numerical solution

The integral equation which was presented by the previous section is solved numerically using the collocation method. The hull surface and a part of the free surface are paneled with flat quadrilateral panels. Figure 2.2 shows an example of a panel distribution. The potential and it's normal derivative are taken to be constant on a panel. In the center of each panel a collocation point is defined. Satisfaction of the integral equation in the collocation points leads to the following linear system of equations:

$$\phi_l = \frac{1}{2\pi}\sum_{k=1}^{N}\Big[\frac{\partial\phi_k}{\partial n_k}\underset{\text{panel }k}{\int\int}G(\vec{x}_l,\vec{x}')dS' - \phi_k\underset{\text{panel }k}{\int\int}\frac{\partial}{\partial n_k}G(\vec{x}_l,\vec{x}')dS'\Big] \qquad (2.34)$$

where $l = 1,\ldots,N$ and N is the number of panels or collocation points.

The normal derivative of ϕ on the hull surface follows from the (Neumann) boundary condition on the hulls. The normal derivative of ϕ on the free surface
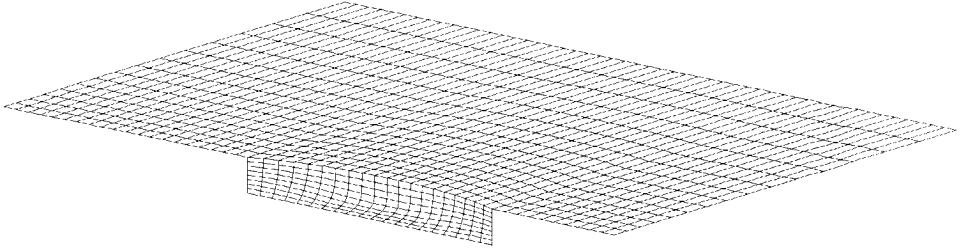
Figure 2.2: Paneling of the port side of a Wigley hull and the free surface

is expressed in tangential derivatives of ϕ using the (Kelvin) free surface boundary condition. Differentiating ϕ tangentially seems to be in contradiction with the assumption that ϕ is constant on a panel. In the continuous case ϕ is however a smooth function which can be differentiated many times. The approximation of ϕ and $\partial\phi/\partial n$ by constant values should be interpreted as samples of otherwise smooth functions. Therefore differentiation of this function does make sense.

Two schemes to calculate the tangential derivatives of ϕ have been tried: a finite difference scheme, and a bi-quadratic spline scheme. The finite difference scheme uses the potential on the eight neighboring panels and on the actual panel itself to compute the first and second tangential derivatives by means of finite difference operators.

In the bi- quadratic spline scheme the potential and it's derivatives follow from a bi-quadratic spline representation of the potential. The potential is written as the sum of bi-quadratic B-spline basis functions:

$$\phi(x, y) = \sum_{k=1}^{N} x_k \cdot B_k^{(2,2)}(x, y) \tag{2.35}$$

where x_k is the weight factor of basis function $B_k^{(2,2)}$. $B_k^{(2,2)}$ is zero except on panel k and it's neighboring panels. A two-dimensional basis function $B^{(2,2)}$ follows from the product of two one-dimensional quadratic basis functions:

$$B^{(2,2)}(\xi, \eta) = b^{(2)}(\xi) \cdot b^{(2)}(\eta) \tag{2.36}$$

where ξ and η are the local non-orthogonal coordinates which are defined by Figure 2.4. Figure 2.3 shows a one-dimensional quadratic basis function. It can be
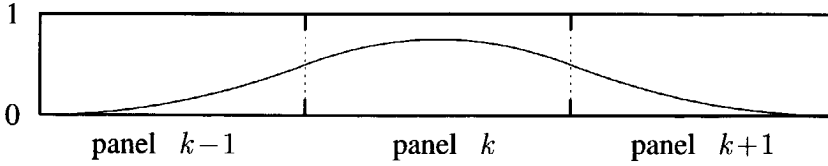
Figure 2.3: One-dimensional quadratic basis function

differentiated two times analytically. $b^{(2)}(\xi)$ follows from:

$$
b^{(2)}(\xi) = \begin{cases}
\dfrac{(h_\xi^{k-1} + \frac{1}{2}h_\xi^k + \xi)^2}{h_\xi^{k-1}(h_\xi^{k-1} + h_\xi^k)} & -h_\xi^{k-1} - \frac{1}{2}h_\xi^k \le \xi \le -\frac{1}{2}h_\xi^k \\[3ex]
1 - \dfrac{(\frac{1}{2}h_\xi^k - \xi)^2}{h_\xi^k(h_\xi^k + h_\xi^{k-1})} - \dfrac{(\frac{1}{2}h_\xi^k + \xi)^2}{h_\xi^k(h_\xi^k + h_\xi^{k+1})} & -\frac{1}{2}h_\xi^k \le \xi \le \frac{1}{2}h_\xi^k \\[3ex]
\dfrac{(h_\xi^{k+1} + \frac{1}{2}h_\xi^k - \xi)^2}{h_\xi^{k+1}(h_\xi^{k+1} + h_\xi^k)} & \frac{1}{2}h_\xi^k \le \xi \le h_\xi^{k+1} + \frac{1}{2}h_\xi^k
\end{cases}
$$

$$(2.37)$$

where h_ξ^k is the dimension of panel k in ξ-direction. The potential and it's derivatives are expressed in the weight factors of the basis functions ($\vec{x}$). These weight factors are solved for. Nakos[44] also used this bi-quadratic spline scheme, but he also implemented a quadratic singularity distribution on the panels. In the present method the *mean* value of ϕ and $\partial\phi/\partial n$ on a panel are used.

In both schemes (finite difference scheme and spline scheme) the differentiation of the potential is carried out along the local coordinates ξ and η. The dashed lines in Figure 2.4 show that ξ and η are, at least in the continuous case, curvilinear coordinates. Therefore tangential derivatives need to be transformed to the global coordinates x, y and z by means of the following relations:

$$
\phi_x = \phi_\xi \frac{1}{\cos\theta} + \phi_\eta \tan\theta
$$

$$
\phi_y = \phi_\eta
$$

$$
\phi_{xx} = \phi_{\xi\xi} \frac{1}{\cos^2\theta} + 2\phi_{\xi\eta} \frac{\tan\theta}{\cos\theta} + \phi_{\eta\eta} \tan^2\theta +
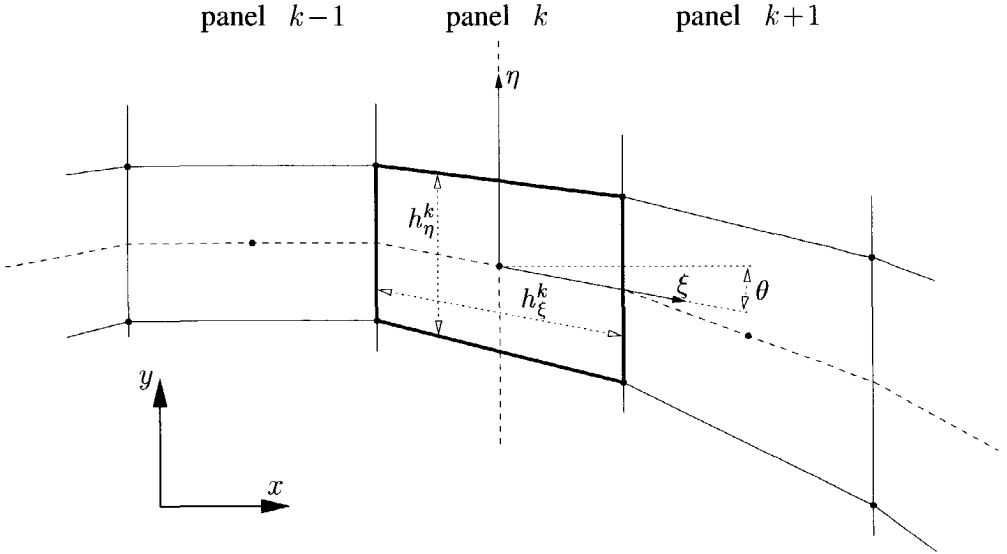$$

panel $k-1$ panel k panel $k+1$

Figure 2.4: The local non-orthogonal curvilinear coordinates on panel k

$$2 \cdot \left(\phi_\xi \frac{\sin \theta}{\cos^2 \theta} + \phi_\eta \frac{1}{\cos^2 \theta} \right) \cdot \left(\theta_\xi \frac{1}{\cos \theta} + \theta_\eta \tan \theta \right)$$

$$\phi_{xy} = \phi_{\xi\eta} \frac{1}{\cos \theta} + \phi_{\eta\eta} \tan \theta + \left(\phi_\xi \frac{\sin \theta}{\cos^2 \theta} + \phi_\eta \frac{1}{\cos^2 \theta} \right) \cdot \theta_\eta$$

$$\phi_{yy} = \phi_{\eta\eta} \tag{2.38}$$

where θ is the skew angle of the panel as defined by Figure 2.4. The terms within brackets are due to the curvature of the curvilinear coordinates. It must be noted that the free surface grid must be generated in such a way that the direction of the η-axis and the y-axis are the same for all free surface panels.

In both schemes a row of artificial end panels surrounding the grid panels has been added. In case of the finite difference scheme this enables the use of central discretization on panels next to the waterline and the truncations of the free surface grid. In case of the spline scheme this enables a complete spline representation of the unknown potential, because the basis functions spill over the boundaries of their panel. This causes the number of unknowns to exceed the number of equations which follows from collocation. Therefore extra end conditions have been formulated. At the center line the symmetry condition $\partial \phi / \partial y = 0$ is used. At the waterline two end conditions must be imposed: one for the end panels of the hull

surface, and one for the end panels of the free surface. For the hull surface the condition of continuity of the potential when passing from the hull surface to the free surface is used. For the free surface the rather 'impartial' condition $\partial^2\phi/\partial y^2 = 0$ is used. The more physical condition of zero normal velocity to the hull resulted in transverse point to point oscillations in the steady solution near the stem and stern of the vessel. This is probably caused by the local singular behavior of the solution. The condition of zero curvature leads to a much smoother solution. This condition is also used for the end panels of the hull surface at the stem and stern. The next section treats the end conditions at the upstream, downstream and transverse truncations of the free surface grid in relation with the radiation condition.

The finite difference scheme appears to have significant numerical damping and dispersion. The performance of the spline scheme is superior on these points. In the steady solutions some transverse oscillations appear near the waterline when the grid is refined. This phenomenon was also reported by Sclavounos and Nakos[51]. They attribute the oscillatory behavior to aliasing of the energy of very short waves to the shortest waves that can be resolved by the grid. The spline scheme already leads to wiggles on a much coarser grid than the finite difference scheme. The wiggles do not seem to have an important effect on the convergence of the hydrodynamic forces. Therefore the spline scheme is used in most cases.

2.2.3   Radiation condition

The radiation condition has a double function. First it should ensure a unique solution to the problem. This implies that it should prevent waves which are traveling into the computational domain. Secondly it should absorb the waves which are generated by the vessel. As the number of panels is bounded by the available computer capacity, only a part of the free surface can be covered with panels. Generally the effect of truncating the free surface does not vanish in the vicinity of the vessel when the truncation is moved towards infinity. This is caused by the (partial) reflection of waves by the truncation.

For the present method reflections from the truncations of the free surface grid are not important. The method is designed to compute the hydrodynamics of fast ships. When the forward speed is high, the Strouhal number $\tau = U\omega/g$ is much larger than $1/4$ in the frequency range of interest. This means that waves cannot travel upstream. Therefore they will not reach the upstream truncation. Moreover, when the transverse truncations are sufficiently far away from the vessel, the reflections of this truncation will end up behind the vessel. Reflections from the downstream

truncation cannot travel upstream and therefore will not reach the vessel.

A unique solution is effectively ensured by requiring flat water at the upstream truncation of the free surface. Therefore the following conditions are enforced at the upstream truncation in both steady and unsteady cases:

$$\zeta = 0$$

$$\frac{\partial \phi}{\partial z} = 0$$

(2.39)

These conditions were also used by Nakos[44]. The conditions are very similar to the conditions that require a smooth detachment of the flow at the transom (equations 2.18 and 2.19).

The two conditions at the upstream truncation of the free surface are implemented as the end conditions for the upstream and for the downstream truncation of the free surface grid. The fact that both end conditions only involve unknowns at the upstream truncation does not lead to an ill-conditioned system of equations. At the transverse truncation the condition $\partial^2 \phi / \partial y^2 = 0$ is used. When the vessel has a transom stern an extra sheet of free surface panels is added behind the transom. Analogous to the radiation condition, both transom flow conditions are implemented as the upstream and downstream end conditions of this sheet.

The system of equations is solved using simple LU-decomposition, although an iterative solver might give a considerable reduction of computational time. The method is suitable for symmetrical problems (i.e. head or following waves) only.

2.3   Results of the panel method

This section presents results of the panel method. First it displays some examples of computed wave patterns. Thereafter it presents a convergence study of the hydromechanic coefficients, the wave pumping volume of the air cushion and the wave height of the seals. The results of the finite difference scheme and the spline scheme are compared. Finally this section presents a comparison of computational and experimental results.
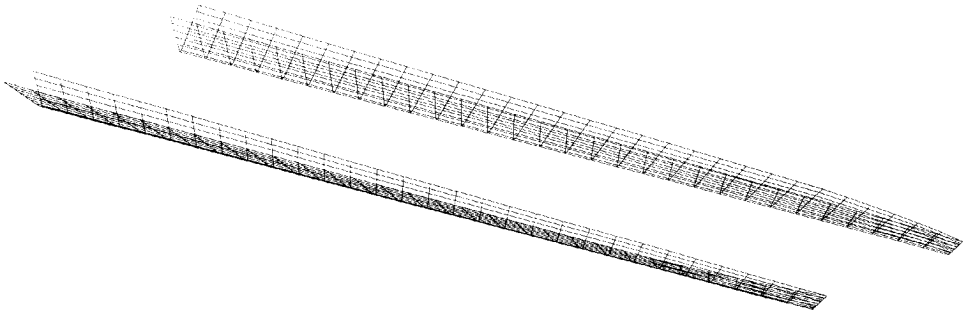
Figure 2.5: Panel distribution on the hulls of the DUTSES model (30 × 13 panels on one hull)

2.3.1   Wave patterns

This section presents some examples of computed wave patterns around the DUT-SES model. The DUTSES model is an SES model that was subjected to an extensive series of experiments. Chapter 4 describes the DUTSES model and these experiments. Figure 2.5 shows the panel distribution on the hulls that was used in the computations.

Figure 2.6 and Figure 2.7 both show the computed steady wave pattern around the DUTSES model sailing at $Fn = 0.603$. The gaps in the free surface mesh is due the piercing hulls. The large wave trough between the demi-hulls is due to the air cushion. Figure 2.6 shows the wave pattern as computed by means of the finite difference scheme, while the wave pattern that is shown in Figure 2.7 was computed by means of the spline scheme. Generally the solutions are in good agreement, although the result of the finite difference scheme are much smoother than the results of the spline scheme. Both computational schemes result in a wave pattern that slightly oscillates in transverse direction. These oscillations are much more pronounced in the results of the finite difference scheme, especially in the vicinity of the rooster tail like wave system aft of the transoms. These oscillations become worse upon panel refinement.

Many authors report a poor convergence of the wave pattern close to the water line of surface piercing bodies. Nakos and Sclavounos [52] also report a poor convergence of their solution upon panel refinement. They attribute this behavior to the strong singularity exhibited by the underlying continuous (linear) solution. In the regions where highly non-linear phenomena like wave breaking and spray occur,
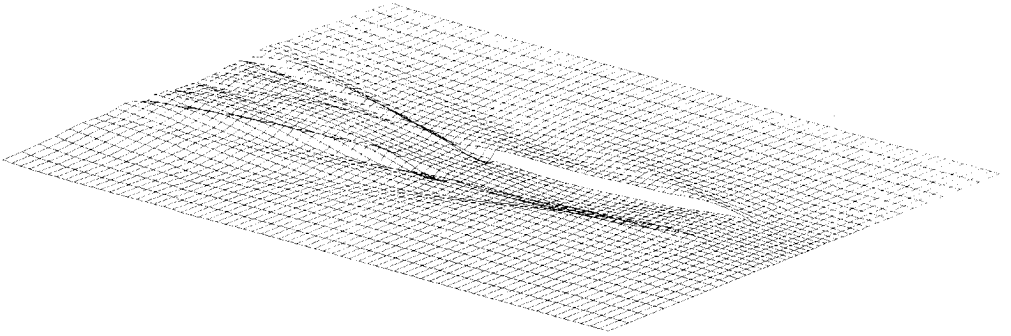
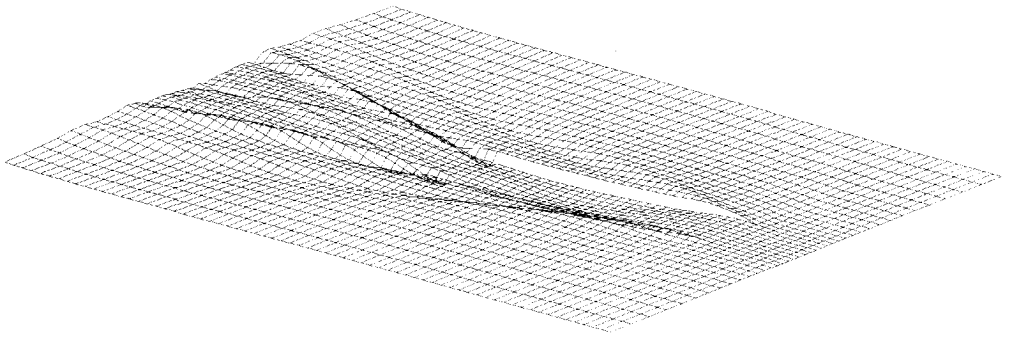Figure 2.6: Steady wave pattern around the DUTSES model (finite difference scheme)

Figure 2.7: Steady wave pattern around the DUTSES model (quadratic B-spline scheme)

the linear continuous solution contains (if it exists at all) very short wave lengths which contain a considerable amount of energy. This energy is aliased to the shortest wave lengths that can be represented by the computational grid (Nyquist wave numbers). Therefore Nakos and Sclavounos [52] introduced a filtering scheme for the forcing terms in the free surface boundary condition in order to obtain a full convergence. For the present method we will not mind this oscillatory behavior, as we are particularly interested in the hydromechanic forces, the wave pumping volume and (mean) wave height at the seal. The next section presents an investigation into the convergence of these quantities.
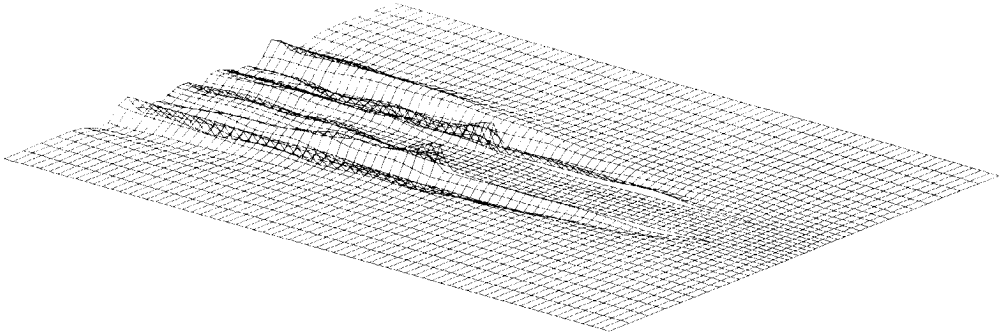
Figure 2.8: Unsteady wave pattern around the DUTSES model due to heaving hulls (finite difference scheme)
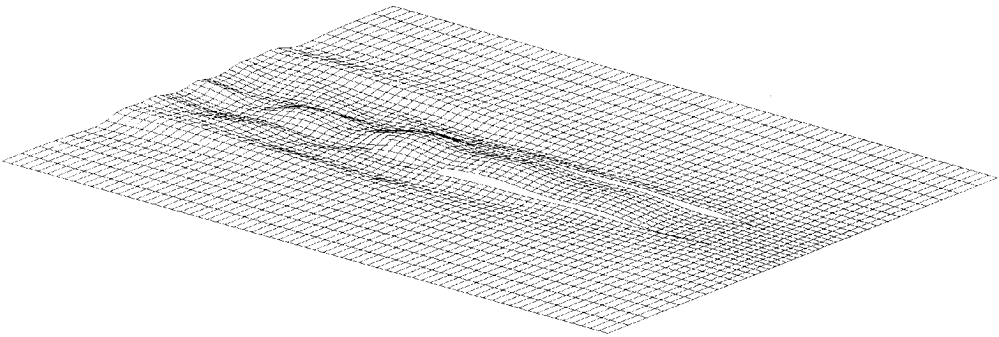

Figure 2.9: Unsteady wave pattern around the DUTSES model due to oscillating air cushion pressure (finite difference scheme)

Figure 2.8 shows a snap shot (actually the real part) of the unsteady wave pattern due to harmonically heaving hulls. This figure does not include the steady waves. The figure is the result of a computation for $Fn = 0.603$ and $\omega\sqrt{(L/g)} = 5.530$ using the finite difference scheme. This frequency is by far over critical ($\tau = 3.333 \gg 0.25$), hence no waves occur upstream of the vessel. The hulls generate relatively small waves in the air cushion (between the demi-hulls). This is due to the shape of the hulls: vertical inner side-walls, and inclined outer side walls. Downstream of the transoms large waves can be observed. This is due to the smooth flow detachment at the transom.

Table 2.1: Principal characteristics of the systematically refined free surface grids for the DUTSES model

name	number of f.s. panels	h_x	h_y	expansion factor
Grid A	438	0.1992	0.0875	1.226
Grid B	760	0.1494	0.0656	1.161
Grid C	1190	0.1195	0.0525	1.125
Grid D	1692	0.0996	0.0438	1.102

Figure 2.9 shows a snap shot (real part) of the unsteady wave pattern due a harmonically oscillating air cushion excess pressure. This figure is also the result of a computation for $Fn = 0.603$ and $\omega\sqrt{(L/g)} = 5.530$ using the finite difference scheme. The waves in the the air cushion are considerable. These waves have an important effect on the air cushion volume and therewith on the air cushion pressure. The importance of this interaction is investigated in Section 3.5.3.

2.3.2 Convergence of the hydrodynamic coefficients e.t.c.

This section presents some results of the panel method that were obtained using systematically refined free surface grids. It illustrates the convergence of the hydrodynamic coefficients, the wave pumping volume and the wave height at the seals upon panel refinement.

Figure 2.10 shows the modified heave added mass and damping curves for the DUTSES model sailing at $Fn = 0.603$. The curves were computed by means of the spline scheme. They are presented in a non-dimensional form. Table 2.1 presents the principal characteristics of the systematically refined free surface grids. It subsequently shows the grid name, the total number of free surface panels, the longitudinal panel dimension h_x, the transverse panel dimension h_y and the transverse expansion factor for the panels next to the vessel (i.e. $h_y^{(n+1)}/h_y^{(n)}$, the transverse panel dimension of transversely neighboring panels).

The convergence of the added mass is quite satisfactory. The convergence of the damping is however much slower. A cause for the slow convergence is that the hulls are very slender. For a good representation of the wave exiting due to the hulls one should use panels with a transverse dimension which is significantly smaller than the beam of a demi-hull. Furthermore the high speed of SESs results in relatively
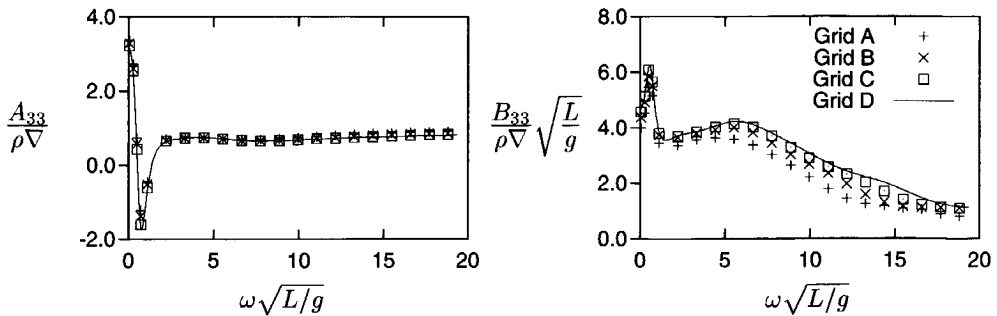
Figure 2.10: Convergence of the heave added mass and damping curves of the DUT-SES model (spline scheme)

high frequencies of encounter and therefore in very short transverse wavelengths. The representation of these waves also requires a very small transverse panel dimension.

Figure 2.11 shows the heave added mass and damping curves for the Wigley model 1 hull sailing at $Fn = 0.300$. A Wigley hull is a hull form which follows from a simple mathematical expression. The next section describes Wigley Model I. These curves were also computed by means of the spline scheme. The Wigley I hull is slender too, but it is much wider than a demi-hull of the DUTSES model. The speed is also considerably lower. Table 2.2 presents the principal characteristics of the free surface grids that were used.

The convergence of both the added mass curve and the damping curve is excellent. This indicates that the results of the panel method do converge upon panel refinement. In the case of the DUTSES model the convergence is probably delayed due to the inability of the grid to represent the very short transverse wave lengths.

Table 2.2: Principal characteristics of the systematically refined free surface grids for the Wigley Model I (spline scheme)

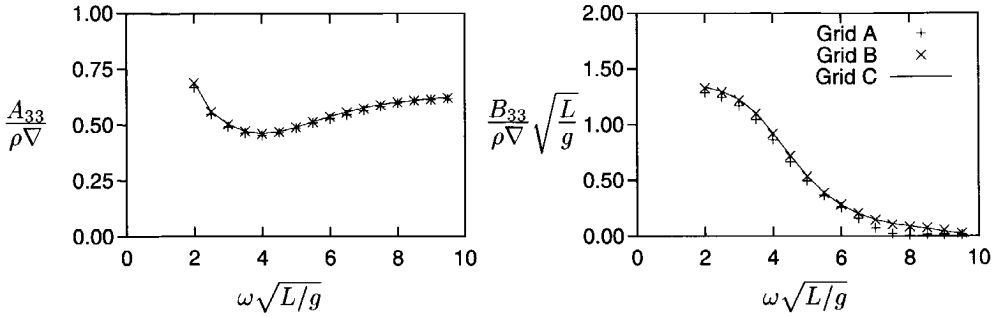| name	number of f.s. panels	h_x	h_y	expansion factor
Grid A	244	0.3000	0.2121	1.108
Grid B	804	0.2000	0.1061	1.076
Grid C	1680	0.1000	0.0707	1.056

Figure 2.11: Convergence of the heave added mass and damping curves of Wigley Model I

Figure 2.12 shows the real and the imaginary part of the wave pumping volume due to oscillating cushion pressure of the DUTSES model sailing at $Fn = 0.603$. These results were also computed by means of the spline scheme. In the low and medium frequency range the convergence is very satisfactory. In the high frequency range the method turns unstable when the coarser grids are used, which leads to erroneous results.

Figure 2.13 shows the same results as Figure 2.12 except that these results were obtained by means of the finite difference scheme. Both schemes converge to the same result, but the spline scheme converges much faster than the finite difference scheme. The finite difference scheme turns unstable at much lower frequencies. The spline scheme can represent shorter wave lengths on the same grid. In the remainder of this thesis we will always use the spline scheme because of it's superior convergence properties.

Figure 2.14 shows the real and imaginary part of the mean wave height at the stern seal due to oscillating cushion pressure of the DUTSES model sailing at $Fn = 0.603$. These results were again obtained by means of the spline scheme. The wave height at the seals does not converge that fast as the wave pumping volume. The convergence of the wave steepness at the seals is even slower.
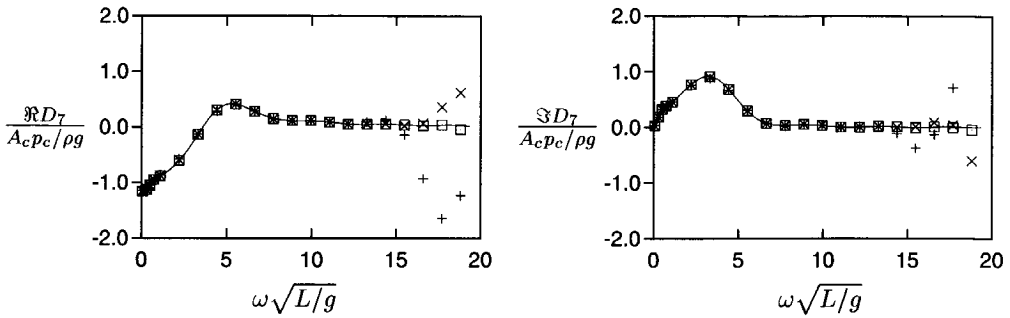
Figure 2.12: Convergence of the wave pumping volume due to oscillating cushion pressure (spline scheme)
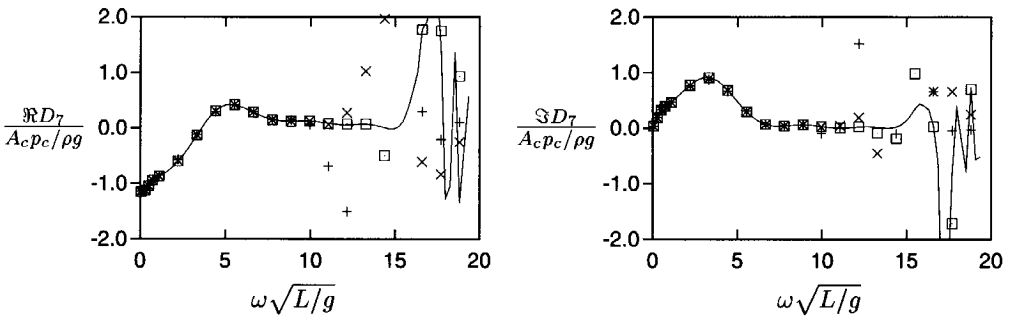

Figure 2.13: Convergence of the wave pumping volume due to oscillating cushion pressure (finite difference scheme)
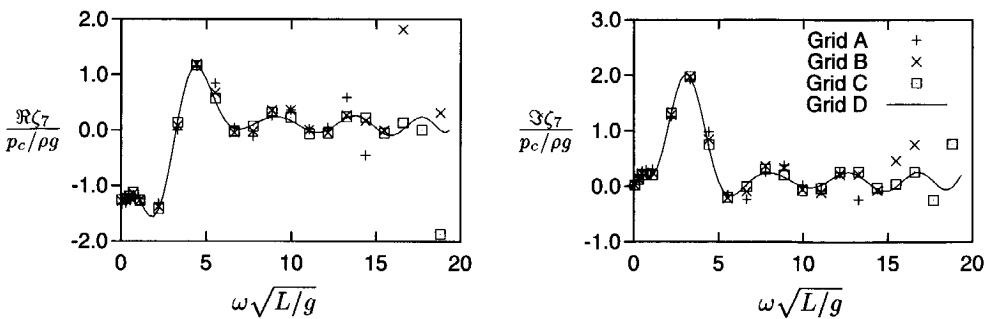

Figure 2.14: Convergence of the wave height at the stern seal due to oscillating cushion pressure (spline scheme)

Table 2.3: Main dimensions of Wigley model I

Length to beam ratio	L/B	10	
Length to draft ratio	L/T	16	
Midship section coefficient	C_M	0.909	
Block coefficient	C_B	0.561	
Length	L	3.000	m
Beam	B	0.300	m
Draft	T	0.188	m
Pitch radius of gyration	k_{yy}	0.750	m

2.3.3 Comparison of the results to experimental data

This section presents a comparison of results of the panel method with experimental data. It presents hydrodynamic coefficients, wave exiting forces and motions for Wigley Model I. The experimental data for Wigley Model I were extracted from a report by Journée[53].

The hull shape of Wigley Model I follows from the following formula:

$$\frac{2y}{B} = \left(1 - \frac{z^2}{T^2}\right)\left(1 - \frac{x^2}{L^2}\right)\left(1 + 0.2\frac{x^2}{L^2}\right) + \frac{z^2}{T^2}\left(1 - \frac{z^8}{T^8}\right)\left(1 - \frac{x^2}{L^2}\right)^4 \quad (2.40)$$

Table 2.3 presents the main dimensions of Wigley model I.

Figure 2.15 shows a comparison of the computed and the experimentally determined hydrodynamic coefficients of Wigley Model I sailing at $Fn = 0.30$. The computational and experimental data are generally in good agreement. Timman and Newman[46] derived the following symmetry relations for the coupling coefficients of slender fore-aft symmetrical vessels at forward speed: $A_{35} = -A_{53}$ and $B_{35} = -B_{53}$. These relations are adequately reproduced by the experimental data but not by the computational results. This is due to the use of uniform flow m-terms. Nakos[44] and van 't Veer[45] showed that the use of double body flow m-terms leads to a better preservation of these symmetry relations.

Figure 2.16 shows a comparison of the computed and the experimentally determined amplitude and phase of the wave exiting forces on Wigley Model I sailing at $Fn = 0.30$. The data are in good agreement.
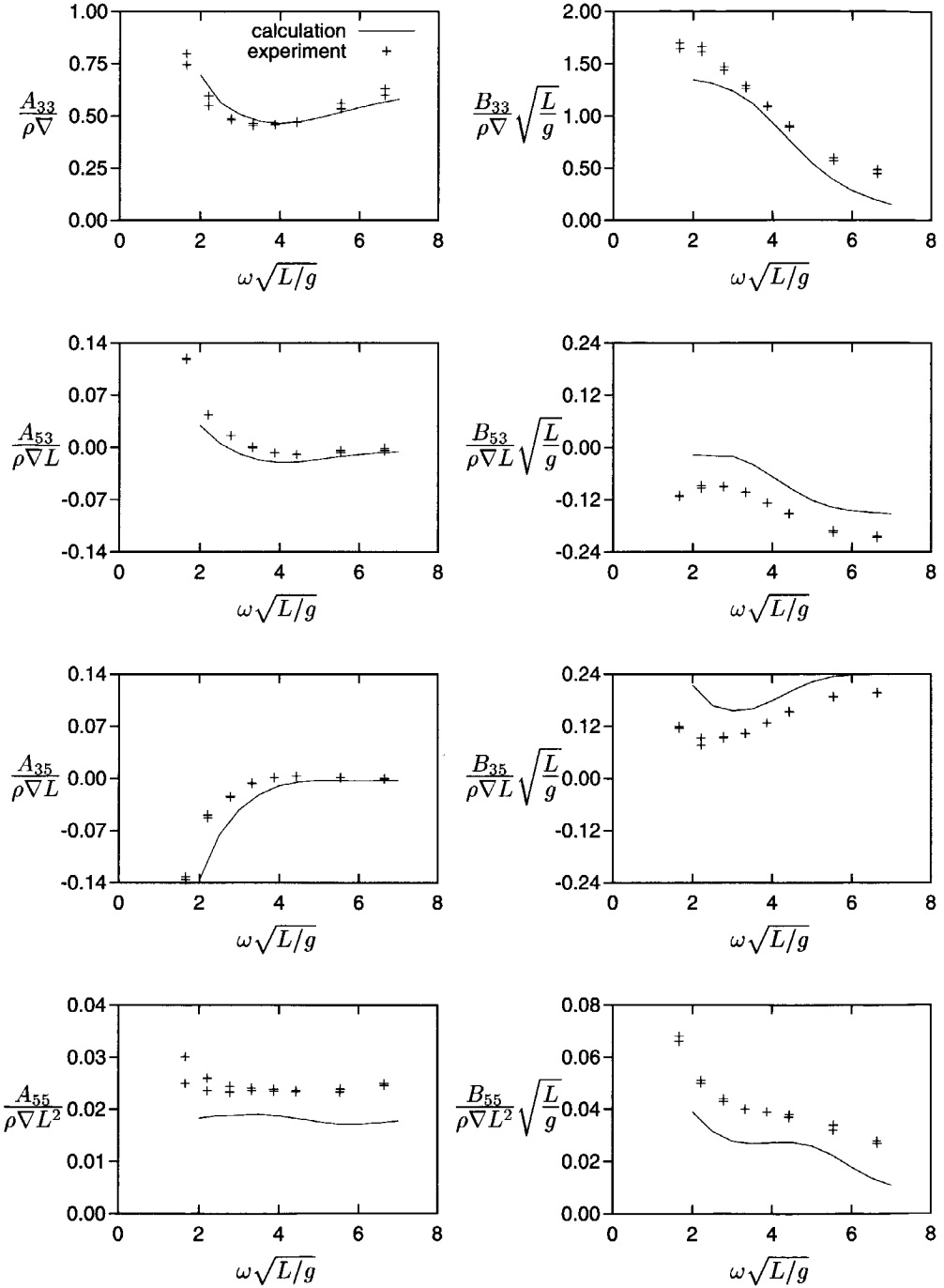
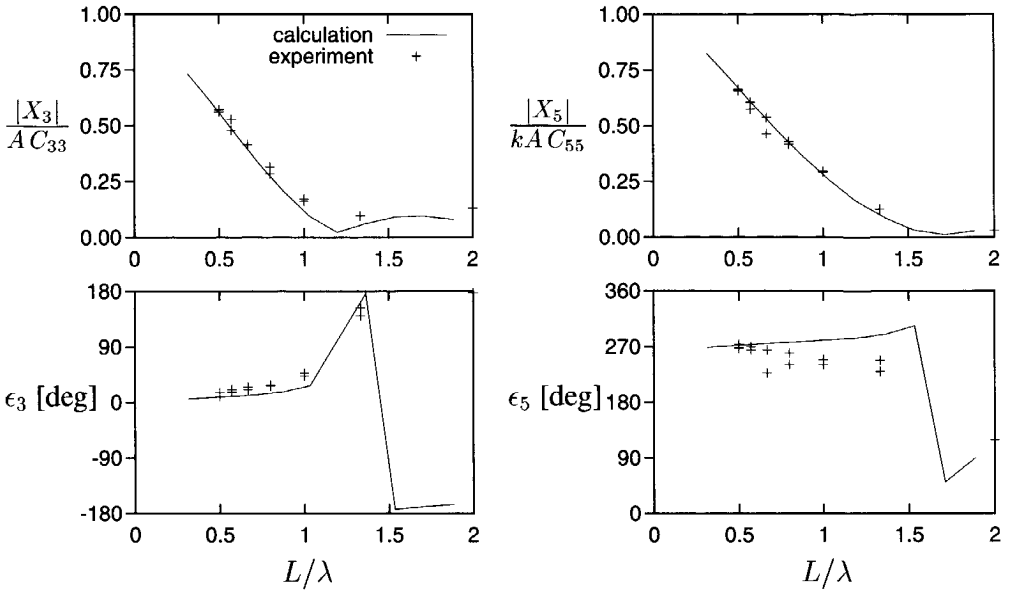Figure 2.15: Hydrodynamic coefficients of Wigley model I

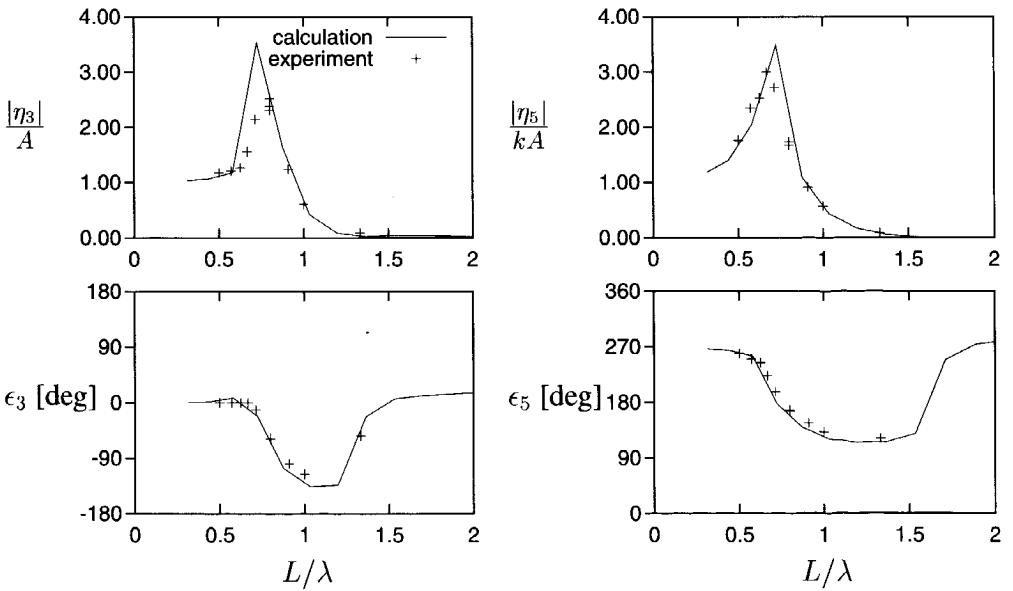Figure 2.16: Wave exiting forces on Wigley model I

Figure 2.17: Heave and pitch motions of Wigley model I

Figure 2.17 shows a comparison of the computed and experimentally determined amplitude and phase of the heave and pitch motions of Wigley Model I sailing at $Fn = 0.30$. The computed motions follow from the following equations of motion:

$$\sum_{k=3,5} \left([-\omega^2(M_{jk} + A_{jk}) + i\omega B_{jk} + C_{jk}]\hat{\eta}_k \right) = X_j \qquad j = 3, 5 \qquad (2.41)$$

where M_{jk} is the kth component of the jth row of the generalized mass matrix. The computational and experimental data are in reasonable agreement. The overestimation of the heave motions (and to a smaller extend also pitch motions) is caused by the somewhat poor prediction of the coupling coefficients. van 't Veer[45] showed that the use of double body flow m-terms leads to a better prediction of the coupling coefficients and the motions of a Wigley model. The present method is however intended for use in a method for the prediction of motions and added resistance of SESs. The forces acting on the hulls are relatively unimportant for the prediction of the motions because the largest part of the vessel's weight is carried by the air cushion. Therefore the present method is considered sufficiently accurate.

This chapter presented a three dimensional Rankine panel method. This method can compute the hydromechanic forces on the hulls of an SES, the wave volume in the air cushion of an SES and the mean wave height and wave slope at the bow and stern seal of an SES. The panel method is a frequency domain method. The results of the panel method will be used in the non-linear time simulation method that is presented by Chapter 3. Appendix A treats the transformation of the frequency domain results of the panel method to the time domain.

Chapter 3

Non-linear simulation method

This chapter presents a non-linear time simulation method for the motions and added resistance due to waves of Surface Effect Ships. The most important non-linear effects occur in the air cushion and seal dynamics. Especially the leakage of air from the cushion is a highly non-linear phenomenon. The motions and ambient waves are considered to be relatively small. Therefore linearized equations of motions and linearized hydrodynamics are used, while the non-linear form of the cushion and seal dynamics is retained.

The first section presents the equations of motion and a decomposition of all forces that act on the vessel. The second section treats the dynamics of the air cushion and the seals. It presents equations which govern the pressures in the air cushion and stern seal plena. Thereafter this section pays attention to the modeling of the fans and the modeling of the air air leakage flow. Subsequently it describes the models for the bag-type stern seal and the finger-type bow seal. The third briefly comments on the numerical time integration scheme. Section 3.4 treats the topic of added resistance due to waves. It presents an expression for the added resistance of the air cushion which was considered to be the most important contribution to the total added resistance. Section 3.5 presents results of the non-linear simulation method. The computational results are compared with experimental results of MARIN. Furthermore this section presents an investigation into the sensitivity of the simulation method to simplifications. Finally Section 3.5 presents preliminary conclusions concerning the validity of the method and a plan for further research.

3.1 Equations of motion

This section presents the equation of motion. Furthermore, it presents a decomposition of the forces that act on the vessel into force components due to gravitation, propulsion, hydromechanics, the air cushion and the seals.

The forces that act on the vessel are computed in a body-fixed coordinate system. Therefore the motions of the SES are also solved in the body-fixed coordinate system. In that case the motions follow from the Euler equations which can be derived from Newton's second law. The motions of the vessel are assumed to be small. Therefore the quadratic terms in the Euler equations can be neglected. This leads to the following system of equations of motion:

$$\sum_{k=1}^{6} M_{jk} \frac{d^2 \eta_k}{dt^2} = F_j \qquad j = 1, \dots, 6 \tag{3.1}$$

where M_{jk} is the kth element of the jth row of the generalized mass matrix, η_k is the displacement in k^{th} direction and F_j is the force (or moment) in j^{th} direction.

The total force which acts on the vessel in j^{th} direction can be decomposed into the following components:

$$F_j = F_j^{(g)} + F_j^{(p)} + F_j^{(h)} + F_j^{(a)} + F_j^{(s)} \tag{3.2}$$

where the affix denotes gravitational force (g), propulsive force (p), hydromechanic force (h), force due to the air cushion (a) or seal force (s).

The gravitational forces $F_j^{(g)}$ follow (up to linear order) from:

$$F_j^{(g)} = -gM\delta_{j3} - gM(y_g + z_g\eta_4)\delta_{j4} + gM(x_g + z_g\eta_5)\delta_{j5} \tag{3.3}$$

where M is the total mass of the vessel, g is the gravitational acceleration constant, x_g, y_g and z_g are the coordinates of the center of gravity, and δ_{jk} is the Kronecker delta.

The propulsive forces $F_j^{(p)}$ are equal to the thrust of the water jets. However, the propulsion and resistance characteristics of SESs are not within the scope of this thesis (except for the added resistance due to waves). Therefore we will assume that the propulsive force is balanced by the mean resistance of the vessel. Moreover, the surge motion (η_1) is up to now not included in the actual program. The effect of surge on the heave and pitch motions and the added resistance is generally considered to be small.

The hydromechanic forces $F_j^{(h)}$ are computed by means of a three-dimensional Rankine panel method which is presented in Chapter 2. Appendix A treats the transformation of the frequency domain results of the panel method to the time domain. The time domain expression for the hydromechanical force includes a convolution of an impulse response function (retardation function) with the motions and cushion pressure from the past.

The forces due to the air cushion follow from integration of the air cushion excess pressure over the deck and the dry part of the inner side of the hulls:

$$F_j^{(a)} = - \iint_{B_c} p_c n_j dS \tag{3.4}$$

where $(n_1, n_2, n_3)^T = \vec{n}$ and $(n_4, n_5, n_6)^T = \vec{x} \otimes \vec{n}$, where $\vec{n}$ is the normal vector to the hull or deck surface and $\vec{x}$ is the vector to the surface element dS. B_c is the part of the hulls and the deck that bounds the air cushion.

The forces that act on the seals follow from the the appropriate seal models. Section 3.2.4 describes the stern seal model, while the bow seal model is presented by Section 3.2.5.

3.2 Air cushion and seal dynamics

This section treats the dynamics of the air cushion and the seals. It presents equations which govern the pressures in the cushion and stern seal plena. Thereafter this section pays attention to the modeling of the fan system and air leakage flow. Subsequently it presents the models for the bag-type stern seal and the finger-type bow seal. The seals have an important effect on the pressures in the air cushion and stern seal plena.

3.2.1 Equations for the cushion and stern seal pressures

The equation which governs the excess pressures in a plenum follows from a combination of the conservation of mass equation for this plenum with the equation of state for the air inside this plenum. The pressure and density of the air in the plenum are assumed to be constant in space. Therefore conservation of mass can be written as:

$$\rho(Q^{(in)} - Q^{(out)}) = \frac{d}{dt}(\rho V) \tag{3.5}$$

where $Q^{(in)}$ is the air volume flux into the plenum, $Q^{(out)}$ is the air leakage volume flux from the plenum, ρ is the density of air and V is the volume of the plenum.

The process of compression of the air inside a plenum is assumed to be isentropic. In the frequency range of interest there is not sufficient time for the exchange of heat. Moreover the temperature differences are only small because of the relatively small pressure variations, so heat exchange will take much time. The isentropic gas law reads:

$$\frac{p + p_a}{\rho^\kappa} = constant \tag{3.6}$$

where p is the excess pressure in the plenum, p_a is the ambient pressure and κ, is the ratio of specific heats of air; $\kappa = c_p/c_v \approx 1.4$. The following expressions for ρ and $d\rho/dt$ can be derived from Equation 3.6:

$$\rho = \left(\frac{p + p_a}{\bar{p} + p_a}\right)^{\frac{1}{\kappa}} \cdot \bar{\rho} \tag{3.7}$$

$$\frac{d\rho}{dt} = \left(\frac{p + p_a}{\bar{p} + p_a}\right)^{\frac{1}{\kappa}} \cdot \frac{\bar{\rho}}{\kappa(p + p_a)} \cdot \frac{dp}{dt} \tag{3.8}$$

where $\bar{p}$ and $\bar{\rho}$ are the design excess pressure and the corresponding density.

Substitution of Equation 3.7 and Equation 3.8 into Equation 3.5 leads to the desired equation for the pressure in the plenum:

$$\frac{V}{\kappa(p + p_a)} \cdot \frac{dp}{dt} = Q^{(in)} - Q^{(out)} - \frac{dV}{dt} \tag{3.9}$$

The term $V/(\kappa(p + p_a))$ in the left hand side of Equation 3.9 governs the stiffness or compressibility of the air cushion. This equation can be linearized by replacing the stiffness term by $\bar{V}/(\kappa(\bar{p} + p_a))$, where $\bar{V}$ and $\bar{p}$ are the design volume of the plenum and design excess pressure in the plenum. In the present method the non-linear form of Equation 3.9 will be retained.

Figure 3.1 shows a sketch of the complete system of plena and the air-volume fluxes of an SES. One fan pumps air directly into the air cushion plenum ($Q_{c,f}^{(in)}$). The other fan pumps air into the stern seal plenum ($Q_s^{(in)}$). Air subsequently flows from the seal plenum to the cushion plenum ($Q_s^{(out)} = Q_{c,s}^{(in)}$). Furthermore air leaks from the cushion under the bow and stern seal ($Q_{c,b}^{(out)}$ and $Q_{c,s}^{(out)}$).

The equations for the pressures in the air cushion and stern seal plena read:

$$\frac{V_c}{\kappa(p_c + p_a)} \cdot \frac{dp_c}{dt} = Q_c^{(in)} - Q_c^{(out)} - \frac{dV_c}{dt} \tag{3.10}$$

$$\frac{V_s}{\kappa(p_s + p_a)} \cdot \frac{dp_s}{dt} = Q_s^{(in)} - Q_s^{(out)} - \frac{dV_s}{dt} \tag{3.11}$$
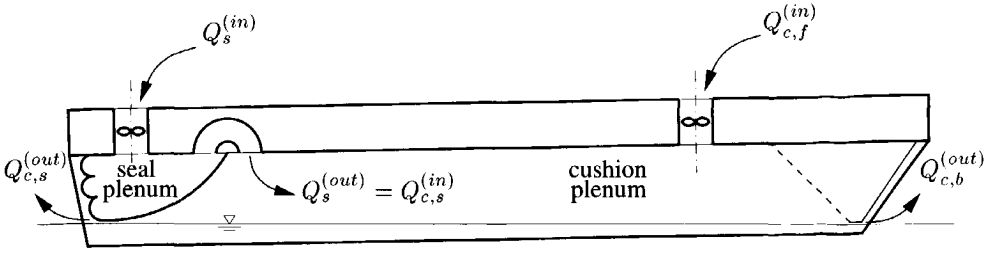
Figure 3.1: The system of plena and the air volume fluxes of an SES

where V_c and V_s are the volumes of the air cushion and stern seal plena, p_c and p_s are the excess pressures in the cushion and stern seal plena, $Q_c^{(in)}$ is the sum of $Q_{c,f}^{(in)}$ and $Q_{c,s}^{(in)}$, and $Q_c^{(out)}$ is the sum of $Q_{c,b}^{(out)}$ and $Q_{c,s}^{(out)}$. Section 3.2.2 presents an expression for the the air volume flux through a fan. Section 3.2.3 presents an expression for the air leakage flux from a plenum. The air cushion volume follows (up to linear order in $\eta_1, \ldots, \eta_6$) from:

$$V_c = \bar{V}_c - V_{sc} + V_{bc} - V_\zeta + \iint_{deck} (\eta_3 + y\eta_4 - x\eta_5)dS \qquad (3.12)$$

where $\bar{V}_c$ is the design cushion volume, V_{sc} is the part of the cushion volume that is taken up by the stern seal, V_{bc} is the extra cushion volume that is supplied by the bow seal, and V_ζ is the part of the cushion volume that is taken up by the free surface waves. V_ζ is often referred to as *wave pumping volume*. The stern seal volume V_s and the part of the cushion volume that is taken up by the stern seal V_{sc} follow from the stern seal model. Section 3.2.4 treats the stern seal model. The extra cushion volume that is supplied by the bow seal V_{bc} follows from the bow seal model, which is presented by Section 3.2.5. The wave pumping volume is computed by means of a three-dimensional Rankine source panel method which is presented in Chapter 2. Appendix A treats the transformation of the frequency domain results of the panel method to the time domain. The time domain expression for the wave pumping volume includes a convolution of an impulse response function (retardation function) with the motions and cushion pressure from the past.

3.2.2 The fan system

The air cushion and stern seal plena are pressurized by means of a system of fans. The volume flux through a fan into a plenum is approximated by the stationary fan

characteristic, which is linearized around the design operation point:

$$Q^{(in)} = Q_{\bar{p}} + \left(\frac{dQ}{dp}\right)_{\bar{p}} \cdot (p - \bar{p}) \qquad (3.13)$$

where $\bar{Q}$ is the the design flux through the fan.

In reality the fan will however not respond in a static way. Durkin and Luehr[18], Sullivan et al.[19], Masset et al.[17] and Witt[20] all show that fans respond in a dynamical way to oscillating pressure in the plenum. Sullivan et al.[19] determined the dynamical response of a model scale air cushion lift fan. They found that the response of the fan was quite linear (i.e. an increase in the pressure variations resulted in a proportional increase of the flow variations). At higher frequencies the response appeared to have a considerable phase lag. Sullivan et al.[19] also showed that the dynamic response of the fan has a large effect on the heave response of a hovering box. Section 3.5.3 presents an investigation into the importance of the fan system for the overall motions of an SES.

3.2.3   Air leakage

Air will leak from the cushion under the bow and stern seals. In rough conditions air will also leak under the hulls. Up to now the air leakage under the hulls is neglected. The air leakage flow has been studied elaborately by Ulstein[12]. He found that the following one-dimensional analysis yields good results compared to results obtained by means of a two-dimensional non-linear panel method.

The flow is assumed to be steady, inviscid and incompressible. The unsteady effects will be small because the outflow velocity is relatively high. The flow can be considered inviscid outside a thin boundary layer. Therefore the boundary layer thickness must be small compared to the leakage gap. The flow behaves like an incompressible flow when the Mach number is much smaller than 1. The outflow velocity is quite high ($Ma \approx 0.25$). Therefore compressibility effects might occur locally.

In the air cushion at some distance from the leakage gap the velocity of the air equals zero. The flow under the seal is assumed to separate at the lowest point of the seal. At this point the pressure is atmospheric. The outflow velocity follows from Bernoulli's equation:

$$u_e = \sqrt{\frac{2\Delta p}{\rho}} \qquad (3.14)$$

where Δp is the pressure jump across the leakage gap. This pressure jump is small compared to the atmospheric pressure p_a, so $\rho \approx \rho_a$. Under the bag-type stern seal no contraction of the air-jet will occur because of the smoothly rounded orifice (the radius of curvature of the seal canvas is much larger than the leakage gap height). If the outflow orifice has a sharp edge, for instance at a finger-type bow seal, the air-jet will contract. In the case of a sharp edge the height of the contracted air-jet is equals 0.61 times the leakage gap height. Now the air leakage flux follows from:

$$Q^{(out)} = c_l A_l \sqrt{\frac{2\Delta p}{\rho}} \tag{3.15}$$

where A_l is the leakage gap area and c_l is the orifice leakage coefficient which accounts for the contraction of the air-jet ($c_l = 1.0$ for a smoothly rounded orifice, while $c_l = 0.61$ for a sharp orifice).

3.2.4 The bag-type stern seal

This section presents the model for the bag-type stern seal. Bag-type seals are commonly used to close the air cushion plenum of SESs at the stern. The bag is made of thin flexible material. Internal webs restrain the aft side of the bag. The webs divide the bag into two or three lobes. The bag is open to the sides, where it is closed by the inner side of the hulls. Figure 3.2 shows a sketch of a three-lobe stern seal. The seal is pressurized by a fan at a slightly higher pressure than the air cushion. Air flows from the seal plenum to the cushion plenum. When the lowest point of the seal does not touch the water surface, air will leak from the cushion. This air leakage flow results in a dynamic pressure distribution under the seal.

This paragraph presents the underlying assumptions of the stern seal model. The stern seal model is a two-dimensional model (in a longitudinal plane). This implies that the wave height is assumed to be constant in transverse direction. This assumption is reasonable when head and following waves are considered, because the waves that are generated by the hulls and the air cushion are small compared to the incident waves. Therefore the mean wave height and wave slope across the cushion width are used.

Furthermore the wave curvature is neglected, but the wave slope is taken into account. The negligence of the wave curvature is reasonable as long as the wave length is not too short. Furthermore, the wave surface is assumed to be rigid. This assumption is valid because of the high speed of SESs. The Froude number based on a characteristic length like the radius of the lower lobe of the seal (R_1 in Figure B.3) is of the order of 10!
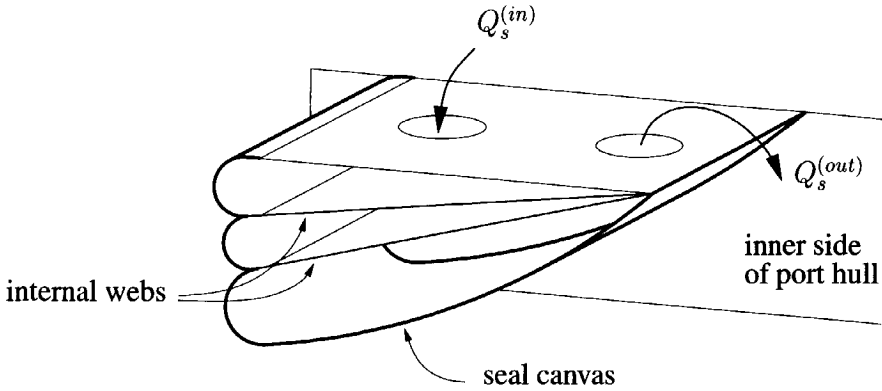
Figure 3.2: Three-lobe bag stern seal

The gravitational and inertial forces that act on the seal canvas are small when compared to the forces due to the excess pressure in the seal. Therefore the inertial and gravitational forces can be neglected. Ulstein[12] showed that the inertial forces are only important in the very high frequency range. Furthermore the seal canvas is assumed to have no bending stiffness; it only transmits tension .

The air leakage flow under the seal is assumed to be stationary, inviscid and incompressible. Ulstein[12] showed that a one-dimensional approach leads to good results. Section 3.2.3 presents a brief discussion of these assumptions. Now the problem of computing the stern seal bag geometry does not depend on time any more. The only time dependency of the seal geometry is through the seal and cushion excess pressures.

Appendix B deals with the actual computation of the stern seal bag geometry. First this appendix presents a simple expression for the pressure distribution under the seal. Thereafter it presents a method to compute the geometry of the cushion-facing part of the seal. Then a non-linear system of equations for the parameters that define the bag geometry is derived from force equilibrium and geometrical considerations. This system of equations is solved by means of Newton-Raphson's method. For a given seal configuration the geometry depends on the following input parameters: the heave displacement (η_3), the pitch displacement (η_5), the cushion excess pressure (p_c), the seal excess pressure (p_s), the mean wave height at the seal (ζ) and the mean wave slope at the seal (ζ_x). When the bag geometry is known, it is easy to calculate the seal volume (V_s), the part of the cushion volume that is taken up by the seal (V_{sc}), the seal forces ($F_j^{(s)}$) and the area of the leakage gap (A_l). The details are sown in Appendix B. Figure 3.3 shows some examples of computed bag geometries. The seal may either touch the water surface or leave a leakage gap. In

the bottom case the cushion pressure is larger than the seal pressure, which results in a concave cushion-facing part of the seal.

The time derivatives of V_s and V_{sc} occur in the equations for the cushion and seal pressure (Equation 3.10 and Equation 3.11). Direct evaluation of dV_s/dt and dV_{sc}/dt is difficult. Lee[15] applies a finite difference scheme using previous time steps. He needs however a filtering technique to prevent amplification of the truncation error. Therefore the present seal model uses the following expression:

$$\frac{dV}{dt} = \frac{\partial V}{\partial \eta_3}\dot{\eta}_3 + \frac{\partial V}{\partial \eta_5}\dot{\eta}_5 + \frac{\partial V}{\partial p_c}\dot{p}_c + \frac{\partial V}{\partial p_s}\dot{p}_s + \frac{\partial V}{\partial \zeta}\dot{\zeta} + \frac{\partial V}{\partial \zeta_x}\dot{\zeta}_x \qquad (3.16)$$

where V is either V_{sc} or V_s, and the dot above a parameter denotes differentiation with respect to time. The partial derivatives of V_{sc} and V_s follow from finite differences of solutions for slightly different inputs. The mean wave height and wave slope at the stern seal (ζ and ζ_x) and their derivatives with respect to time follow from the three-dimensional panel method which is presented by Chapter 2.

Unfortunately the stern seal model is not as robust as one might wish. Sometimes, when the relative motions at the stern seal become very large, the iterative solution procedure does not converge. In that case the stern seal is linearized around the last solution that was found until a new solution is obtained. This linearization implies that the partial derivatives of V_{sc} and V_s of the last solution are used, and that the seal forces and the leakage gap height follow from expressions similar to Equation 3.16. In extreme cases the iterative solution algorithm might find a spurious solution. This usually results in diverging simulation that leads to a run-time error.

3.2.5 The finger-type bow seal

This section presents the model for the finger-type bow seal. Most SESs have a finger type bow-seal. The seal consists of a row of vertical loops of thin flexible material. Each loop represents a *finger*. The loops are open to the cushion side. Figure 3.4 shows an example of a six-finger bow seal.

The modeling of the finger-type bow seal is much more simple than the modeling of the bag-type stern seal. When the local relative deck height at the bow is smaller than the height of the seal, the lower part of the fingers is simply bent backwards at the water surface, and no air will escape under the seal. When the local relative deck height is larger than the height of the seal, the seal will leave a gap above the
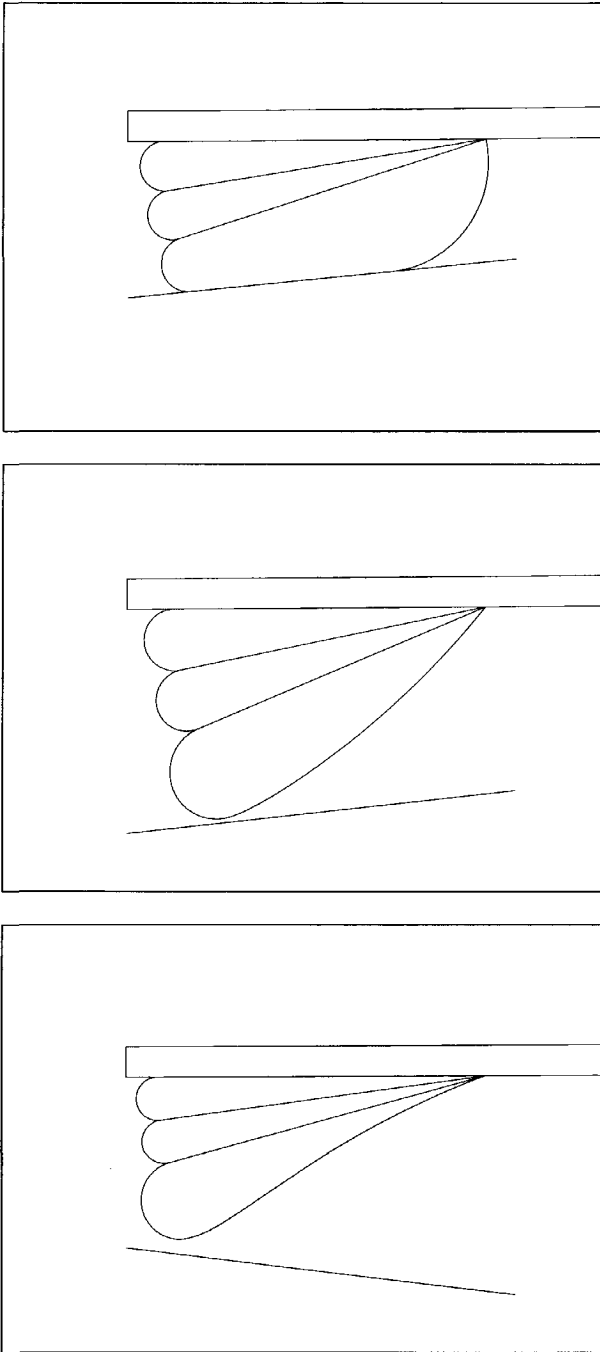
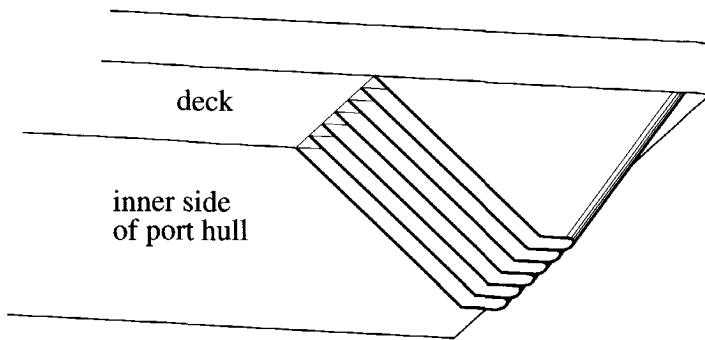Figure 3.3: Examples of computed bag geometries

Figure 3.4: Finger-type bow seal

water surface, and air will escape from the cushion plenum.

The bow seal model is also two-dimensional (in a longitudinal plane). Again the mean wave height and wave slope at the seal are used. The horizontal row of fingers is represented by a flat boundary which roughly coincides with the foremost part of the fingers which actually closes the cushion plenum. The boundary may either leave an air gap or touch the water surface. The part of the seal that is bent away by the water surface is neglected. This implies that the frictional forces that act on the bow seal are neglected. The pressure distribution due to air leakage under the seal is neglected. In the case of a finger seal this pressure distribution has no effect on the height of the gap under the seal. The pressure distribution does only have a small effect on the forces that act on the seal, which is neglected.

The computation of the bow seal geometry basically implies computing the intersection point of the seal boundary and the water surface, if this point exists. Otherwise it implies computing the leakage gap height under the seal. The bow seal geometry depends on the heave displacement (η_3), the pitch displacement (η_5), the mean wave height at the seal (ζ) and the mean wave slope at the seal (ζ_x). The mean wave slope still has a small effect because the point where the mean wave height is computed does generally not coincide exactly with the position of the bow seal. When the bow seal geometry is known, the seal forces follow from integration of the (spatially constant) cushion excess pressure over the plate and the part of the deck that is not included in B_c (Equation 3.4). The extra cushion volume that is supplied by the bow seal (V_{bc}) can also be calculated. The time derivative of V_{bc}

follows (analogous to V_s and V_{sc} in Section 3.2.4) from:

$$\frac{dV_{bc}}{dt} = \frac{\partial V_{bc}}{\partial \eta_3}\dot{\eta}_3 + \frac{\partial V_{bc}}{\partial \eta_5}\dot{\eta}_5 + \frac{\partial V_{bc}}{\partial \zeta}\dot{\zeta} + \frac{\partial V_{bc}}{\partial \zeta_x}\dot{\zeta}_x \qquad (3.17)$$

where the partial derivatives of V_{bc} again follow from finite differences of solutions for slightly different inputs. The mean wave height and wave slope at the bow seal (ζ and ζ_x) and their derivatives with respect to time follow from the three-dimensional panel method which is presented by Chapter 2.

3.3 Numerical time integration

We have now arrived at a system of eight coupled equations (six equations of motion, the equation for the cushion pressure and the equation for the stern seal pressure) for eight unknowns ($\eta_1, \ldots, \eta_6, p_c, p_s$). The actual computer program only includes heave and pitch displacement, and is therefore only suitable for head and following waves. It can be extended to six degrees of freedom. This system of equations is solved in time by means of a Runge-Kutta scheme. The time step must be smaller than about one quarter of the Helmholtz resonant period of the air cushion in order to achieve stable numerical integration. Usually a smaller time step is used. A quick estimate of the Helmholtz resonant frequency follows from:

$$\omega^H = \sqrt{\frac{\kappa g}{h}\left(1 + \frac{p_a}{p_c}\right)} \qquad (3.18)$$

where h is the height in the air cushion. This formula was taken from a paper by Nakos et al.[9]. Helmholtz resonance occurs when the inertia of the SES is balanced by the compressibility of the air cushion.

3.4 Added resistance due to waves

This section goes into the added resistance due to waves. Surface Effect Ships appear to have a large speed loss when sailing in a seaway. The major cause for this speed loss is the increase of the resistance of the vessel due to the ambient waves. First this section presents a qualitative discussion of the added resistance of SESs. Subsequently this section presents an expression for the added resistance of the air cushion, which was expected to be the largest contribution to the total added resistance.

3.4.1 Qualitative discussion of the added resistance of SESs

This section presents a qualitative discussion of the added resistance of Surface Effect Ships. The added resistance of an SES can be split up into two contributions:

- the added resistance of the hulls,

- the added resistance of the air cushion.

There are three mechanisms which cause the added resistance of an SES:

- radiation of waves

- sinkage

- momentum of escaping air

The first mechanism also causes the added resistance that is experienced by conventional ships. It is associated with the momentum of the waves which are radiated by the vessel (far field approach). These waves are caused by diffraction of the incident waves by the hulls, and by the motions and air cushion pressure variations of the SES. This mechanism is relevant for both the added resistance of the hulls and the added resistance of the air cushion.

The second mechanism is only found with Surface Effect Ships. When an SES sails in a seaway the amount of air leakage under the seals increases, which results in a decrease of the cushion pressure. This causes the SES to sink deeper into the water as a larger part of the vessel's weight must be carried by the buoyancy of the hulls. The sinkage of the vessel leads to an increase of the (calm water) wave making resistance of the hulls, a decrease of the (calm water) wave making resistance of the air cushion, and also an increase of the viscous resistance of the hulls.

The third mechanism only contributes to the added resistance of the air cushion. The velocity of the leaking air under the seals is quite high. The corresponding outflow of momentum must be compensated by a force that acts on the vessel. Air leakage under the bow seal results in a resistance while air leakage under the stern seal leads to a propulsive force (negative resistance). Furthermore the air which is pumped into the air cushion by the fans must be accelerated up to the vessel's speed. Any changes in one of these air flows result in a change of the resistance. When the air flow changes are caused by the ambient waves, the corresponding resistance change should be included in the added resistance due to waves.

When this research project was started the major part of the large added resistance of SES was believed to be caused by the air cushion. The added resistance of the hulls was assumed to be small because of several reasons. The hulls are extremely slender, and therefore will not radiate much waves. Furthermore only a small part of the vessel's weight is carried by the hulls. The added resistance due to sinkage should mainly act on the hulls. Kapsenberg[25] found however from an experiment that the added resistance due to sinkage was only small. He carried out one test run with an increased fan RPM. The cushion excess pressure was raised from 0.79 times the calm water excess pressure to 0.99 times the calm water excess pressure. This only resulted in a six percent drop of the added resistance. When the added resistance of the hulls is small, the major part of the large added resistance of SESs must be caused by the air cushion.

In view of the considerations that were presented by the previous paragraph we choose to focus on the added resistance of the air cushion and to neglect the added resistance of the hulls for the time being. The next section presents a computational method for the added resistance of the air cushion.

3.4.2   The added resistance of the air cushion

This section presents a computational method for the added resistance of the air cushion of a Surface Effect Ship. The expression follows from a near field approach as far as hydromechanics are concerned. On the other hand the resistance of the air cushion does *not* follow from direct pressure integration over the part of the vessel that bounds the air air cushion. We choose to calculate the resistance of the air cushion from the rate of change of the linear momentum of the air inside the air cushion. This has the advantage that the added resistance due to the momentum of escaping air can easily be accounted for.

Figure 3.5 shows the air cushion and the control surface S (dotted line) that bounds the air cushion. It also presents a detailed view of the air leakage flow under the bow seal. The leakage flow under the stern seal is very similar although no contraction of the air jet occurs because of the smoothly rounded orifice. Furthermore the figure indicates the air flows into and out of the air cushion, as well as the wave heights and wave slopes at the bow and stern seals.

The (full) resistance of the air cushion is calculated from the rate of change of the linear momentum of the air inside the air cushion. The total longitudinal force that acts on the air cushion must equal the rate of change of the linear momentum inside
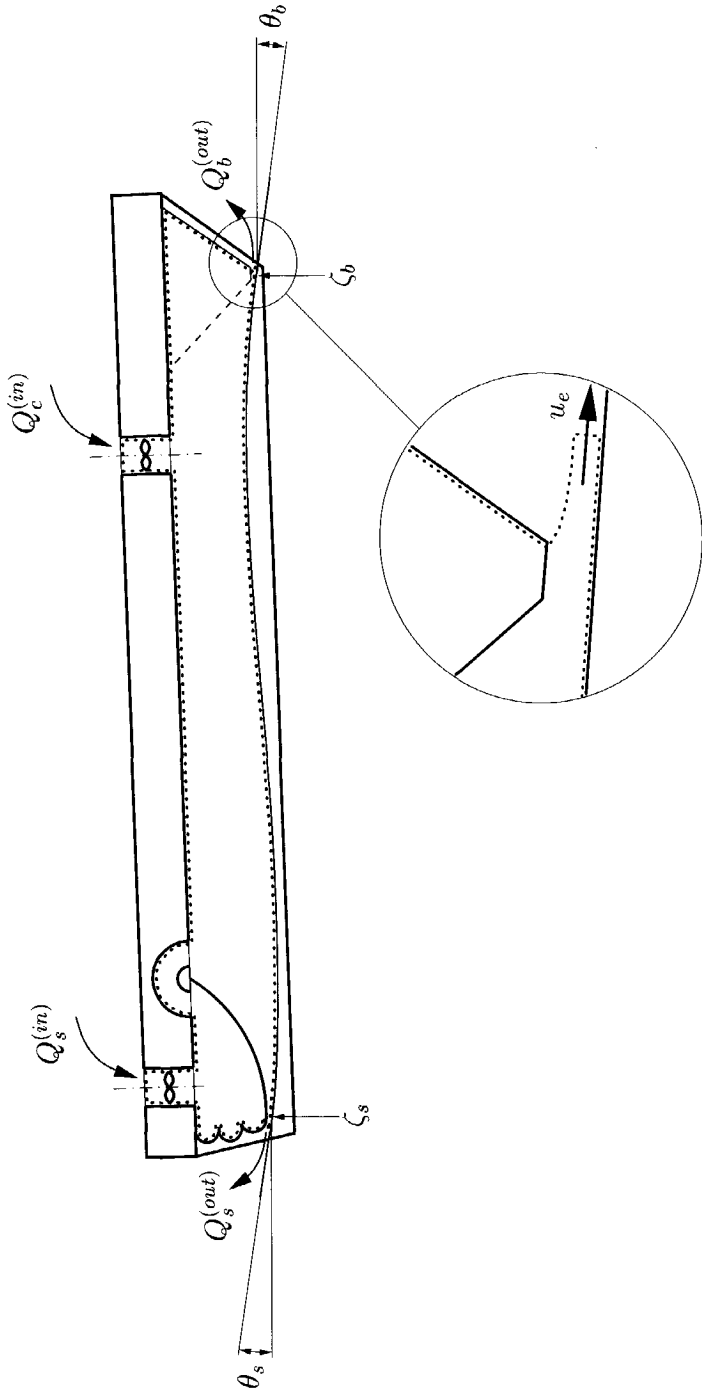
Figure 3.5: The control volume around the air cushion

the air cushion:

$$F_1^{(ac)} = \frac{d}{dt} M_1^{(ac)} \tag{3.19}$$

It should be noted that the longitudinal direction is the x-direction in a directionally fixed coordinate system.

The total longitudinal force that acts on the air cushion follows from pressure integration over the control surface S:

$$
\begin{aligned}
F_1^{(ac)} &= \iint_S p n_1 dS \\
&= \iint_{S_v} p n_1 dS + \iint_{S_w} p n_1 dS
\end{aligned}
\tag{3.20}
$$

where p is the (local) excess pressure, S_v is the part of S that is adjacent to the vessel (i.e. the parts of the deck, hulls and seals that bound the air cushion), S_w is the part of S that is adjacent to the wave surface, and n_1 is the instantaneous x-component (w.r.t. the directionally fixed coordinate system) of the normal vector to S which points into the air cushion. The integration over the part of S which bounds the escape air jets vanishes because the local pressure equals the ambient pressure. The integral over S_v is just the resistance of the air cushion which must be calculated. The integral over S_w can be approximated by $(\zeta_b - \zeta_s) \cdot B_c \cdot p_c$, where ζ_b is the mean wave height at the bow seal, ζ_s is the mean wave height at the stern seal, B_c is the air cushion width and p_c is the (spatially constant) cushion excess pressure. Therefore

$$F_1^{(ac)} = -R^{(ac)} + (\zeta_b - \zeta_s) \cdot B_c \cdot p_c \tag{3.21}$$

In this approximation a small error is made in the integration of the pressure in the vicinity of the seals. In the vicinity of the seals the pressure is not equal to the spatially constant cushion pressure (p_c). In this area the excess pressure drops from p_c to zero. This effect is however very local, and when the wave steepness at the seals is relatively small it is negligible.

The rate of change of the linear momentum of the air inside the air cushion follows from the integration of the inflow of momentum over the control surface. It can be expressed in terms of the air volume fluxes into and out of the air cushion:

$$\frac{d}{dt} M_1^{(ac)} = \iint_S \rho \cdot \vec{u} \cdot \vec{n} \cdot u_1 \, dS =$$

$$= \rho \cdot Q_c^{(in)} \cdot (-U) \; +$$

$$\rho \cdot Q_s^{(in)} \cdot (-U) \; +$$

$$\rho \cdot (-Q_b^{(out)}) \cdot u_e \cdot \cos \theta_b \; +$$

$$\rho \cdot (-Q_s^{(out)}) \cdot (-u_e) \cdot \cos \theta_s \qquad\qquad (3.22)$$

where $\vec{u}$ is the air velocity, u_1 is the x-component of $\vec{u}$. Further U is the forward speed of the SES and u_e is the air escape velocity. Please see Figure 3.5 for the definition of the air volume flows $Q_c^{(in)}$, $Q_s^{(in)}$, $Q_b^{(out)}$ and $Q_s^{(out)}$, and the wave slope angles θ_b and θ_s. Section 3.2 presents expressions for these air volume flows and the air escape velocity.

The required equation for the resistance of the air cushion follows when Equation 3.21 and Equation 3.22 are substituted into Equation 3.19:

$$R^{(ac)} = (\zeta_b - \zeta_s) \cdot B_c \cdot p_c \; +$$

$$\rho \cdot Q_c^{(in)} \cdot U \; +$$

$$\rho \cdot Q_s^{(in)} \cdot U \; +$$

$$\rho \cdot Q_b^{(out)} \cdot u_e \cdot \cos \theta_b \; -$$

$$\rho \cdot Q_s^{(out)} \cdot u_e \cdot \cos \theta_s \qquad\qquad (3.23)$$

Subsequently the *added* resistance of the the air cushion follows from:

$$R_{aw}^{(ac)} = \overline{R^{(ac)}(\text{in waves})} \; - \; R^{(ac)}(\text{in calm waters}) \qquad (3.24)$$

where the overlining denotes that the time averaged value of $R^{(ac)}(\text{in waves})$ should be used.

This section presented a computational method for what is expected to be the most important contribution to the added resistance of Surface Effect Ships. This method is implemented in the time simulation method for the motions that was presented by the previous sections. The next section presents results of the simulation method.

Table 3.1: Main particulars of the HYDROSES target vessel

symbol	description	unit	value
L_{oa}	length over all	m	160.60
L_{pp}	length at the perpendiculars	m	153.00
L_c	length of the air cushion	m	144.00
B	beam	m	35.00
B_{cf}	beam of the air cushion (fore)	m	26.25
B_{ca}	beam of the air cushion (aft)	m	25.25
T_0 (off)	off-cushion draft at Station 0	m	4.41
T_{20} (off)	off-cushion draft at Station 20	m	5.85
T_0 (on)	on-cushion draft at Station 0	m	2.76
T_{20} (on)	on-cushion draft at Station 20	m	0.99
p_c	air cushion excess pressure	kPa	11.04
p_s	stern seal excess pressure	kPa	11.17
Δ	mass	t	5050.0
X_G	length c.o.g. forward of Station 10	m	-2.37
k_{yy}	pitch radius of gyration	m	49.74

3.5   Results of the simulation method

This section presents results of the non-linear simulation method. First it presents some time signals as they directly follow from the simulation method. Thereafter it presents a comparison of harmonically analyzed results of the simulation method to experimental results of MARIN. Subsequently this section presents an investigation into the sensitivity of the simulation method to simplifications. Finally the section presents preliminary conclusions concerning the validity of the method and a motivation for further research.

All results that are presented by this section concern the target vessel of the HYDRO-SES project. The HYDROSES project was an extensive collective research project on seakeeping of Surface Effect Ships (see for instance Kapsenberg and Blume[5]). The HYDROSES target vessel was designed as a large car/passenger ferry by FIN-CANTIERI in Italy. It served as a study object in the HYDROSES project. Table 3.1 presents the main particulars of the HYDROSES target vessel. The air cushion lift to weight ratio of the vessel is about 0.85. The results are presented on full scale. The air cushion of the model that was used in the MARIN experiments was equipped with a diaphragm in order to obtain a correctly scaled stiffness of the air

cushion. Chapter 4 presents a discussion of the scaling of air cushion dynamics and the diaphragm technique. All results concern simulations and experiments in regular sinusoidal head waves at a forward speed of 45 knots ($Fn = 0.61$). For the computations with the panel method the draft was taken according to the on-cushion drafts as presented by Table 3.1. This position of the vessel corresponds to $\eta_3 = 0.0$ and $\eta_5 = 0.0$.

3.5.1 Time signals

Figure 3.6 shows the time signals of a non-linear simulation in regular waves. It presents time traces of the following quantities: the incident wave height at the center of gravity (ζ), the heave displacement (η_3), the pitch displacement (η_5), the air cushion and stern seal excess pressures (p_c and p_s), the leakage areas under the bow and stern seal ($A_{e,b}$ and $A_{e,s}$), and the vertical acceleration at Station 0 ($\ddot{z}_0$), Station 10 ($\ddot{z}_{10}$) and Station 20 ($\ddot{z}_{20}$). The figure shows the results of a simulation in regular head waves. The wave frequency was 2.2 [rad/s] which corresponds to a wave length of 102 [m]. The wave steepness was relatively large ($kA = 0.10$, i.e. a wave amplitude of 1.63 [m]). Time signals are however not very practical for presentation and comparison of the results. Therefore the next section presents results which were analyzed harmonically. The time signals are an illustration of the (non-linear) process.

The heave and pitch time signals do not show significant higher harmonic components. There is however a significant shift of the mean values of the heave and pitch displacements. The heave and pitch displacements in calm water are 0.26 [m] and -0.192 [deg] respectively. This is caused by an increased amount of air leakage, which results in a drop of the mean cushion pressure, and consequently in a change of the sinkage and trim of the vessel.

In the air cushion and stern seal excess pressure signals higher harmonic components are clearly present. Please note that the shape of the vertical acceleration at Station 10 signal and the cushion pressure signal are very much alike. This is due to the fact that the air cushion is responsible for the major contribution to the heave force.

The most obvious non-linear effects occur in the leakage areas under the seals. The waves, motions and pressure variation cause a sudden opening and closure of the air leakage gaps. This highly non-linear effect cannot be captured by some kind of linearization.

Figure 3.7 shows subsequent solutions of the stern seal geometry. It presents the
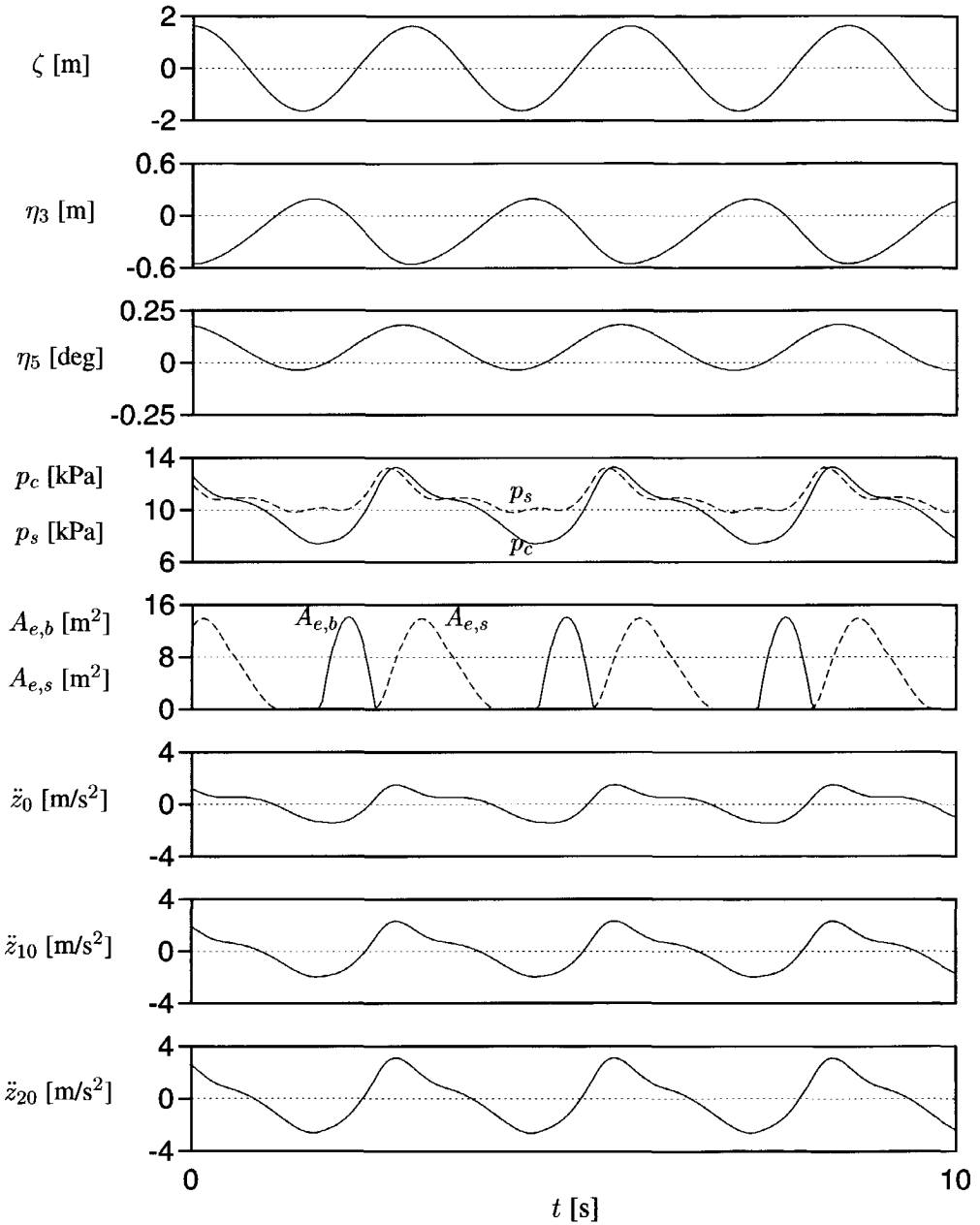
Figure 3.6: Time traces of a non-linear simulation; $\omega_e = 2.2$ [rad/s], $kA = 0.10$
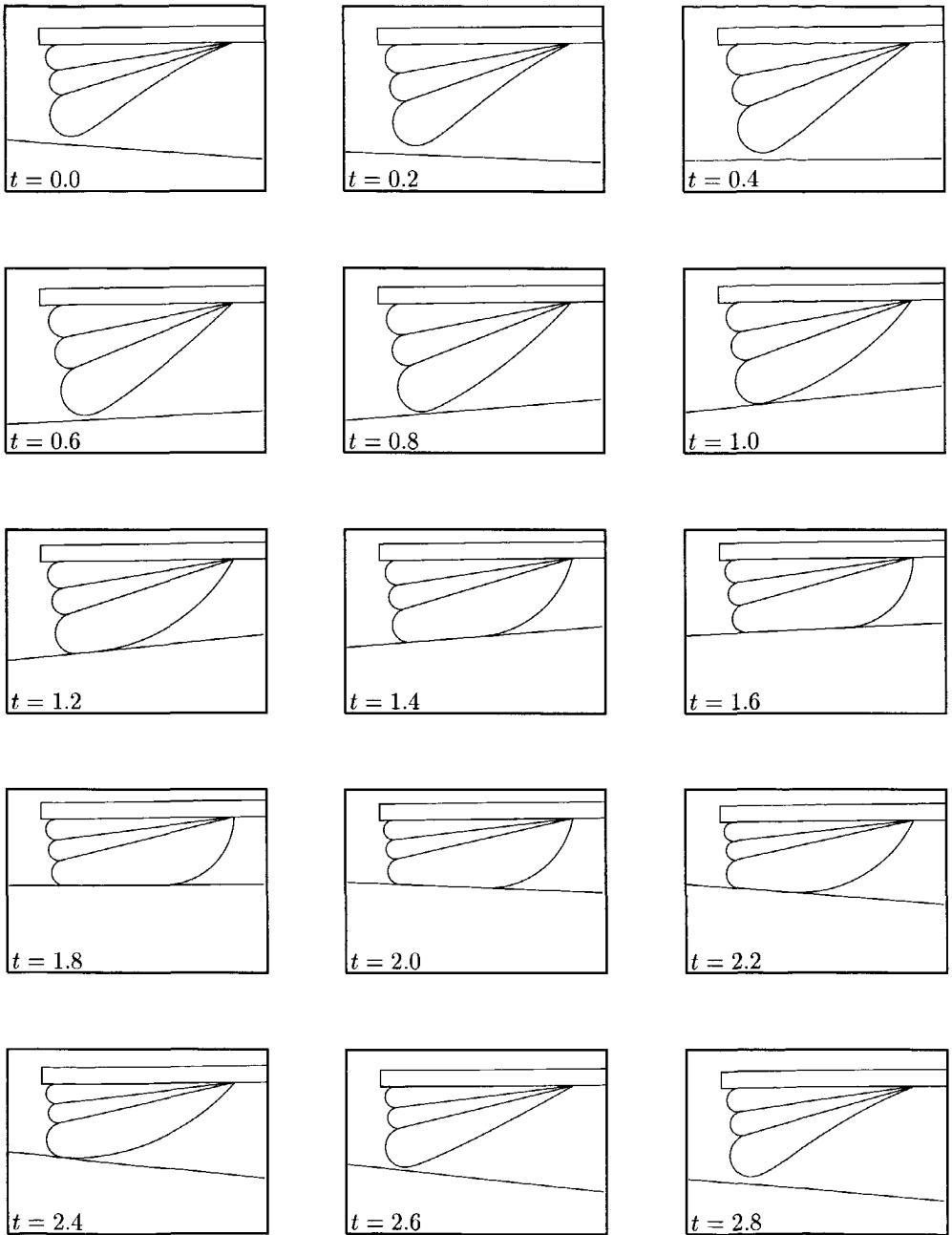
Figure 3.7: Subsequent stern seal solutions; $\omega_e = 2.2$ [rad/s], $kA = 0.10$

seal geometry at every fourth time step (the time step was 0.05 s). Each time step requires four seal geometry computations; one for each predictor in the Runge-Kutta time integration. Figure 3.7 follows from the same simulation as Figure 3.6. At $t = 0.0$ the seal pressure is smaller than the cushion pressure which results in a concave cushion facing part of the seal and a large air leakage gap. At $t = 1.8$ the seal pressure is much larger than the cushion pressure. This results in a stern seal geometry that touches the water surface over a considerable length. The height of the leakage gap under the stern seal depends for a large extent on the ratio of the seal and cushion excess pressures.

3.5.2   Comparison to experimental data of MARIN

This section presents a comparison of results of the non-linear simulation method with results of experiments that were carried out by Kapsenberg et al.[1] at MARIN. The results of the simulations and of the experiments were processed by means of harmonic analysis.

Figure 3.8 shows the heave response of the HYDROSES target vessel to regular head waves. The figure presents the mean heave displacement, the amplitude of the heave motion divided by the amplitude of the incident waves (Response Amplitude Operator, RAO) and the phase of the heave motion with respect to the incident waves at the origin which is located at the center of gravity. The results are presented as a function of the air cushion length divided by the wave length (L/λ). Results for several levels of wave steepness (kA) are shown. The computations and the experiments are in good agreement. When L is a multiple of the wave length, the incident waves do not change the air cushion volume. This causes the RAO to be small at $L/\lambda = 1, 2, \ldots$. The effect of the wave height on the RAO is not very large. The waves cause however a significant decrease of the mean heave displacement. This sinkage is caused by the increased air leakage which result in a drop of the mean cushion pressure which must be compensated by a larger buoyancy of the hulls.

Figure 3.9 shows the pitch response of the HYDROSES target vessel. The figure again presents the mean pitch displacement, the pitch RAO and the phase of the pitch motions. In the very low frequency range where the pitch resonance occurs, the computed pitch motions are larger than the pitch motions found in the experiments. The correlation of the computational end experimental phase relation is also not fully satisfactory. In the low frequency range this is probably caused by difference in resonant behavior. In the higher frequency range one can question the
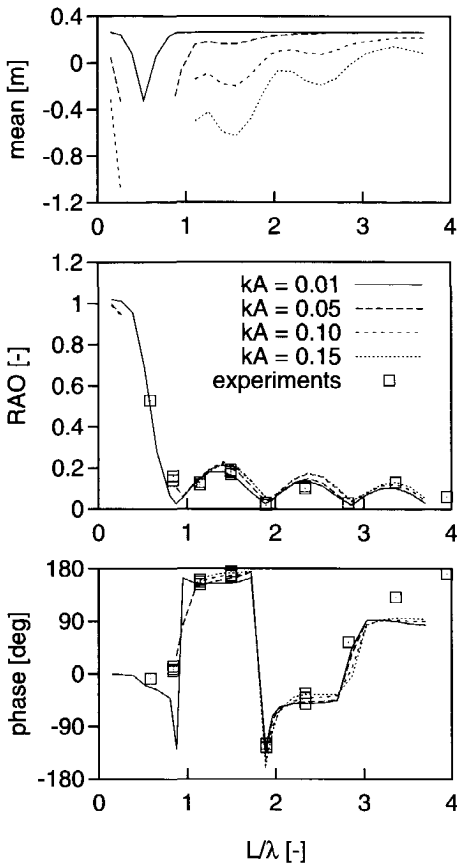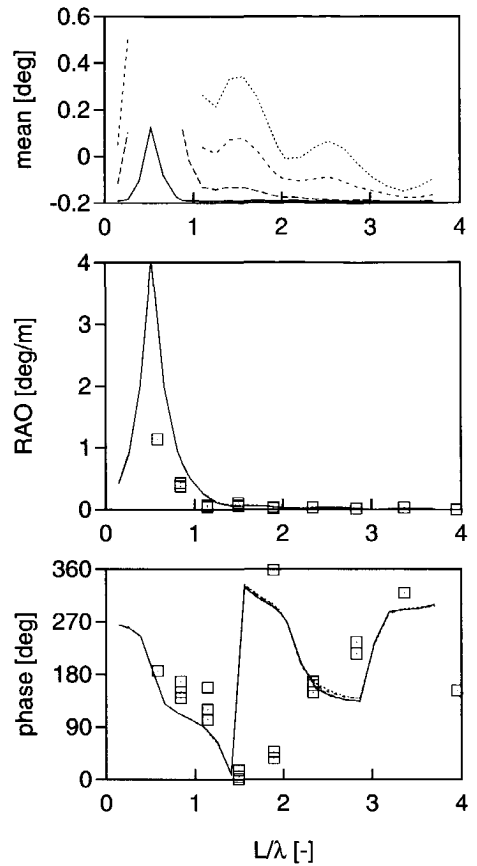
Figure 3.8: Heave response

Figure 3.9: Pitch response

relevance of the phase of an almost zero amplitude motion. Close to the pitch resonance the iterative stern seal geometry solver does not converge. This is caused by the large relative motions at the stern seal which lead to extreme stern seal geometries, or even to the non-existence of a relevant stern seal geometry (for instance when the deck touches the water surface). Therefore this section does not present results for higher waves around the pitch resonance.

Figure 3.10 shows the response of the air cushion excess pressure. The correlation of computations and experiments is generally good for the cushion pressure. The deviation in the low frequency range is probably caused by the overestimation of the pitch motions by the computational method. The large pitch motions result in the opening of large air leakage gaps which excites the cushion pressure. The deviation
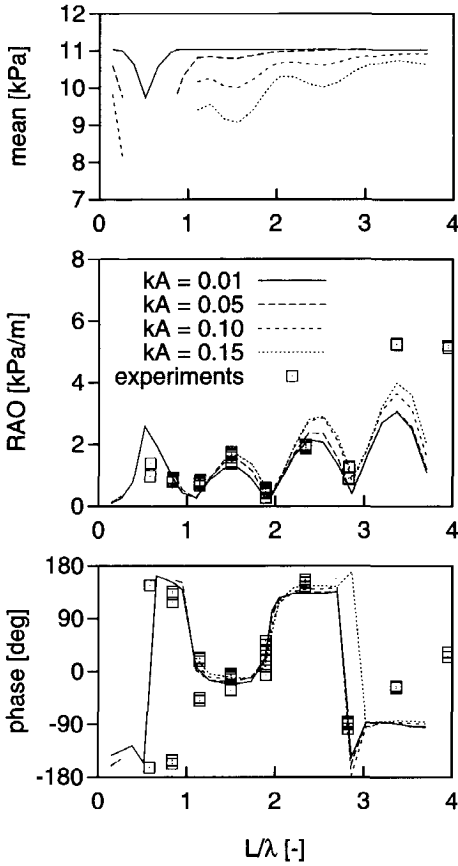
Figure 3.10: Air cushion excess pressure response
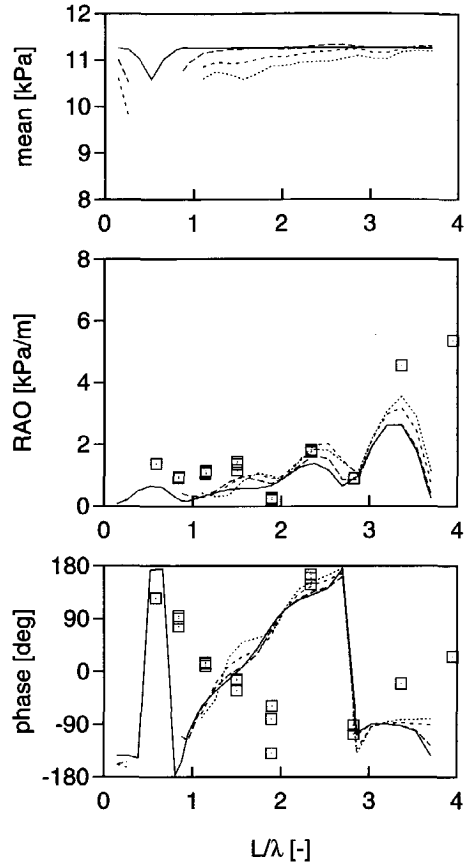
Figure 3.11: Stern seal excess pressure response

in the high frequency range is due to an underestimation of the Helmholtz resonance of the air cushion. The prediction of the amplitude response at the Helmholtz resonance is difficult as it highly depends on the damping due to the fans. The next section presents an investigation into the importance of the fans and several other aspects.

Figure 3.11 shows the response of the stern seal excess pressure. The correlation of the computations and the experiments is rather poor. From a comparison of the cushion pressure response with the seal pressure response it can be concluded that during the experiments the stern seal pressure followed the cushion pressure to a large extent, while in the computations the seal pressure is much more independent.

There are several explanations for this discrepancy. First the overestimation of the pitch motions has of course an important effect on the dynamics of the stern seal. Furthermore there are some important differences in the air supply system of the stern seal. In the computations the air supply system was according to Figure 3.1. In the experiments the aft fan pumped air into an air distribution box which distributed the air over the stern seal and cushion plena. The air flowed subsequently via separate ducts from the stern seal plenum to the cushion plenum. In the computations all air flowed from the aft fan through the stern seal plenum into the cushion plenum. In the experiments only a part of the air from the aft fan flowed via the seal plenum to the cushion plenum. In addition to this the stern seal plenum was not equipped with a diaphragm during the experiments. This results in a much too large stiffness of this plenum. The computations were carried out at full scale.

Figure 3.12 and Figure 3.13 show the added resistance due to waves. Figure 3.13 presents the same computational data as Figure 3.12 without the experimental results in order to show the behavior of the computational results. The computed added resistance only includes the added resistance due to the air cushion (see Section 3.4). There seems to be no correlation at all between the experimental and computational data. From these results it can be concluded that the air cushion does not give a significant contribution to the added resistance of Surface Effect Ships, which is completely contrary to the line of reasoning that was presented by Section 3.4. Figure 3.14 and Figure 3.15 present the added resistance divided by the wave amplitude squared. Both experimental and computational result show that the quadratic relation of the added resistance with wave height does not hold for an SES.

The important discrepancy between the computed added resistance of the air cushion and the measured (complete) added resistance requires further research. The next chapter presents an extensive series of model experiments. The main goal of these experiments is to find the origin of the large added resistance of Surface Effect Ships.

3.5.3 Sensitivity of the simulation method to simplifications

This section presents an investigation into the sensitivity of the non-linear simulation method to simplifications. The goal of this investigation is to address the importance of several components of the simulation method. All results that are presented by this section concern simulation in waves with steepness $kA = 0.05$.
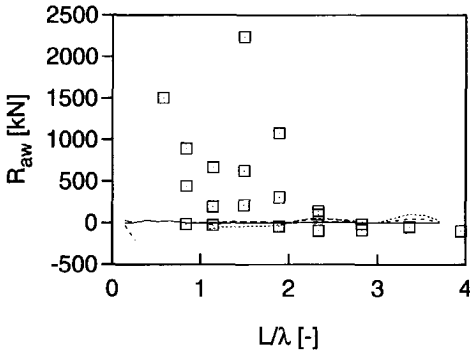
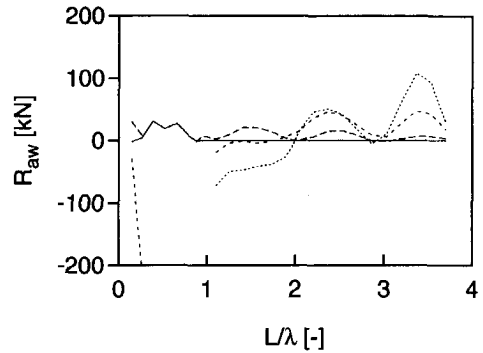Figure 3.12: Added resistance

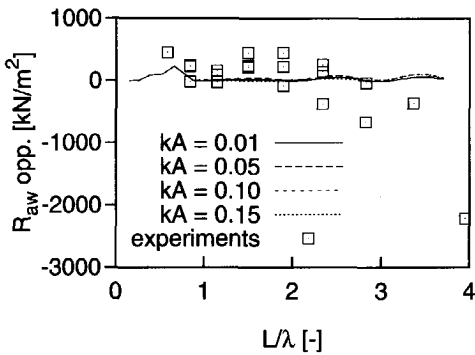Figure 3.13: Added resistance

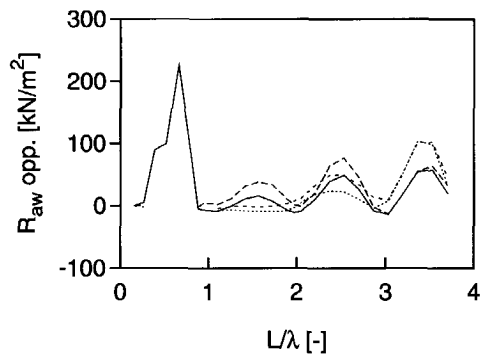Figure 3.14: Quadratic added resistance operator

Figure 3.15: Quadratic added resistance operator

Figure 3.16 and Figure 3.17 show the effect of a very attractive simplification on the heave and pitch motion. This simplification is the linearization of the stern seal. It implies that the seal geometry only needs to be computed once. This saves a lot of computational time and also leads to a more robust computational model. The linearization of the stern seal also implies that the leakage area under the seal can turn negative, which is not very realistic. Therefore the leakage area is set equal to zero when this occurs, because otherwise a negative air leakage flux would occur. Therewith the most important non-linear feature of the stern seal is retained. The effect of the stern seal linearization on the heave and pitch motions is remarkably small. The results however depend on the solution around which the seal is
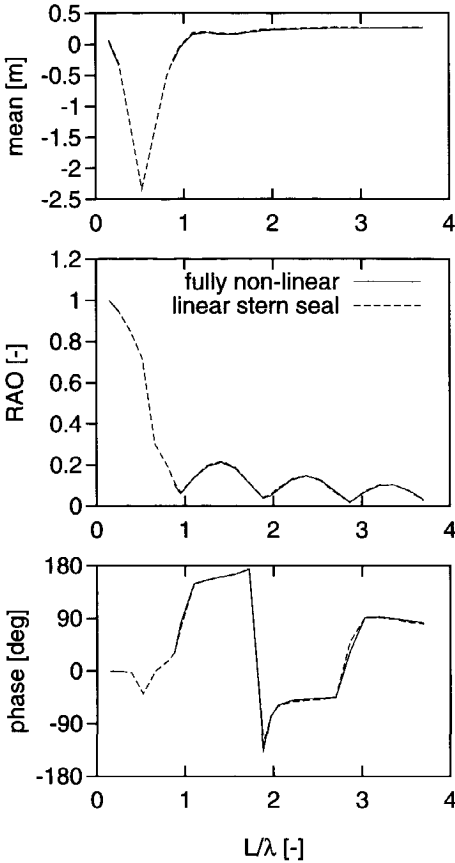
Figure 3.16: The effect of stern seal linearization on the heave response
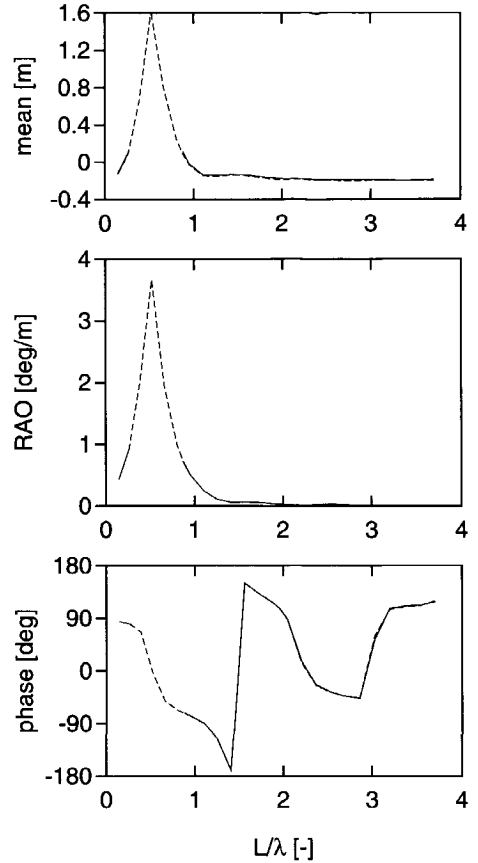
Figure 3.17: The effect of stern seal linearization on the pitch response

linearized. Therefore one should apply this simplification with care. In the investigation into the sensitivity of the method to all other simplifications, the linearization of the stern seal was applied.

Figure 3.18 and Figure 3.19 show the effect of neglecting the seal forces on the heave and pitch motion. In the computation without seal forces the stern seal force was replaced by cushion pressure times an extension of the deck area over the longitudinal extent of the seal. The bow seal force was simply neglected. The effect of the seals on the air cushion dynamics were however taken into account. Especially the stern seal force was expected to have an important (damping) effect on the pitch motions because of the great distance to the center of gravity which results in large
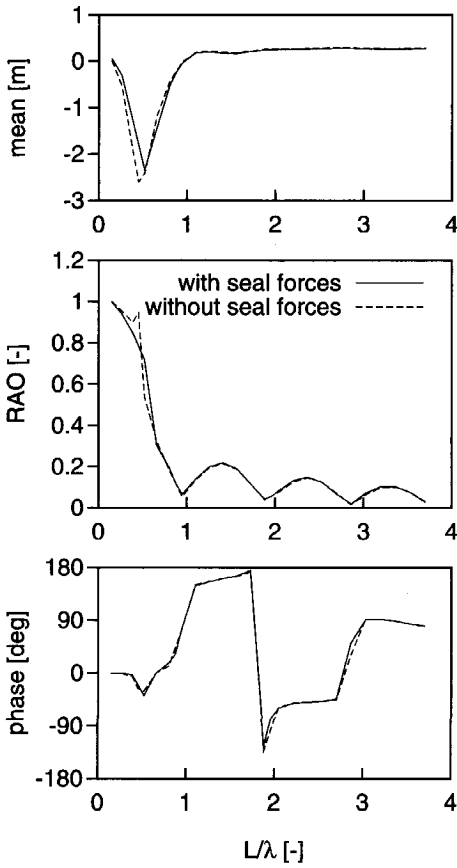
Figure 3.18: The effect of neglecting the seal forces on the heave response
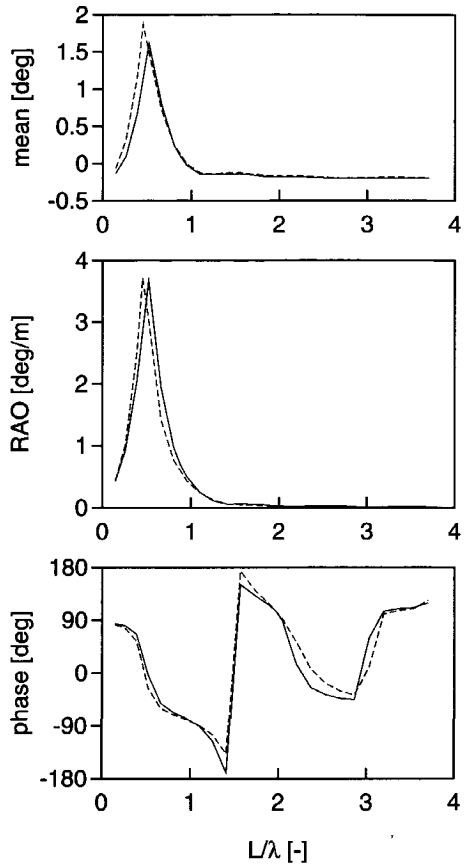
Figure 3.19: The effect of neglecting the seal forces on the pitch response

seal moments. Other investigators have found that the stern seal has an important effect on pitch motions of SESs (See the discussion to a paper by Moulijn[54]). Figure 3.18 shows however that the only effect is a small shift of the pitch resonance frequency. The effect of the seal forces on the heave motions is also small. One should however not conclude from these results that the effect of the seals on motions is small in general. The seals have a very important effect on the leakage gaps, and therefore on the air cushion dynamics. This results in a significant indirect effect of the seals on the heave motions.

Figure 3.20 shows the effect of neglecting air leakage on the heave motions. This simplification also includes neglecting the mean air flow trough the fans and the
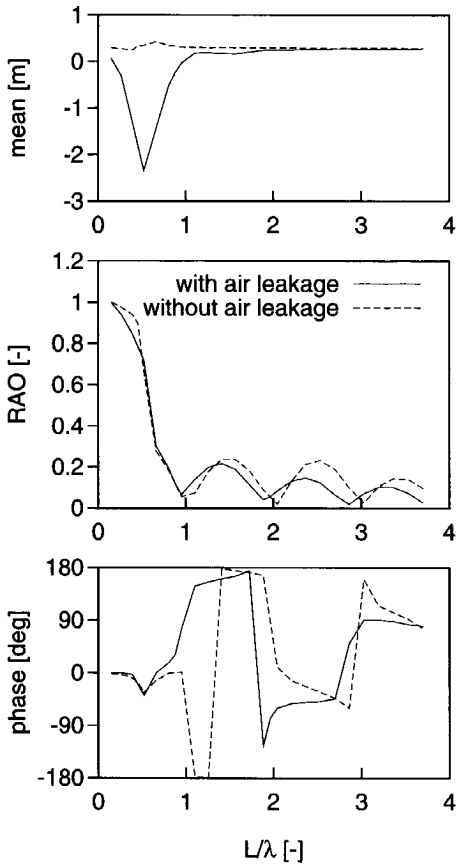
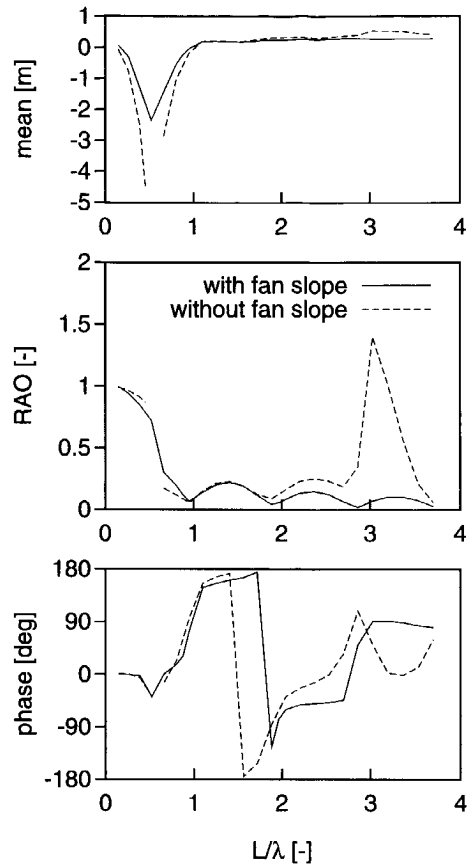Figure 3.20: The effect of neglecting air leakage on the heave response

Figure 3.21: The effect of neglecting the fan slope on the heave response

mean air flows from the stern seal plenum to the cushion plenum, in order to compensate for the lack of mean air leakage flow. The instationary flow through the fans and the instationary flow from the seal to the cushion were taken into account. Figure 3.20 shows that air leakage has a significant effect on the heave motions. The most important and obvious effect of neglecting air leakage is that no sinkage is predicted. Furthermore air leakage appears to have a significant damping effect on the cushion pressure variation and therewith on the heave motions. Air leakage also appears to shift the frequency at which the RAO reaches it's minimum values. The effect on the phase characteristics is also considerable. The effect of air leakage on trim was similar to the effect on sinkage. The effect on the pitch RAO and phase characteristics is very small.

Figure 3.21 shows the effect of neglecting the fan slope on the heave motions. This simplification implies that the air volume flux through the fans is assumed constant. The fan slope appears to have a huge effect on the heave motions. The large peak in the RAO around $L/\lambda = 3$ is due to the Helmholtz resonance of the air cushion. Helmholtz resonance occurs when the inertia of the SES is balanced by the compressibility of the air cushion. Apparently the fans have a very important damping effect on this resonant phenomenon. This means that a correct prediction of the amplitude response at the Helmholtz resonance requires a very accurate fan model. It remains to be seen whether the simple static fan model which is applied in the present study will suffice. Neglecting the fan slope also has a considerable effect on sinkage. This can be explained by the fact that the mean flow through the fans does not increase when the mean cushion pressure drops. At the pitch resonance the sinkage was that large that the cushion volume turned negative which resulted in the abortion of the simulation. The effect of the fans on the pitch motions is generally small.

Figure 3.22 shows the effect of neglecting the interaction of the air cushion with the wave surface on the heave motions. This simplification implies that only incident waves are considered when computing the wave pumping volume and the wave height at the seals. The forces on the hulls due to cushion pressure variations are also neglected. The effect is relatively small though still significant. Figure 3.23 shows a similar comparison where in both cases the fan slope was neglected too. From Figure 3.23 it appears that the cushion-surface interaction causes a considerable shift of the Helmholtz resonant frequency. Nakos et all.[9] also reported this effect. In Figure 3.22 the Helmholtz resonance is damped by the fans, thus concealing this important effect of the cushion surface interaction.

Figure 3.24 shows the effect of linearizing the stern seal on the computed added resistance of the air cushion. The added resistance appears to be more sensitive to the stern seal linearization than the motions. The effect is however still not very large.

Figure 3.25 shows the effect of neglecting the impulse of the air flows into and out of the air cushion on the added resistance of the air cushion. In this case the resistance of the air cushion simply follows from $(\zeta_b - \zeta_s) \cdot B_c \cdot p_c$, where ζ_b and ζ_s are the wave height at the bow and stern seal, B_c is the air cushion width and p_c is the air cushion excess pressure. Especially the air leakage under the bow seal gives a significant contribution to the added resistance of the air cushion. Leakage under the stern seal gives rise to a propulsive force. The contribution due to the impulse
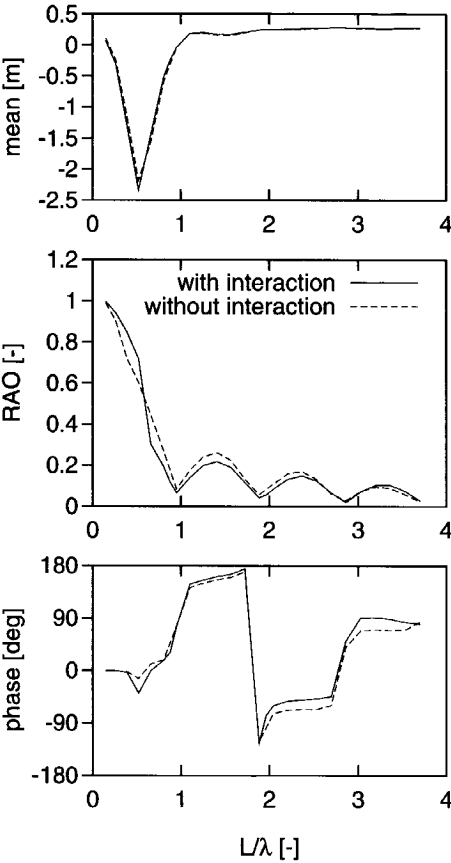
Figure 3.22: The effect of neglecting the cushion-surface interaction on the heave response
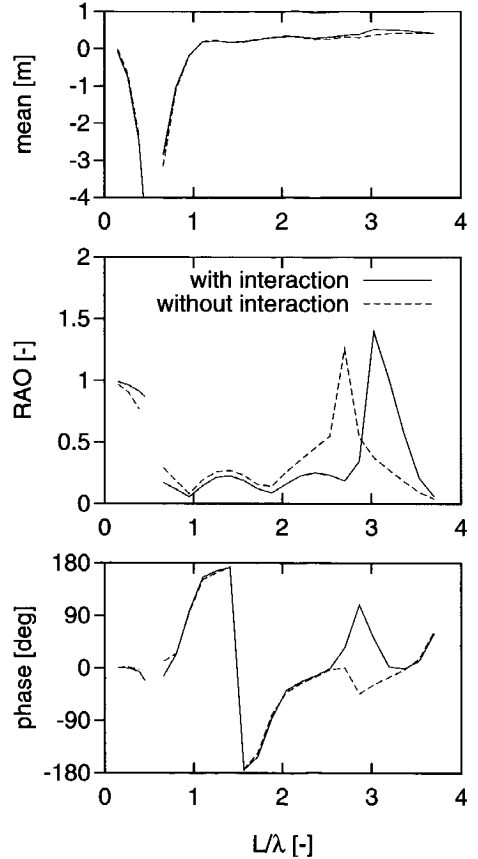
Figure 3.23: The effect of neglecting the cushion-surface interaction on the heave response (fan slope was also neglected)
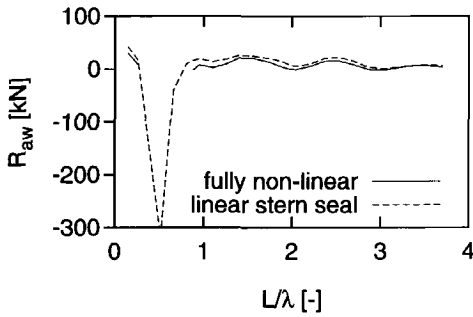
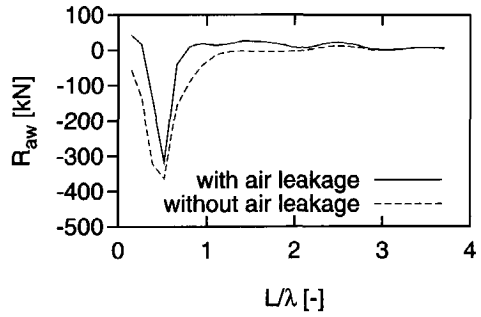Figure 3.24: Effect of stern seal linearization on added resistance

Figure 3.25: Effect of neglecting the impulse of the leaking air on added resistance

of the air flow through the fans is relatively small because the forward speed of the ship is small when compared to the leakage velocity.

3.6   Conclusions

From the results that were presented by Section 3.5 the following conclusions can be drawn:

- The computational end experimental results are in good agreement as far as the heave motions and the air cushion excess pressures are concerned. The correlation for the pitch motions and the stern seal excess pressure still require some improvement.

- There is a huge discrepancy between the computational and experimental added resistance due to waves. The computed added resistance only includes the added resistance of the air cushion. Probably the hypothesis that the air cushion is responsible for the major contribution to the added resistance due to waves of Surface Effect Ships is not valid. The computed added resistance is negligible in comparison with the added resistance that follows from the experiments.

- From the computational results the seals appear to have only a small direct effect on the motions of SES. The seals do however have an important effect on the air cushion dynamics by means of their influence on the air leakage gap. Therefore the seals have an important indirect effect on the heave motions. The computations indicate that the seals do *not* have a significant (damping)

effect on pitch motions. Other investigators found however that the stern seal does have an important effect on the pitch motions of SESs.

- The linearization of the stern seal is an attractive simplification which does not need to have a great effect on the results. It must however be applied with care because the solution around which the linearization is carried out can have an effect on the results.

- Air leakage appears to have a significant damping effect on the cushion pressure variations and the heave motions. Air leakage is also very important for the prediction of the drop of the cushion pressure and the consequent sinkage.

- The fan system appears to have a very important damping effect on the cushion pressure variations and the heave motions. It remains to be seen whether the simple static fan model which is applied in the present study will suffice. The fan system is also important for the prediction of the cushion pressure drop and the consequent sinkage.

- The effect of the interaction of the air cushion with the wave surface is significant though not very large. The interaction appears to cause a considerable shift of the Helmholtz resonant frequency of the air cushion. This resonance is however damped to by the fans to a large extent.

- According to the computations the impulse of the leaking air gives rise to a significant contribution to the added resistance of the air cushion.

From these conclusions it appears that several questions remain unanswered. The most important question is: what causes the large added resistance of SES? In order to find an answer to this questions an extensive series of model experiments were carried out. Chapter 4 presents a description of these model experiments. The experiments particularly focus on the origin of the added resistance of Surface Effect Ships. Furthermore the experiments will be used in a further validation of the computational method which is presented by Chapter 5.

Chapter 4

Model experiments

This chapter presents an extensive series of model experiments that was carried out at the Ship Hydromechanics Laboratory of Delft University of Technology. After an introduction this chapter discusses the scaling of air cushion dynamics. Section 4.3 and Section 4.4 subsequently describe the model and the various types of experiments that were carried out. Section 4.5 goes into the actual measurement of the added resistance, and Section 4.6 presents and discusses the results of the experiments. This chapter ends with conclusions concerning the origin of the added resistance of Surface Effect Ships.

4.1 Introduction

At the end of the previous chapter it appeared that the large added resistance of SESs does not originate from the air cushion, as was expected. The computed added resistance of the air cushion was negligible in comparison to the added resistance that followed from model experiments of MARIN. Therefore a series of new experiments was carried out. The main goal of these experiments was to get more insight into the origin of the (large) added resistance due to waves of Surface Effect Ships.

In Section 3.4.1 two components which contribute to the added resistance of SES were distinguished:

- the added resistance of the hulls,

- the added resistance of the air cushion.

An attempt was made to measure the two added resistance components separately. As a part of the investigation of the added resistance of the hulls two versions of

the model were tested: one with extremely slender side-hulls, and one with realistic side-hulls. The aim of the experiments with the first version was to isolate the effects of the air cushion to a large extent. Alongside of the two components three mechanisms which cause the added resistance of an SES were distinguished:

- radiation of waves

- sinkage

- momentum of escaping air

The importance of the mechanism of sinkage (a drop of the cushion pressure in waves that leads to a larger draft and consequently to a larger resistance) was investigated.

The model with extremely slender hulls lacks buoyancy and restoring capabilities, and could therefore not be tested in a set-up where it was free in heave and pitch. Therefore this model and the model with realistic side-hulls were subjected to wave force and forced oscillation experiments, where a model is rigidly connected to the carriage. The model with realistic side-hulls was also tested in a set-up where it was free in heave an pitch (motion experiments).

It is however not common practice to measure the added resistance during wave force and oscillation tests, because the added resistance that is measured during these experiments cannot be used in the prediction of the added resistance of a free sailing vessel. The added resistance is a higher order quantity, or at least a non-linear quantity. This implies that the added resistance does not simply follow from a superposition of a wave force test and a forced oscillation experiment.

4.2   Scaling of air cushion dynamics

This section discusses the scaling of air cushion dynamics. Scale effects play an important role in the model testing of air cushion vehicles. Just as with normal ships the scaling law of William Froude is applicable. Special attention must be payed to the scaling of the dynamics of the air cushion. The scaling problems of air cushion dynamics were amongst others distinguished by Lavis et al.[26]. Figure 4.1 illustrates the scale effect on the air cushion dynamics. It presents a comparison of the computed heave RAOs for the full scale HYDROSES target vessel and a geometrically scaled 1:20 scale model.
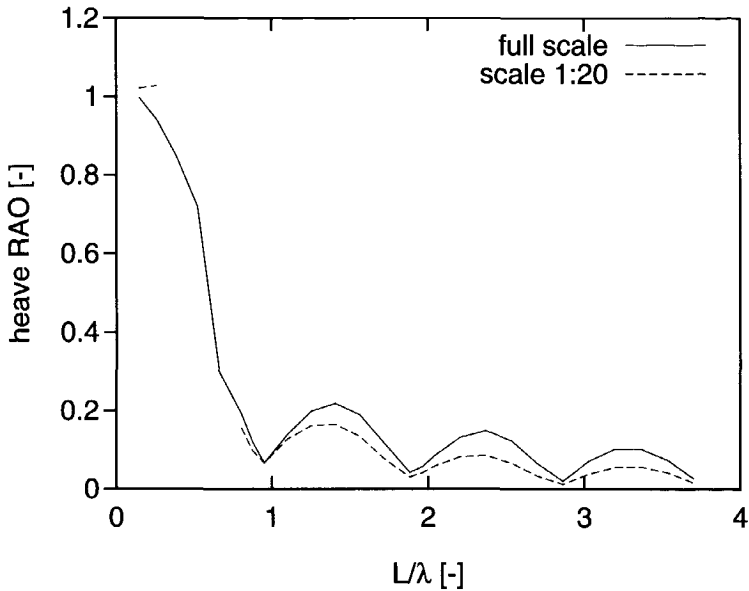
Figure 4.1: The effect of an incorrect scaling of the cushion dynamics on the heave RAO of the HYDROSES target vessel

The Froude scaling law requires that the ratio of gravitational and inertial forces that act on the water is the same at both model and full scale. When the Froude scaling law is obeyed, the generated wave pattern is geometrically identical on full scale and model scale as far as viscosity plays an subordinate part. Table 4.1 presents the Froude scale factors for several relevant quantities. These factors presuppose that the density of the water ρ and the gravitational acceleration g are the same on full scale and model scale.

In order to investigate how the dynamics of an air cushion can be scaled in a correct way, the equation which governs the dynamics of a plenum is examined. This equation reads:

$$\frac{V}{\kappa(p + p_a)} \cdot \frac{dp}{dt} = Q^{(in)} - Q^{(out)} - \frac{dV}{dt} \tag{4.1}$$

where V is the volume of the plenum, p is the excess pressure in the plenum, p_a is the ambient pressure and Q^{in} and Q^{out} are the air volume fluxes into and out of the plenum. This equation was derived from the equation of continuity and the equation of state for the air in the plenum. The derivation was carried out in Section 3.2.1. The Froude scaling law requires that Equation 4.1 is scaled by a factor $\alpha^{2\frac{1}{2}}$. This follows from the term dV/dt in the right hand side of equation 4.1. The volume V is

Table 4.1: Froude scale factors

description	symbol	unit	factor
length	L	[m]	α
area	A	[m^2]	α^2
volume	V	[m^3]	α^3
mass	M	[t]	α^3
force	F	[kN]	α^3
pressure	p	[kPa]	α
time	t	[s]	$\alpha^{\frac{1}{2}}$
velocity	V	[m/s]	$\alpha^{\frac{1}{2}}$
frequency	ω	[rad/s]	$\alpha^{-\frac{1}{2}}$

scaled by α^3 while the time t is scaled by $\alpha^{\frac{1}{2}}$, leading to a scale factor $\alpha^{2\frac{1}{2}}$ for dV/dt.

The stiffness of the air cushion is governed by the term $V/(\kappa(p + p_a))$ in the left hand side of Equation 4.1. According to Froude scaling, this term should be scaled by α^2, since dp/dt is scaled by $\alpha^{\frac{1}{2}}$ (p is scaled by α while t is scaled by $\alpha^{\frac{1}{2}}$). This can be achieved in two direct ways: scaling of the ambient pressure p_a by α, or scaling of the cushion volume V by α^2. In the second case the absolute pressure $p + p_a$ is almost constant because $p_a >> p$.

Unfortunately both ways are not very practical. A reduction of the ambient pressure can be achieved in the Depressurized Towing Tank at MARIN. Kapsenberg[27] carried out oscillation experiments in the Depressurized Towing Tank. A reduction of the ambient pressure is however impossible at other facilities. Moreover it causes air leakage to scale erroneously, as is pointed out later. Scaling of the cushion volume by α^2 is not very useful because it leads to an impractical height of the air cushion. The length and width of the air cushion are scaled by α resulting in scaling of the cushion height by 1. Then it will be impossible to scale the inertial properties of the model in a realistic way.

The stiffness of the air cushion can also be scaled correctly in an indirect way by mounting a device on the cushion, which supplies some extra volume when the excess pressure increases. Then equation 4.1 becomes:

$$\frac{V^{(c)} + V^{(d)}}{\kappa(p + p_a)} \cdot \frac{dp}{dt} = Q^{(in)} - Q^{(out)} - \frac{dV^{(c)}}{dt} - \frac{dV^{(d)}}{dp} \cdot \frac{dp}{dt} \tag{4.2}$$

where $V^{(d)}$ is the extra volume of this device and $V^{(c)}$ is the volume of the cushion.

This equation can be rewritten as:

$$\left[\frac{V^{(c)} + V^{(d)}}{\kappa(p + p_a)} + \frac{dV^{(d)}}{dp}\right] \cdot \frac{dp}{dt} = Q^{(in)} - Q^{(out)} - \frac{dV^{(c)}}{dt} \tag{4.3}$$

Now the device can be designed to have a "$dV^{(d)}/dp$" which results in a correctly scaled stiffness of the air cushion (the term within square brackets).

The device must be very light. Otherwise the inertia of the device can cause a dynamical response of the device. The most simple design of such a device is a flexible membrane mounted on top of the air cushion. In literature this membrane is called *diaphragm*. It has amongst others been used by Kapsenberg and Blume[5]. Appendix C presents an elaborate analysis of the diaphragm which was used in the present model tests.

The flow through the fans into the air cushion can be approximated by the linearized steady fan characteristic:

$$Q^{(in)} = Q_{\bar{p}} + \left(\frac{dQ}{dp}\right)_{\bar{p}} \cdot (p - \bar{p}) \tag{4.4}$$

where $\bar{p}$ is the design excess pressure. All terms in Equation 4.1 should be scaled by $\alpha^{2\frac{1}{2}}$. Therefore $Q_{\bar{p}}$ has to be scaled by $\alpha^{2\frac{1}{2}}$, while $\left(\frac{dQ}{dp}\right)_{\bar{p}}$ must be scaled by $\alpha^{1\frac{1}{2}}$ as $(p - \bar{p})$ scales by α. This may be used when choosing the fans for the model.

The air leakage flow can be approximated by the orifice flow formula (see also Section 3.2.3):

$$Q^{(out)} = c_l A_l \sqrt{\frac{2\Delta p}{\rho}} \tag{4.5}$$

where c_l is a coefficient which depends on the geometry of the leakage gap, A_l is the leakage area, Δp is the pressure difference across the leakage gap, and ρ is the density of the air at ambient pressure. The coefficient c_l accounts for the contraction of the escape air jet.

$Q^{(out)}$ should also be scaled by $\alpha^{2\frac{1}{2}}$ (see Equation 4.1). The coefficient c_l is the same on model scale and full scale when viscous effects of the leakage flow are of minor importance. The leakage area A_l scales by α^2. The pressure difference across the leakage gap scales by α. Then the air leakage flux scales correctly provided that ρ is the same on model and full scale.

When the ambient pressure is reduced by a factor α in order to achieve a correctly scaled stiffness of the air cushion ρ is also reduced by a factor α (provided that the temperature is constant). In that case $Q^{(out)}$ scales by α^2 in stead of $\alpha^{2\frac{1}{2}}$.

Then the effects of air leakage will become too great on model scale.

For the present series of experiments there is not a prescribed scale factor. The main goal of the experiments is to get insight into the origin of the added resistance of Surface Effect Ships rather than to predict the behavior of a full scale vessel.

Nevertheless we chose to equip the model with a diaphragm. This choice was made in order to limit the amplitude of the cushion excess pressure. When a model without a diaphragm is subjected to wave force or forced oscillation experiments, the large stiffness of the air cushion results in very large cushion pressure variations. Then the cushion excess pressure can easily turn negative, which is not very realistic (the seals might collapse and cease to function). The large pressure variations also result in large forces which might cause a considerable deformation of model. These effects were reported by van den Berg[55]. Furthermore a realistic scaling of the stiffness of the air cushion has the advantage that the conclusions drawn from these experiments are more generally valid.

On the other hand a diaphragm also introduces new unrealistic effects. Appendix C shows that the "$dV^{(d)}/dp$" of a diaphragm is not constant, particularly when the cushion excess pressure is close to zero. Therefore a diaphragm will introduce (unwanted) non-linear effects. When the pressure variations are not too large these non-linear effects will be small. Furthermore a diaphragm can introduce (unwanted) dynamic effects. These dynamic effects are not expected to be very large in the relevant frequency range because the rubber membrane is very light.

Appendix C presents a computational and experimental analysis of the diaphragm that was applied in the present experiments. The "$dV^{(d)}/dp$" of the diaphragm turned out to be $3.1 \cdot 10^{-5}$ [m^3/Pa]. This suits a scale factor of about 1:15. A scale factor of 1:50 would have been preferable as that would lead to a better similarity with the results of the HYDROSES project. This however required diaphragm dimensions that did not fit the model. The applied diaphragm was the largest that fitted the model in a reasonable way; the width was already greater than the beam of the vessel.

4.3   Description of the DUTSES model

This section presents a description of the model, that will be referred to as the DUTSES model. Two versions of the DUTSES model were tested. One version had extremely slender side-hulls which were in fact 12 mm thick plates. The other version was equipped with more realistic side-hulls. The model version with ex-

Table 4.2: Main particulars of the DUTSES model

symbol	description	unit	value
L_{oa}	Length over all	m	3.200
L_{pp}	Length at the perpendiculars	m	3.000
L_c	Length of the air cushion	m	3.000
B_p	Beam of the model with plates	m	0.549
B_h	Beam of the model with hulls	m	0.739
B_c	Beam of the air cushion	m	0.525
D_u	Depth to the upper deck	m	0.325
D_l	Depth to the lower deck	m	0.225
T_0	On-cushion draft at station 0	m	0.103
T_{20}	On-cushion draft at station 20	m	0.053
∇	Displacement of the hulls (on-cushion)	m^3	0.0168
p_c	Design air cushion excess pressure	Pa	300
p_s	Design stern seal excess pressure	Pa	306

tremely slender side-hulls will be referred to as the model with plates, while the model version with realistic hulls will be designated model with hulls. First this section presents a description of the overall geometry and structure of the model. Thereafter the section describes the seals which closed the air cushion at the bow and stern. Subsequently this section describes the system of fans that pressurized the air cushion.

4.3.1 Overall geometry and structure

The model was partially derived from the target vessel of the HYDROSES project. Section 3.5 presented a description of the HYDROSES target vessel. Figure 4.2 shows a drawing of the DUTSES model that also contains some main dimensions. Table 4.2 presents the main particulars of the model.

The main differences between the DUTSES model and the HYDROSES target vessel are an increased draft of the hulls, an increased depth of the air cushion and a higher air cushion excess pressure.

The draft of the hulls (in on-cushion mode) was increased in order to prevent the occurrence of significant air leakage under the hulls. Air leakage under the hulls is not included in the computational method that was presented in Chapter 3. The
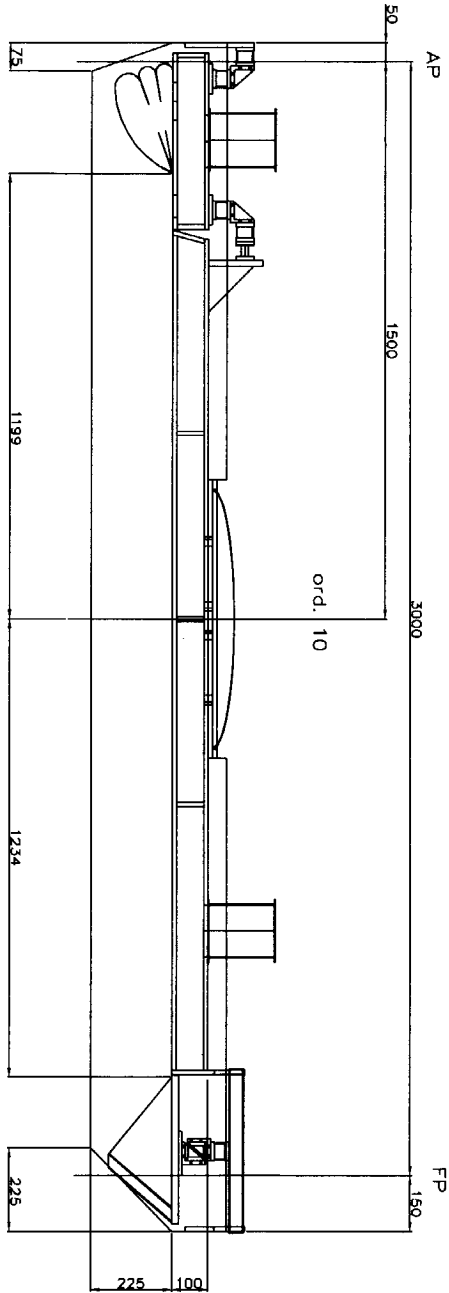
Figure 4.2: Overall structure of the DUTSES model

larger draft of the hulls also leads to a larger displacement of the hulls.

The depth of the air cushion was increased because this leads to larger seals. This results in larger seal forces, and therefore increases the accuracy of the seal force measurement.

The cushion pressure and the related weight of the vessel were increased in order to enable a simple and sufficiently stiff structure.

The side-plates and side-hulls have the same lateral contours (see Figure 4.2). The side-plates were about 12 mm thick. At the bow, keel and stern they were rounded. The plates were constructed of polyurethane foam which was reinforced by glass-fiber and polyester. The hulls were constructed by mounting extra polyurethane bodies to the plates. A smooth transition was achieved by means of filler. Figure 4.3 shows a body plan of the hulls. The hulls were prismatic from the stern up to station number 15. The double deck of the model was constructed of plywood. Table 4.3 presents the inertial properties of the model.

4.3.2 The seals

The bow and stern seals are similar to the seals of the HYDROSES target vessel. The main difference is that they are relatively larger as was pointed out above.

The bow seal is of the finger-type. It consists of vertical loops of flexible material, which are open to the cushion side of the seal. Each loop is a *finger*. The bow seal has nine fingers. Figure 4.4 shows the dimensions of the bow seal.

The stern seal is of the bag type; a bag of flexible material which is pressurized at a slightly higher pressure than the air cushion. The bag is open to the sides, where it is closed by the side-hulls. Two internal webs restrain the aft side of the bag, and divide the bag into three lobes. Figure 4.5 shows the dimensions of the stern seal. Both seals were manufactured of spinnaker cloth.

During the experiments the forces that were acting on the seals were measured separately. For this reason the bow seal was mounted on a plate which was connected to the model by means of force transducers (see Figure 4.4). The stern seal was mounted on an air distribution box which distributes the air flow from the aft fan over the stern seal bag and the air cushion. This box was also connected to the model by means of force transducers (see Figure 4.5). The air distribution box was connected at the front and the rear side in order to achieve a sufficiently stiff structure. This was necessary because the aft fan which was also mounted to the air distribution box might cause considerable vibrations. Table 4.3 presents the inertial properties of the bow seal plate and the air distribution box plus the fan. The mass
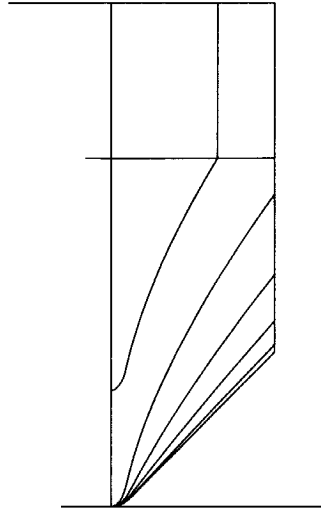
Figure 4.3: Body plan of the DUTSES model

Table 4.3: Inertial properties of the DUTSES model

symbol	description	unit	series		
			1.1 - 1.4	2.1 - 2.6	2.7
M	Total mass of the model	kg	48.12	64.02	62.80
K_{yy}	Pitch radius of gyration w.r.t. G	m	0.964	0.971	0.971
X_G	Horizontal position of G w.r.t. st. 10	m	-0.031	-0.031	-0.031
KG	Vertical position of G w.r.t. keel line	m	0.291	0.284	0.288
M_{bx}	Mass of bow seal for x-forces	kg	3.83	3.83	3.83
M_{bz}	Mass of bow seal for z-forces	kg	3.13	3.13	3.13
M_{sx}	Mass of stern seal for x-forces	kg	6.48	6.48	6.48
M_{sz}	Mass of stern seal for z-forces	kg	7.88	7.88	7.88
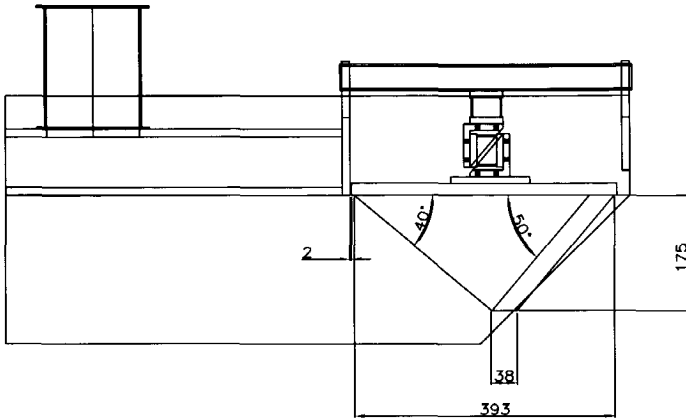
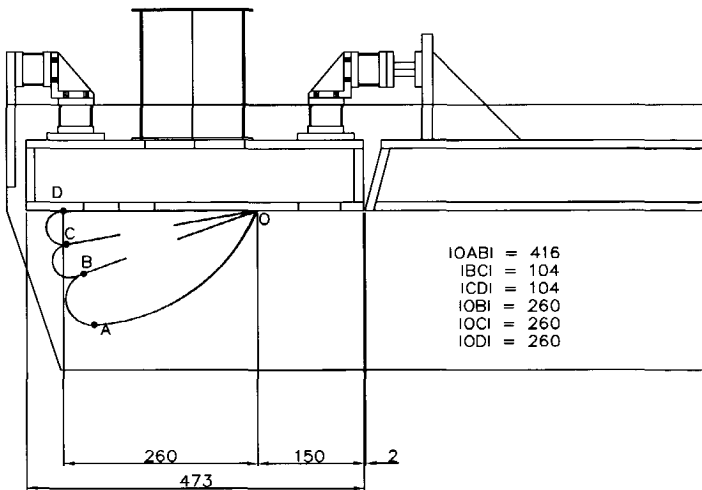Figure 4.4: Geometry and structure of the bow seal

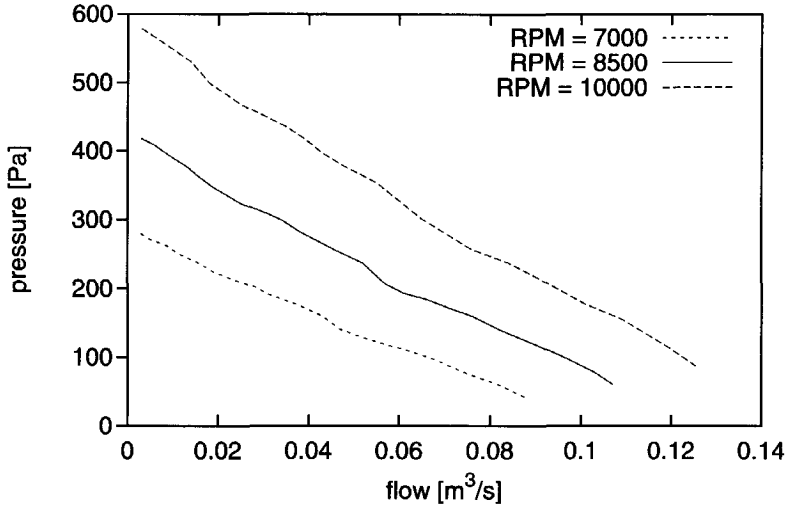Figure 4.5: Geometry and structure of the stern seal

Figure 4.6: The static fan characteristics

of the actual seals was very small.

4.3.3   The fan system

The air cushion and the stern seal plenum were both pressurized by axial fans. The fans were mounted directly on the model. The RPM of the fans was controlled by a computer. This ensured a very stable fan RPM. Figure 4.6 shows the measured static characteristics of the two identical fans. The fans were kindly on loan from MARIN.

The fore fan pumped air directly into the air cushion. The aft fan pumped air into an air distribution box which distributed the air over the stern seal and the air cushion. The ducts between the air distribution box and the stern seal were large. Therefore the volume of the air distribution box could be considered a part of the seal plenum. The duct between the air distribution box and the air cushion was relatively small. This resulted in a considerable resistance for the air flow from the stern seal plenum to the air cushion. The area of this duct could be adjusted by means of two slides. The pressure difference between the stern seal and cushion plena could be controlled by opening or closing the slides.

4.4 Description of the experiments

This section describes the three types of experiments that were carried out: wave force measurements, forced oscillation tests and heave and pitch motion tests. Table 4.4 presents an overview of the experiments that were carried out. The model with side plates was only subjected to wave force and forced oscillation experiments (Series 1.1 to Series 1.4). The model with hulls was subjected to all types of experiments(Series 2.1 to Series 2.7). Table 4.5 presents an overview of the quantities that were measured during the experiments. All model tests were carried out at the towing tank no. 1 of the Ship Hydromechanics Laboratory of Delft University of Technology. This tank is 142 m long and 4.22 m wide. During the experiments the water depth was 2.285 m.

4.4.1 Wave force tests

Figure 4.7 shows the experimental set up for the wave force tests and the oscillation tests. The model was rigidly connected to the carriage by means of the oscillator. During the wave force measurements the oscillator was fixed in its mean position. At the two connecting points (500 mm in front of station 10 and 500 mm aft of station 10) the horizontal and vertical connection forces were measured. The aft connection point was equipped with a slide which enabled pitch oscillation experiments and also prevented large internal stresses in the structure.

Both versions of the model (the model with side-plates and the model with hulls) were subjected to wave force test in on-cushion and off-cushion mode. During the on-cushion and the off-cushion experiments the draft of the model was the same (at the aft perpendicular: $T_0 = 103$ mm and at the fore perpendicular: $T_{20} = 53$ mm).

The wave length varied from 1.00 m to 6.00 m. In order to investigate the dependence of the added resistance on wave height the wave amplitude was varied from 10 mm to 40 mm. The program of the off-cushion experiments was reduced in order to limit the total number of runs. Next to the experiments in waves, some experiments in calm water were carried out. These experiments were repeated regularly because the calm water resistance has an important effect on the added resistance. The model velocity was 3.27 m/s ($Fn = 0.603$), and the RPM of both fans was 8500 1/min.

Table 4.4: Overview of the experiments

name	model	type of experiment	amplitude [mm]/[rad]	wave length [m]	enc. frequency [rad/s]
Series 1.1	plates	wave force experiments, $p_c = 300$ Pa	10 20 30 40	1.00 - 6.00 1.20 - 6.00 1.50 - 3.00 2.00 - 6.00	6.64 - 28.43 6.64 - 24.32 11.39 - 20.13 6.64 - 15.84
Series 1.2	plates	wave force experiments, $p_c = 0$ Pa	20 40	1.20 - 6.00 2.40 & 4.00	6.64 - 24.32 9.07 & 13.64
Series 1.3	plates	forced heave oscillation experiments, $p_c = 300$ Pa	5	-	6.00 - 24.00
Series 1.4	plates	forced pitch oscillation experiments, $p_c = 300$ Pa	0.02	-	6.00 - 18.00
Series 2.1	hulls	wave force experiments, $p_c = 300$ Pa	10 20 30 40	1.00 - 6.00 1.20 - 6.00 1.50 - 6.00 2.00 - 6.00	6.64 - 28.43 6.64 - 24.32 6.64 - 20.13 6.64 - 15.84
Series 2.2	hulls	wave force experiments, $p_c = 0$ Pa	20 40	1.20 - 6.00 2.40 & 4.00	6.64 - 24.32 9.07 & 13.64
Series 2.3	hulls	forced heave oscillation experiments, $p_c = 300$ Pa	5	-	6.00 - 24.00
Series 2.4	hulls	forced pitch oscillation experiments, $p_c = 300$ Pa	0.02	-	6.00 - 18.00
Series 2.5	hulls	forced heave oscillation experiments, $p_c = 0$ Pa	10	-	6.00 - 16.00
Series 2.6	hulls	forced pitch oscillation experiments, $p_c = 0$ Pa	0.01	-	6.00 - 18.00
Series 2.7	hulls	heave and pitch motion experiments $p_c = 300$ Pa	10 20 30 40	1.00 - 6.00 1.20 - 6.00 1.50 - 6.00 2.00 - 4.00	6.64 - 28.43 6.64 - 24.32 6.64 - 20.13 9.07 - 15.84

Table 4.5: Overview of the quantities that were measured

symbol	unit	description
η_3	[mm]	heave displacement
η_5	[deg]	pitch displacement
F_1	[N]	surge force
F_3	[N]	heave force
F_5	[N]	pitch moment
F_{1b}	[N]	longitudinal bow seal force
F_{3b}	[N]	vertical bow seal force
F_{1s}	[N]	longitudinal stern seal force
F_{3s}	[N]	vertical stern seal force
p_f	[Pa]	excess pressure in the air cushion (fore)
p_a	[Pa]	excess pressure in the air cushion (aft)
p_s	[Pa]	excess pressure in the stern seal plenum
Δp	[Pa]	differential pressure between cushion and stern seal
Q_f	[m^3/s]	air flow through the fore fan
Q_a	[m^3/s]	air flow through the aft fan
ζ_{b2}	[mm]	wave height just aft of the bow seal
ζ_{s1}	[mm]	wave height just in front of the stern seal
ζ_{s2}	[mm]	wave height just aft of the stern seal
ζ_{ref1}	[mm]	reference wave height at ord. 10
ζ_{ref2}	[mm]	reference wave height ahead of the model

4.4.2 Forced oscillation tests

The experimental set-up of the forced oscillation tests was identical to the experimental set-up of the wave force measurements (see Figure 4.7). The difference is that the oscillator now forces the model to carry out harmonic heave or pitch motions in calm water. The pitch oscillations were carried out around the center of reference (station 10, 350 [mm] above the keel line).

The model with side-plates was only tested in on-cushion mode, because the forces acting on oscillating vertical plates was considered to be not very relevant. The model with hulls was tested in on-cushion as well as off-cushion mode. The off-cushion tests lead to the well known hydrodynamic coefficients (added mass and damping) of the hulls. During the off-cushion and on-cushion experiments the draft of the model was the same ($T_0 = 103$ mm and $T_{20} = 53$ mm).
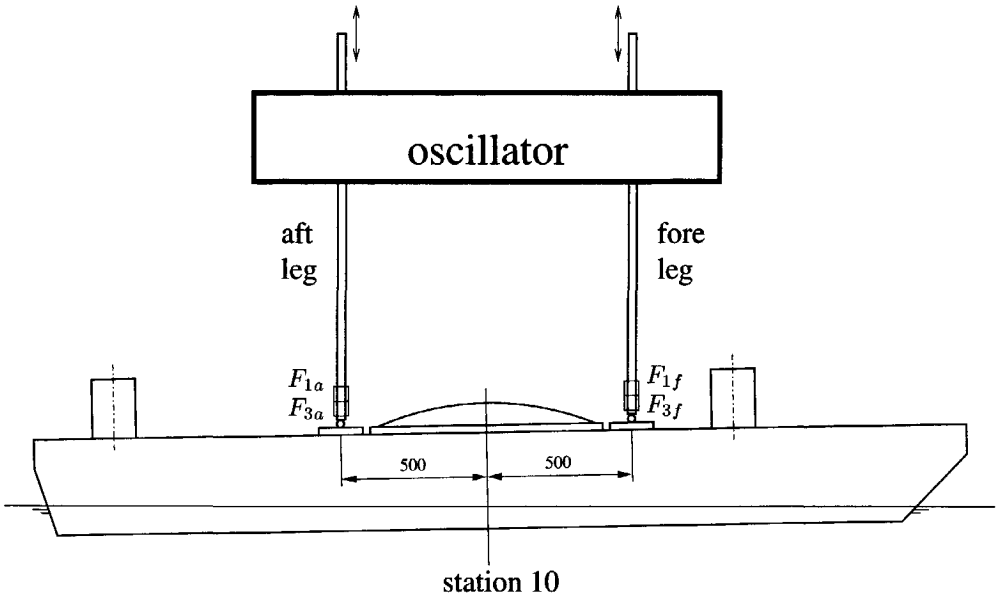
Figure 4.7: Experimental set-up for the wave force tests and the forced heave and pitch oscillation tests

In the on-cushion heave oscillation tests the oscillation frequency varied from 6.0 rad/s to 24.0 rad/s. For the off-cushion heave oscillation tests and all pitch oscillation tests the program had to be reduced at the high frequency end because the forces acting on the vertical force transducers were exceeding the nominal range of these transducers. The heave amplitude was 5 mm in the on-cushion tests and 10 mm in the off-cushion tests. The pitch amplitude was 0.02 rad during the on-cushion tests and 0.01 rad during the off-cushion tests. The on-cushion heave amplitude was small because otherwise the cushion excess pressure might turn negative. The on-cushion pitch amplitude was relatively large when compared with the heave amplitude. This was done because one of the aims of these tests was to investigate the effects of (non-linear) air leakage under the seals. A large pitch amplitude results in significant air leakage gaps. The amplitude of the motions was not varied in order to limit the total number of tests. The model velocity was 3.27 m/s ($Fn = 0.603$), and the RPM of both fans was 8500 1/min.
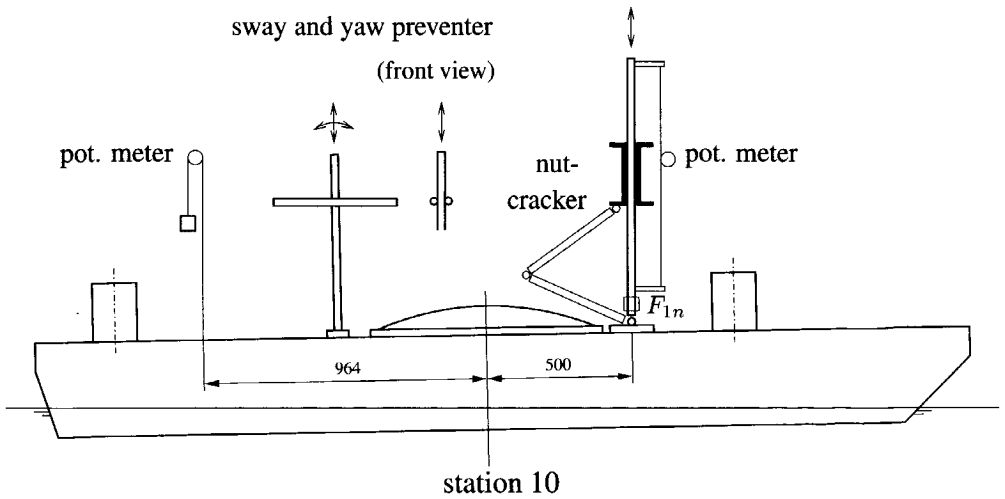
Figure 4.8: Experimental set-up for the heave and pitch motion tests

4.4.3 Heave and pitch motion tests

Figure 4.8 shows the experimental set-up for the heave and pitch motion tests. During these experiments the model was free to carry out heave and pitch motions. The model was connected to the carriage by the so called *nutcracker*; a device which prevents surge, sway, roll and yaw motions. The nutcracker was mounted 500 mm in front of station 10. At the Ship Hydromechanics Laboratory it is common practice to mount the nutcracker at the center of reference. This was however impossible because of the presence of the diaphragm. At 500 mm aft of station 10 an extra sway and yaw preventer was mounted.

The model with side-plates was not subjected to heave and pitch motion tests because it lacked buoyancy and restoring capabilities. The model with hulls was only tested in the on-cushion mode (in off-cushion mode the draft was very large). The calm water trim and sinkage corresponded to the sinkage and trim during the captive experiments ($T_0 = 103$ mm and $T_{20} = 53$ mm). The off-cushion zero velocity drafts of the model were: $T_0^* = 137$ mm and $T_{20}^* = 176$ mm.

The wave length varied from 1.00 m to 6.00 m. In order to investigate the dependence of the added resistance on wave height the wave amplitude was varied from 10 mm to 40 mm. The model velocity was 3.27 m/s ($Fn = 0.603$), and the RPM

of both fans was 9000 1/min. Besides the experiments in waves, some experiments in calm water with a reduced fan RPM were carried out. This was done in order to investigate the importance of the mechanism of sinkage. In these experiments the RPM of both fans was reduced equally.

4.5   Measurement of the added resistance

The *total* added resistance due to waves follows from:

$$R_{aw} = R(in\ waves) - R(in\ calm\ water) \tag{4.6}$$

It is difficult to obtain an accurate measurement of the the added resistance because the relatively small added resistance follows from the difference of two large quantities. Especially in the captive experiments (wave force and forced oscillation tests) the calm water resistance appeared to be very sensitive to small variations of the water level in the towing tank which resulted in a change of the draft of the model. In order to minimize these errors the water level was checked regularly. Furthermore the calm water resistance was measured several times over again, while the experiments were in progress. An actual calm water resistance was used in the calculation of the added resistance.

The added resistance due to waves of an SES can be divided into a contribution due the air cushion and a contribution due to the hulls. The resistance of the air cushion follows from:

$$R^{(ac)} = \overline{-F_{1b} - F_{1s} + p_c A_d \sin\theta - (F_{3b} + F_{3s} + p_c A_d \cos\theta) \cdot \eta_5} \tag{4.7}$$

where F_{1b}, F_{3b}, F_{1s} and F_{3s} are the seal forces (the subscripts b and s indicate bow or stern seal force, and the subscripts 1 and 3 indicate longitudinal or vertical force). Furthermore A_d is the area of the deck, p_c is the cushion excess pressure, θ is the calm water trim angle of the vessel, and η_5 is the pitch displacement, which is assumed to be small. The overlining denotes that the time averaged value of the expression underneath should be used. This definition of the resistance of the air cushion also includes the frictional resistance of the seals. Now the *added* resistance of the air cushion follows from:

$$R_{aw}^{(ac)} = R^{(ac)}(in\ waves) - R^{(ac)}(in\ calm\ water) \tag{4.8}$$

Subsequently the *added* resistance of the hulls can be calculated from:

$$R_{aw}^{(h)} = R_{aw} - R_{aw}^{(ac)} \tag{4.9}$$

where R_{aw} is the total added resistance. The added resistance of the hulls also followed from captive off-cushion experiments. Of course these experiments do not include the interaction of the hulls with the hydrodynamic effects due to the air cushion.

In order to investigate the added resistance due to sinkage, some calm water tests with a reduced fan RPM were carried out. The reduction of the RPM resulted in a drop of the cushion pressure thus simulating sinkage due to an increase of the air leakage flow. From the results of these tests we derived linear relations of resistance (R), resistance of the air cushion ($R^{(ac)}$) and resistance of the hulls ($R^{(h)}$) with the cushion excess pressure (p_c). Subsequently the added resistance was calculated by substituting the measured mean cushion pressure from the experiments in waves into these relations. In the captive experiments the model was restrained, so no sinkage occurred during these experiments. Therefore the investigation of the added resistance due to sinkage was only carried out for the heave and pitch motion experiments.

4.6 Presentation and discussion of the results

This section presents and discusses the results of the model experiments as far as they concern the added resistance due to waves. The other results are presented in Chapter 5 within the scope of an experimental validation of the computational method. First this section goes into the magnitude of the added resistance, also in relation with the the results of the MARIN experiments. Then it discusses the relation of the added resistance with wave height. Subsection 4.6.3 presents the results of the separately measured added resistance components; the added resistance of the air cushion and added resistance of the hulls. Subsection 4.6.4 treats the results of the investigation into the mechanism of sinkage. This section ends with a discussion of the results.

4.6.1 Magnitude of the added resistance

Figure 4.9 shows a comparison of the added resistance as it was measured during the wave force experiments with the model with plates (Series 1.1), the wave force experiments with the model with hulls (Series 2.1) and the motion experiments (Series 2.7). The added resistance is presented on model scale as a function of L/λ, the cushion length divided by the wave length. The figure shows results for several wave amplitudes.
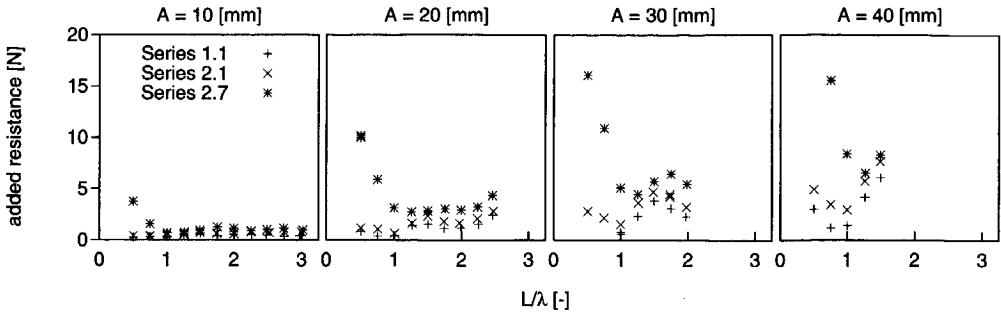
Figure 4.9: Comparison of the added resistance of Series 1.1 (wave force tests, model with plates), Series 2.1 (wave force tests, model with hulls) and Series 2.7 (model free in heave and pitch)

The by far largest added resistance was measured during the experiments where the model was free in heave and pitch (Series 2.7). The largest added resistance occurred in long waves, when the model carried out severe pitch motions. In the wave force tests (Series 1.1 and Series 2.1) the added resistance was much smaller but still significant. The added resistance that was measured during the oscillation experiments was only small (up to about 2 N).

The added resistance that was measured during the present experiments is much smaller than the added resistance that was measured by Kapsenberg et al. [29] at MARIN. They measured added resistance values up to about two times the calm water resistance. In the present experiments the largest measured added resistance was about half the calm water resistance.

There are however several differences between both experiments. The most important difference is that the MARIN model was a self-propelled free sailing model. The added resistance was derived from the thrust increase of the water-jets. The DUTSES model was not free in surge, and the resistance was measured directly. Experiments with a self-propelling model are closer to reality than experiments where the model is only free in heave and pitch. On the other hand the direct measurement of the added resistance that was applied in the present experiments is more reliable, and surge motion is generally considered to be of minor importance for the added resistance.
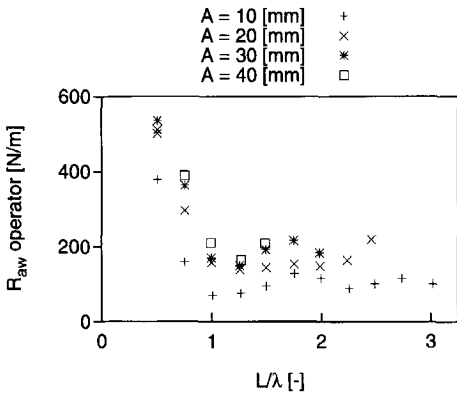
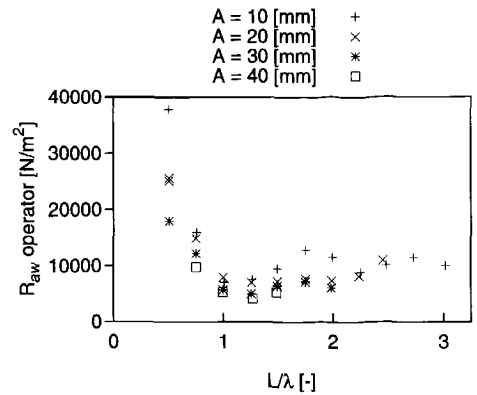Figure 4.10: The added resistance divided by the wave amplitude (Series 2.7: model free in heave and pitch)

Figure 4.11: The added resistance divided by the wave amplitude squared (Series 2.7: model free in heave and pitch)

4.6.2 The relation of the added resistance with wave height

For conventional ships the added resistance has a quadratic relation with the wave amplitude. Figure 4.10 and Figure 4.11 respectively show the added resistance divided by the wave amplitude and the added resistance divided by the wave amplitude squared. Both figures follow from the heave and pitch motion experiments (Series 2.7). They clearly show that the relation of added resistance with wave amplitude is neither linear nor quadratic. The relation of added resistance with wave height is somewhere between linear and quadratic. It probably contains both linear and quadratic terms.

From the off-cushion wave force experiments it appeared that the relation of the added resistance of the hulls with the wave amplitude was not quadratic either (see Figure 4.12 and Figure 4.13). This is quite remarkable because in these off-cushion experiments the model was expected to behave like a regular catamaran.

Apparently there does not exist a simple univocal relation of the added resistance of SESs with the wave amplitude. Therefore the results for the added resistance that are presented by this thesis are *not* divided by some power of the wave height.
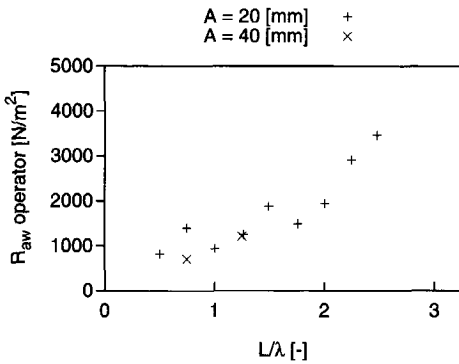
Figure 4.12: The added resistance divided by the wave amplitude squared (Series 1.2: off-cushion wave force tests, model with plates)
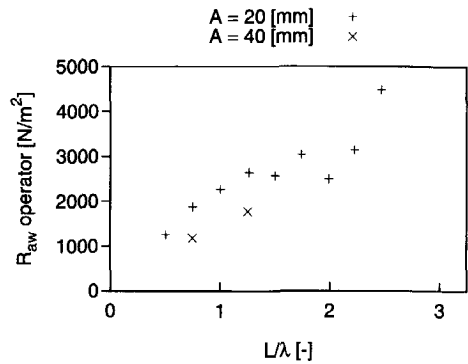
Figure 4.13: The added resistance divided by the wave amplitude squared (Series 2.2: off-cushion wave force tests, model with hulls)

4.6.3   The added resistance components

Figure 4.14, Figure 4.15 and Figure 4.16 respectively show the total added resistance, the added resistance of the air cushion and the added resistance of the hulls. The figures show results of the wave force tests with the model with plates (Series 1.1) and of the wave force tests with the model with hulls (Series 2.1).

This paragraph compares the results of the model with plates with the results of the model with hulls. The total added resistance of the model with hulls is larger than the total added resistance of the model with plates (see Figure 4.14). The difference is however not very large.

The added resistance of the air cushion of the model with plates does not significantly differ from the added resistance of the air cushion of the model with hulls (see Figure 4.15). Apparently the interaction of the hulls and the air cushion is not very important for the added resistance. This also subscribes the accuracy of the measurement of the added resistance of the air cushion.

The model with hulls has a larger added resistance of the hulls than the model with plates (see Figure 4.16). It is however remarkable that the model with plates does have a significant added resistance of the hulls. This also followed from the off-cushion wave force tests with the model with plates (see Figure 4.17). Added resistance is generally considered to be of potential flow origin, i.e. the added resistance is associated with the momentum of radiated waves which are caused by
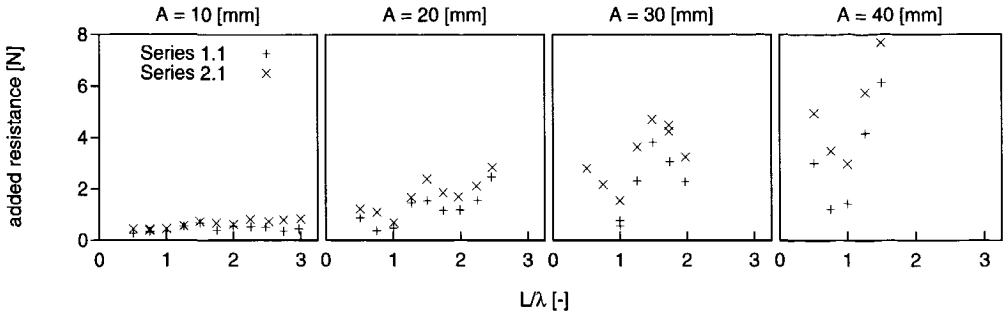
Figure 4.14: Comparison of the total added resistance of the model with plates (Series 1.1) and the model with hulls (Series 2.1) as measured during wave force experiments
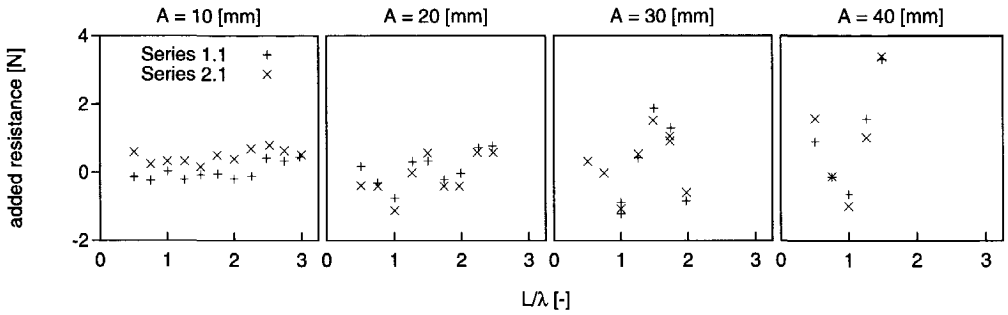

Figure 4.15: Comparison of the added resistance of the air cushion of the model with plates (Series 1.1) and the model with hulls (Series 2.1) as measured during wave force experiments
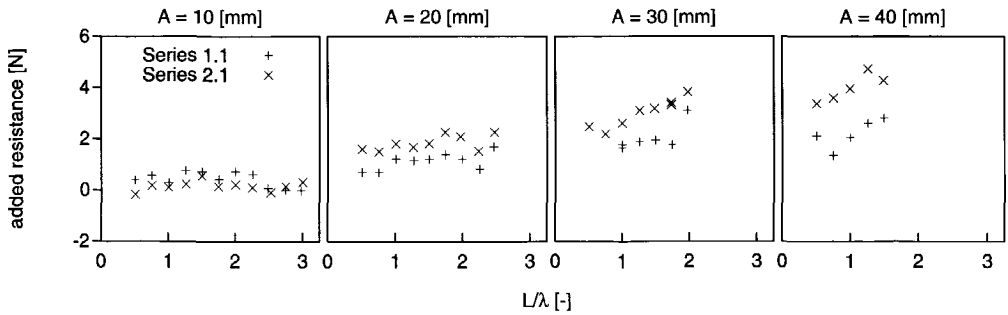

Figure 4.16: Comparison of the added resistance of the hulls of the model with plates (Series 1.1) and the model with hulls (Series 2.1) as measured during wave force experiments
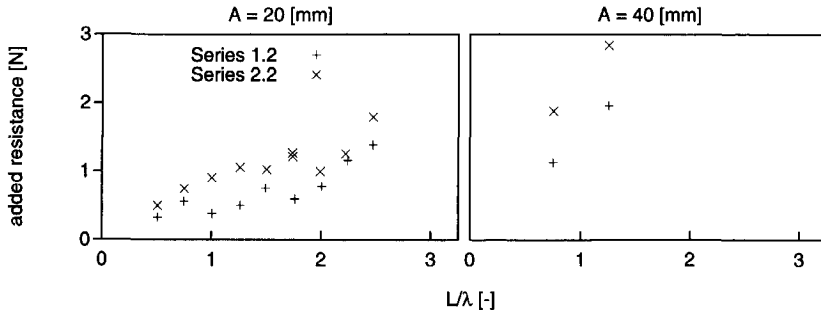
Figure 4.17: Comparison of the total added resistance of Series 1.1 (plates) and Series 2.1 (hulls); wave force experiments

diffraction of the incident waves and by the motions of the vessel. The plates can hardly generate any waves (at least in head and following seas). Therefore the added resistance of the plates was expected to be negligible. This indicates that other mechanisms are important for the added resistance of very slender high speed hulls. One might think of viscous effects or the generation of spray.

This paragraph compares the added resistance of the air cushion with the added resistance of the hulls. From Figure 4.15 and Figure 4.16 it can be concluded that, in the case of wave force tests, the added resistance of the air cushion and the added resistance of the hulls are about of equal importance. The results of the oscillation experiments lead to the same conclusion. In the pitch oscillation tests the added resistance of the air cushion is negative. This is due to a considerable drop of the cushion excess pressure which is caused by the large amount of air leakage under the seals.

Figure 4.18, Figure 4.19 and Figure 4.20 respectively show the total added resistance, the added resistance of the air cushion and the added resistance of the hulls as they were measured during the heave and pitch motion experiments (Series 2.7). It must be noted that during the motion experiments the measurement of the added resistance of the air cushion was not as accurate as during the captive experiments. This was due to a less accurate measurement of the bow seal force. In advance of each test run the model floated in rest at a large draft ($p_c = 0$). As a result the bow seal was wetted during each test run. The wet bow seal was probably *sticking* to the side hulls, thereby affecting the actually measured bow seal force. This sticking is not likely to reproduce very well, and therefore results in some scattering of the added resistance of the air cushion. The sticking occurred in the tests in waves as
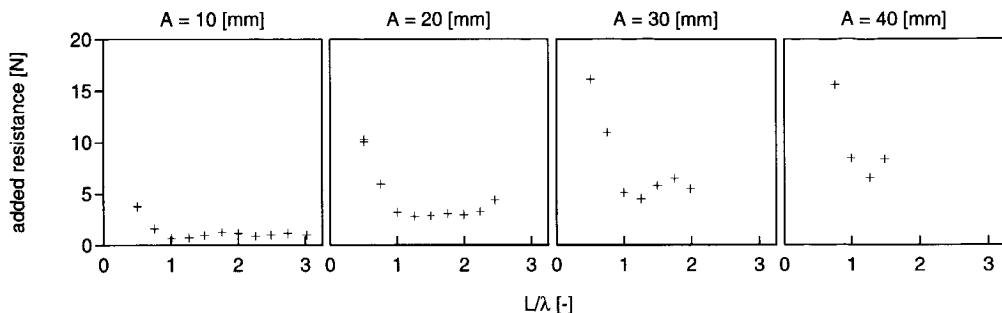
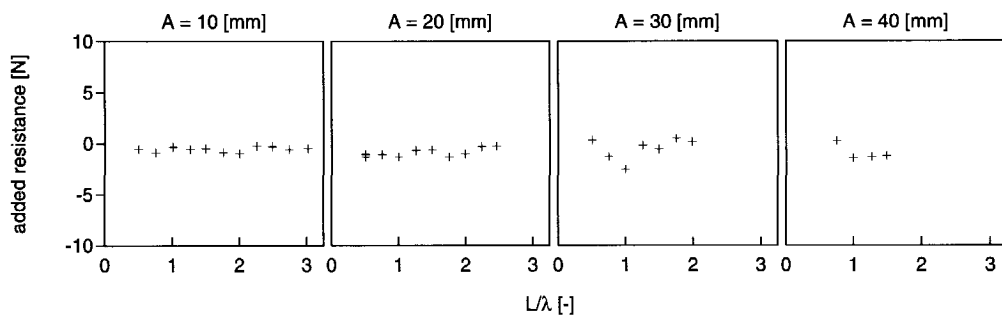Figure 4.18: The total added resistance (model free in heave and pitch)

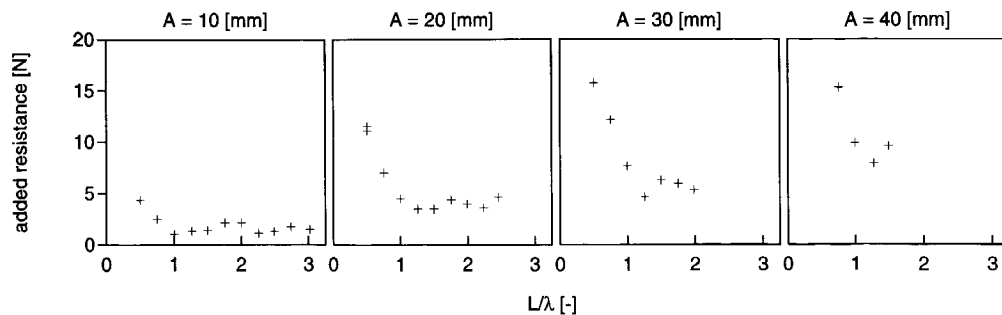Figure 4.19: The added resistance of the air cushion (model free in heave and pitch)

Figure 4.20: The added resistance of the hulls (model free in heave and pitch)

well as in the tests in calm water. Therefore it is not expected that it affects the order of magnitude of the added resistance of the air cushion.

The added resistance of the hulls is much larger than the added resistance of the air cushion (please compare Figure 4.19 and Figure 4.20). The added resistance of the air cushion is only small and in most cases even negative. It can therefore be concluded that, when the model is free in heave and pitch, the contribution of the hulls to the added resistance is much more important than the contribution of the air cushion.

4.6.4   The mechanism of sinkage

When an SES sails in waves the extra amount of air leakage results in a lower mean excess pressure inside the air cushion. Therefore a larger part of the vessel's weight must be carried by the buoyancy of the hulls. This leads to a larger draft of the hulls and consequently to a larger resistance. This increase of the resistance is called the added resistance due to sinkage. It only occurs in the heave and pitch motion tests (Series 2.7). In the captive tests the model was not free to sink deeper into the water.

In order to investigate the mechanism of sinkage, some runs with a reduced fan RPM were carried out. From these runs we derived linear relations of heave displacement (η_3), resistance (R), resistance of the air cushion ($R^{(ac)}$) and resistance of the hulls ($R^{(h)}$) with cushion pressure (p_c). These relations were used to calculate the mean heave displacement and the added resistance due to sinkage for the experiments in waves by substituting the measured mean cushion pressure. Figure 4.21 shows a comparison of the thus calculated mean heave displacement and the directly measured mean heave displacement. The directly measured sinkage is slightly smaller, but the agreement is generally very good. This indicates that this somewhat indirect approach is valid.

Figure 4.22, Figure 4.23 and Figure 4.24 respectively show the total added resistance due to sinkage, the added resistance of the air cushion due to sinkage and the added resistance of the hulls due to sinkage. From a comparison of Figure 4.22 with Figure 4.18 it appears that the mechanism of sinkage is responsible for a large part of the total added resistance; it is more than half the total added resistance. Both air cushion and hulls contribute to added resistance due to sinkage. The added resistance of the hulls due to sinkage is large, while the added resistance of the air cushion due to sinkage is negative. Actually the cushion pressure drop causes a decrease of the wave making resistance of the air cushion, an increase of the wave making resistance of the hulls and an increase of the frictional resistance of the
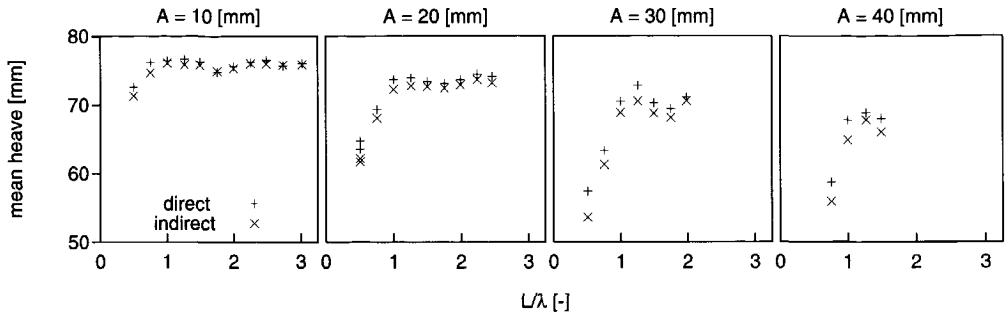
Figure 4.21: The mean heave displacement ($\overline{\eta}_3$) directly measured and computed from the runs with a reduced fan RPM

hulls. Figure 4.25 shows a comparison of the added resistance of the hulls due to sinkage with the total added resistance of the hulls. The full added resistance of the hulls is only slightly larger.

4.6.5 Discussion

The oscillation and wave force experiments led to a conclusion that is quite different from the conclusion that was drawn from the motion experiments. In the first case the conclusion was that the added resistance of the air cushion and the added resistance of the hulls are of equal importance. In the latter case the conclusion was that the added resistance of the hulls is large, while the added resistance of the air cushion is of minor importance.

The difference can be explained by the fact that no sinkage occurred in the oscillation and wave force experiments. Sinkage appeared to be very important for the added resistance of the hulls. In the oscillation and wave force experiments the (mean) position of the model was fixed. The model was not allowed to sink deeper into the water. Therefore the added resistance of the hulls due to sinkage equaled zero, which results in a much smaller added resistance of the hulls and also in a much smaller total added resistance.

The motion experiments, where the model was free in heave and pitch, are most representative for the problem of a real SES sailing in a seaway. Therefore the conclusion of these experiments are the most relevant conclusions concerning the origin of the added resistance of Surface Effect Ships. The conclusions that followed from the oscillation and wave force experiments are only applicable to a situation that
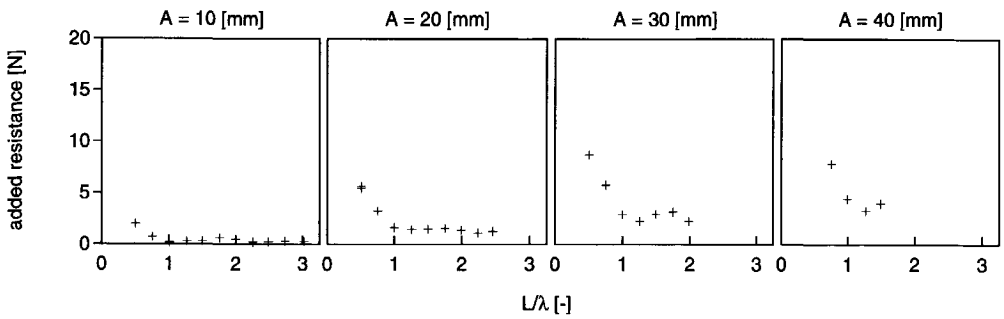
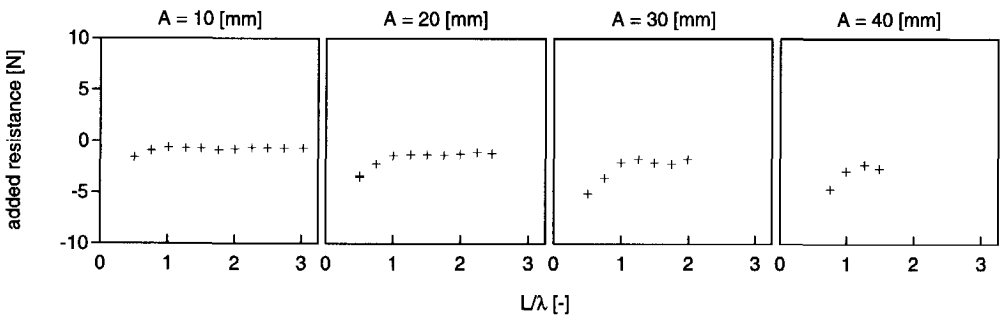Figure 4.22: The total added resistance due to sinkage

Figure 4.23: The added resistance of the air cushion due to sinkage
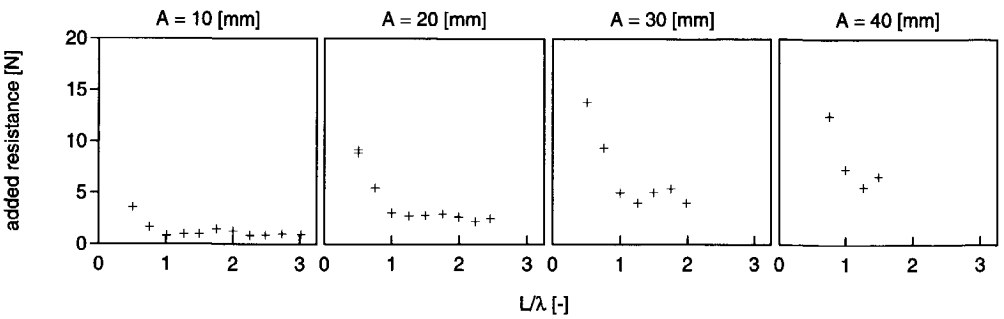

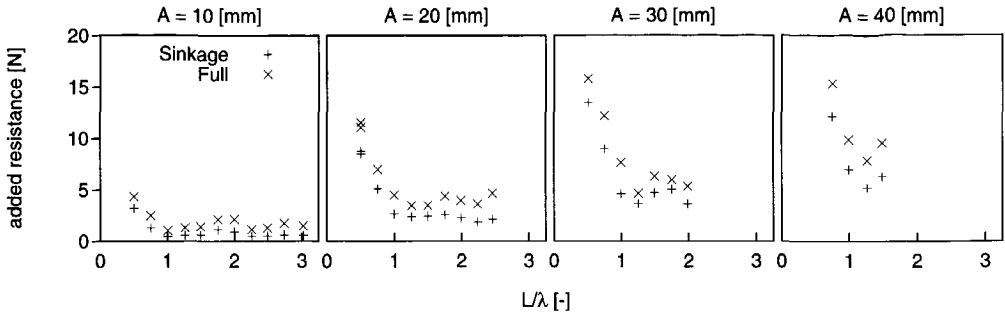Figure 4.24: The added resistance of the hulls due to sinkage

Figure 4.25: Comparison of the added resistance of the hulls due to sinkage with the full added resistance of he hulls (model free in heave and pitch)

only exists in a laboratory.

4.7 Conclusions

The following conclusions concerning the added resistance due to waves of Surface Effect Ships can be drawn from the experiments:

- The contribution of the air cushion to the added resistance is relatively unimportant. The major contribution to the added resistance is due to the hulls. In the wave force experiments the added resistance of the air cushion was significant, but in the experiments where the model was free in heave and pitch the added resistance of the air cushion was only small and in most cases it was even negative.

- The mechanism of sinkage is important for the added resistance of SESs. The large added resistance of the hulls in the heave and pitch motion experiments is almost entirely due to sinkage.

- The added resistance of the model with realistic side-hulls is larger than the added resistance of the model with extremely slender side hulls (model with plates). The difference is however not very large. It is remarkable that the added resistance of the hulls of the model with plates is significant. This indicates that other mechanisms (probably viscosity) might be important for the added resistance of fast and very slender hulls.

- A relatively large added resistance was measured (up to half the calm water resistance). It was however considerably smaller than the added resistance

that was measured by MARIN. It must be noted that there were several differences between both experiments.

- The relation of the added resistance with the wave amplitude is neither linear nor quadratic; the relation is somewhere between quadratic and linear.

Chapter 5

Validation of the computational method

This chapter presents a validation of the computational method. Therefor the results of the computational method are compared to the results of the experiments with the DUTSES model that were described by Chapter 4.

This chapter starts with some remarks on the computations. Thereafter it carries on with the actual comparison of computational and experimental results. This chapter subsequently pays attention to the heave and pitch motions, the pressure variations in the air cushion and stern seal plena, the forces that act on the seals and the behavior of the fans. Thereafter Section 5.6 presents a comparison of the computational and experimental results for the added resistance due to waves.

   The computational method only includes the part of the added resistance that is caused by the air cushion (see Chapter 3). The experiments that were presented by Chapter 4 showed however that the air cushion only gives a minor contribution to the added resistance of SESs. The experiments also showed that the large added resistance of the hulls is mainly caused by sinkage of the vessel while sailing in waves. Therefore Section 5.6 also investigates how the computational method can be applied in a computation of the added resistance due to sinkage.

   This chapter ends with conclusions concerning the validity of the computational method and the applicability of the computational method for the prediction of the added resistance.

In order to limit the amount of results to be presented, this chapter mainly focuses on the results of the experiments in which the DUTSES model was free in heave and pitch. These experiments are the most representative for the problem of a real
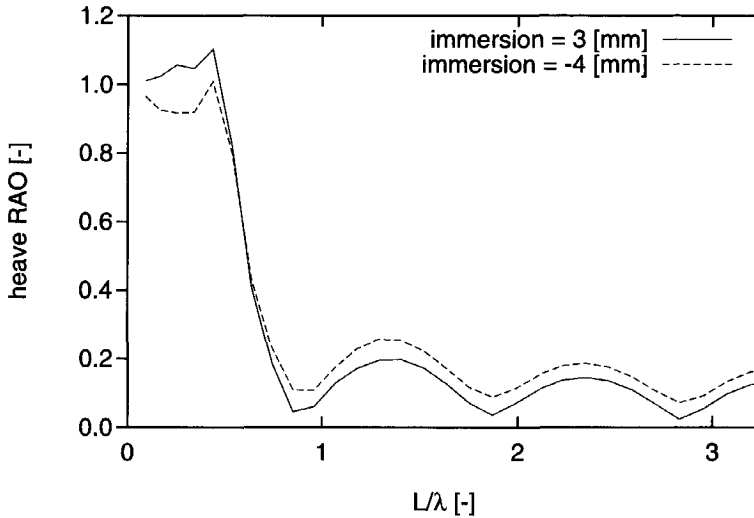
Figure 5.1: The effect of the bow seal immersion on the heave RAO of the DUTSES model

SES sailing in waves. In some cases this chapter also presents results of the forced oscillation and wave force experiments, when these results lead to relevant additional information. All results in this chapter concern the model with realistic hulls sailing in head waves at a forward speed of 3.27 [m/s] ($Fn = 0.603$).

5.1   Some remarks on the computations

Almost every computational method requires some kind of tuning before it yields good results. This also applies to the present method. The tuning that was carried out in the present computations concerned the sinkage and trim of the DUTSES model in calm water. This was particularly important because the bow seal of the DUTSES model was designed to skim over the water surface, just without leaving an air leakage gap (in calm water). The computational results in waves strongly depend on whether the bow seal does or does not leave a leakage gap in calm water, particularly when the wave amplitude is small. This is illustrated by Figure 5.1 which shows the effect of the bow seal immersion on the heave RAO of the DUTSES model in 1 [mm] amplitude waves. The sinkage and particularly the trim have a very important effect on the bow seal immersion. It is therefore of great importance that the computed calm water trim and sinkage are correct.

In order to obtain a computed calm water sinkage and trim that corresponded closely to the calm water sinkage and trim of the experiments, a few small modifications to the input of computational method were made. First of all two small additional leakage areas were introduced: one leakage area for leakage out of the stern seal plenum and one leakage area for leakage out of the air cushion. This extra air leakage resulted in a correct calm water cushion and seal excess pressure, and also in a correct sinkage. In the experiments some extra air leakage between the stern seal bag and the hulls also occurred. Furthermore, in order to obtain a correct trim, the center of gravity was moved about 7 [mm] forward and the bow seal was moved about 5 [mm] aft.

5.2 Heave and pitch motions

This section and the following sections carry on with the actual validation of the computational method. Figure 5.2 shows a comparison of the computed and measured heave motions (η_3) of the DUTSES model. The figure presents the mean value of η_3, the amplitude of the first harmonic component of η_3 divided by the incident wave amplitude, and the phase of the first harmonic component of η_3. The data are plotted as a function of L/λ, the cushion length divided by the incident wave length. Results for several incident wave amplitudes (A) are shown. In some cases (large wave amplitude and close to pitch resonance) the computational results are represented by a dashed line. For these results the stern seal linearization that is discussed in Section 3.5.3 was applied because the non-linear iterative procedure for computing the stern seal geometry did not converge.

The results are generally in good agreement. The computed heave amplitude is slightly larger than the measured value. Both computational and experimental results show a small heave amplitude response when the cushion length is a multiple of the wave length. At these wave lengths the incident waves do not change the air cushion volume, which leads to a small excitation of the cushion pressure and heave motions. The correlation of the phase characteristics is good, and the computed and measured mean heave displacement (sinkage) is also satisfactory.

Figure 5.3 shows a comparison of the computed and measured pitch motions (η_5) of the DUTSES model. A dashed line indicates again that the stern seal linearization was applied. The correlation of the amplitude characteristics is good. The computed pitch motion amplitude is only slightly larger than the measured pitch amplitude. The phase characteristics correlate excellently in the lower frequency range, but in the higher frequency range a large difference occurs. The phase of
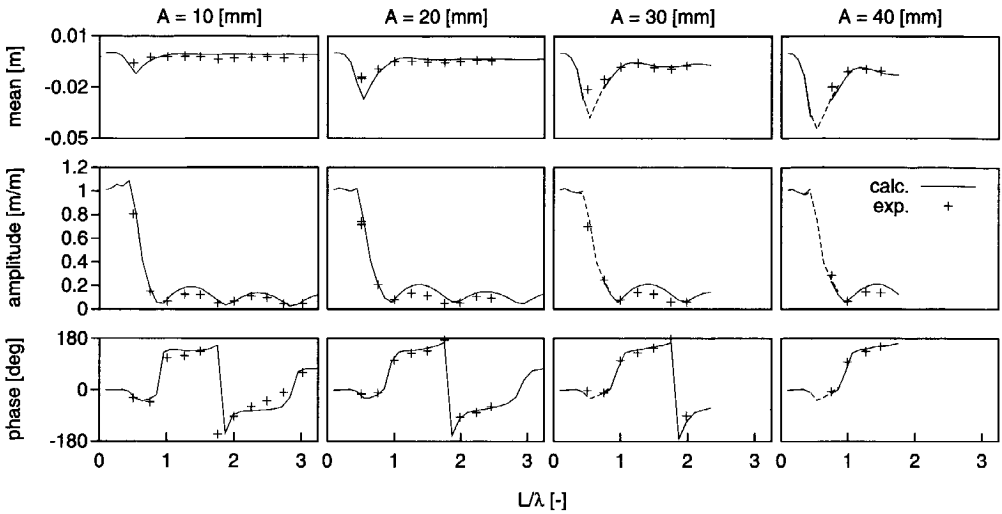
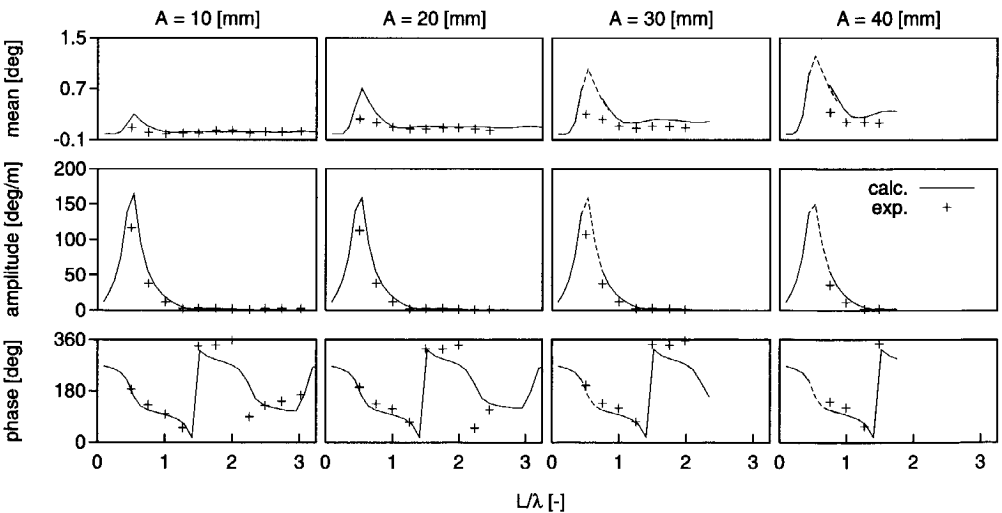Figure 5.2: The mean value, amplitude response and phase of the heave displacement of the DUTSES model

Figure 5.3: The mean value, amplitude response and phase of the pitch displacement of the DUTSES model

an almost zero amplitude signal is however not very relevant. The computed mean pitch displacement is significantly larger than the measured mean pitch displacement, but the trends with wave length and wave height are in good agreement.

Section 3.5.2 presents similar results for the HYDROSES target vessel. When these results are compared to the present results it appears that the correlation for the heave motions is better in the HYDROSES case. The DUTSES results show however a much better correlation for the pitch motions, particularly for the pitch amplitude close to resonance. The latter difference might be explained by the fact that the air cushion of the HYDROSES model was pressurized by fans that were mounted on the carriage, while the air cushion of the DUTSES model was pressurized by fans that were mounted on the model. The tubing which led the air from the fans to the HYDROSES model might have caused a considerable damping of the pitch motions. The HYDROSES results also show the phase difference in the high frequency range.

5.3   Cushion and seal excess pressures

Figure 5.4 presents a comparison of the computed and measured cushion excess pressure (p_c). The air cushion excess pressure was measured at two locations: in the fore and in the aft part of the cushion. The figure presents results of both pressure measurements. The computational and experimental results are in reasonable agreement. The amplitude is again small when the cushion length equals a multiple of the wave length. The computed pressure amplitude is however greater than the measured pressure amplitude. This corresponds to the results for heave motions; the calculated heave amplitude response is also somewhat larger than the experimental one. The correlation of the phase is generally good. The experiments show a phase difference between the fore and aft pressure in the long wavelength range. Such a phase difference does not occur in the computations because the cushion pressure was assumed to be constant in space. The computed and measured mean cushion excess pressure are also in good agreement.

Figure 5.5 shows the computational and experimental results for the stern seal pressure. They are in reasonable agreement. The computed amplitude is again much larger than the measured amplitude, but the correlations for the phase and for the mean value are reasonable.

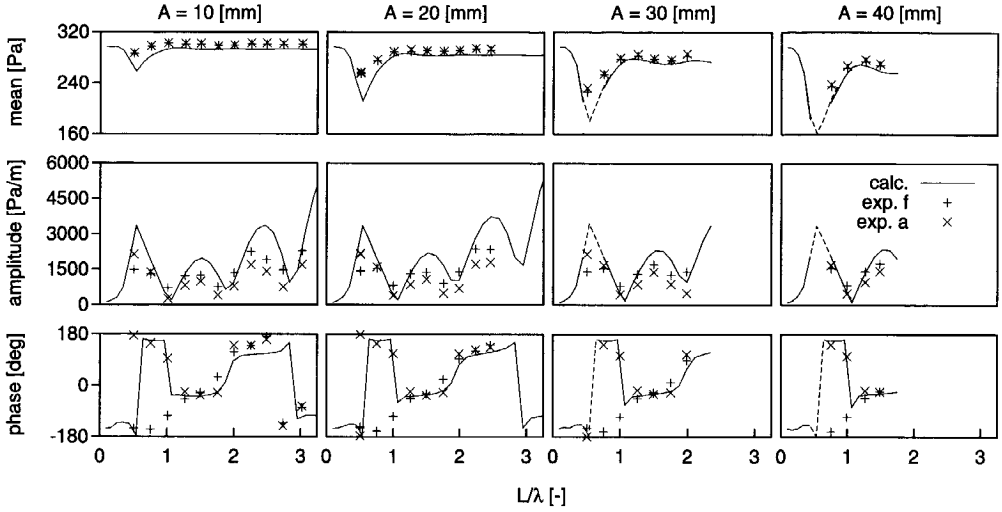The occurrence of higher harmonic components is an important effect of the non-

Figure 5.4: The mean value, amplitude response and phase of the cushion excess pressure p_c (model free in heave and pitch)
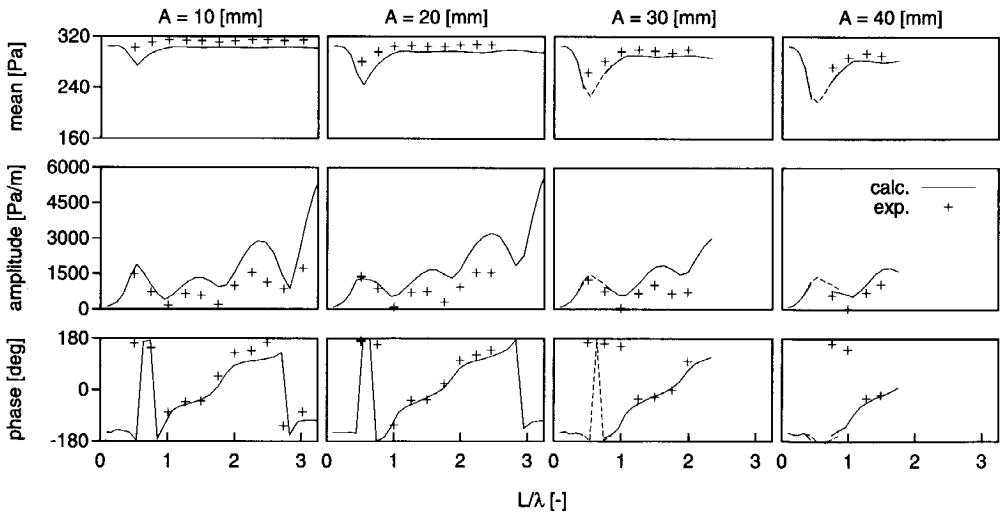

Figure 5.5: The mean value, amplitude response and phase of the stern seal excess pressure p_s (model free in heave and pitch)

linear cushion and seal dynamics. These higher harmonics are most prominent in the cushion and seal excess pressures. Figure 5.6 presents the amplitude and phase of the first, the second and the third harmonic component of the air cushion pressure. The correlation of the amplitude characteristics is good, but the phase characteristics do not agree very well. The phase of the higher harmonic components depends strongly on the opening and closing of the leakage gaps under the seals. Air leakage is the most important non-linear phenomenon in the air cushion dynamics. It is the main cause for the higher harmonics. The exact moment of the opening or the closure of the seals is difficult to predict.

Figure 5.7 also shows amplitude and phase characteristics of the first second and third harmonic component of the cushion pressure. These results follow however from forced pitch oscillation experiments in calm water. The pitch amplitude was 0.02 [rad], and the results are plotted as a function of the oscillation frequency. In this case the second harmonic component is even larger than the first one. Pitch motions do not change the volume of the air cushion. Therefore the cushion pressure is only excited by air leakage under the seals, which results in small pressure variations and relatively large higher harmonics. The correlation of the phase of the second and third harmonic component is good. This is probably due to the fact that in this case the prediction of the moments at which the leakage gaps under the seals open or close is relatively easy.

Another remarkable aspect of Figure 5.7 is the phase shift of the first harmonic components of the pressures that were measured in the fore and aft parts of the air cushion. Such a phase difference also occurred in Figure 5.4 around $L/\lambda = 1$. At this wave length the cushion pressure variations are only small, while the model carried out significant pitch motions, just like during the forced pitch oscillations. This can be explained by the fact that a large amount of air leakage causes internal air flows inside the air cushion, which results in spatial pressure variations. When waves or heave motions induce significant cushion volume variations and consequent pressure variations, the effect of the spatial variations is only small. It is not expected that the phase difference is caused by the vertical acceleration of the pressure transducers since the resonance frequency of the pressure transducers was much higher than the oscillation frequency.

5.4 Seal forces

At the end of Chapter 3 some doubt was cast on the accuracy of the computed seal forces. It appeared that the seal forces had only a small effect on the pitch motions,
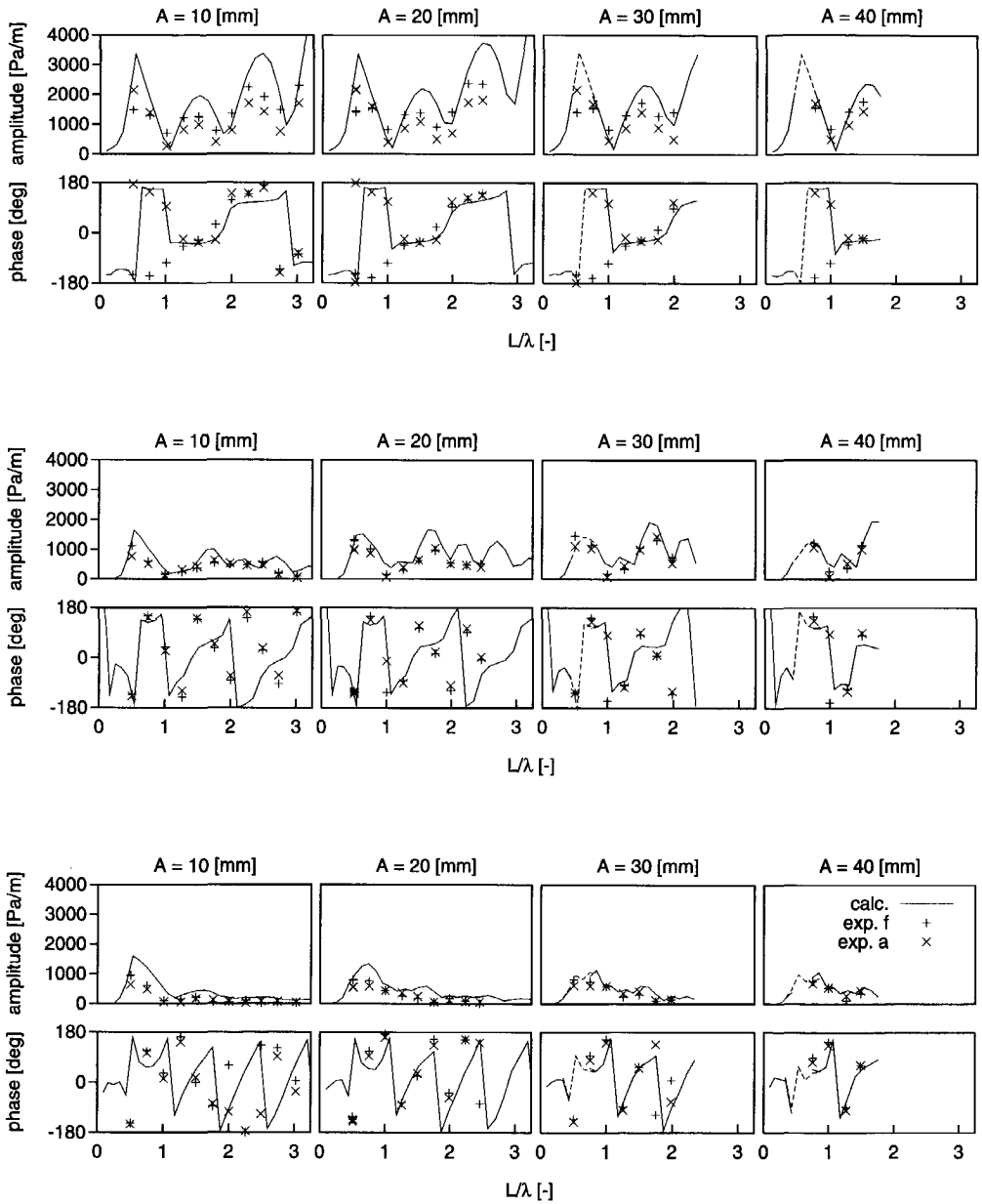
Figure 5.6: The first (top), second (middle) and third (bottom) harmonic component of the cushion excess pressure p_s (model free in heave and pitch)
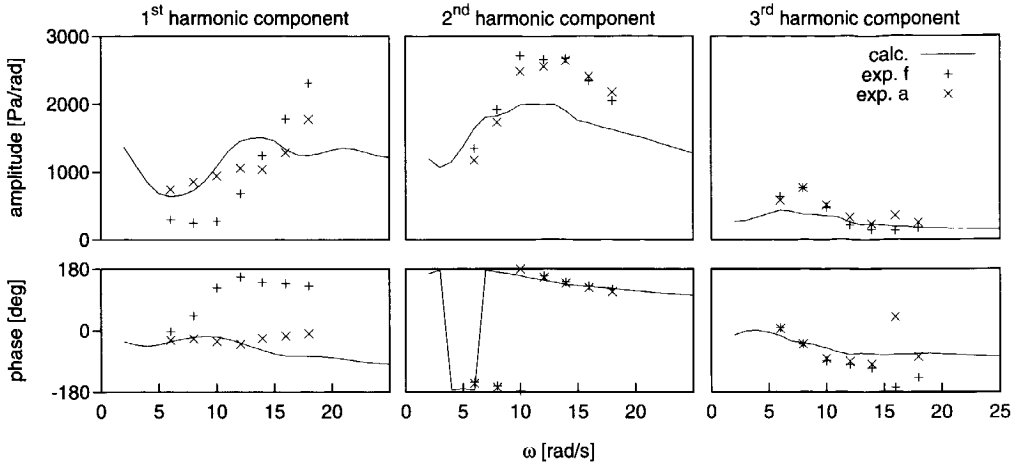
Figure 5.7: The first, second and third harmonic component of the cushion excess pressure (p_s) due to forced pitch oscillations

but other investigators found that the stern seal forces are very important for pitch motions. This section presents a comparison of computed and measured seal forces in order to check the validity of the seal models.

Figure 5.8 and Figure 5.9 show comparisons of the computed and measured bow seal forces, and Figure 5.10 and Figure 5.11 show comparisons of the computed and measured stern seal forces. The correlation of computational and the experimental seal forces is generally good. There are however some differences.

In most cases the computed and measured mean values are shifted with respect to each other. The measured mean longitudinal seal forces (F_{b1} and F_{s1}) are smaller than their computed counter parts. This may be explained by the fact that the viscous resistance of the seals is not included in the calculations. Furthermore the measured vertical bow seal force (F_{b1}) is larger than the computed one. This can be explained by the sticking phenomenon of the bow seal that was discussed in Section 4.6.3. This cannot however explain the complete difference. The trends of the computed and measured mean seal forces are however in excellent agreement.

The amplitude of the longitudinal bow seal force (F_{b1}) does not show the characteristic maxima and minima. This also leads to a somewhat smoother phase characteristic. The most remarkable difference is perhaps that the measured amplitude of the vertical stern seal force (F_{s3}) is much smaller than the computed one. This is remarkable since the results for the longitudinal seal force amplitude, which seems

Figure 5.8: The mean value, amplitude response and phase of the longitudinal bow seal force (F_{b1}) in head waves (model free in heave and pitch)

Figure 5.9: The mean value, amplitude response and phase of the vertical bow seal force (F_{b3}) in head waves (model free in heave and pitch)
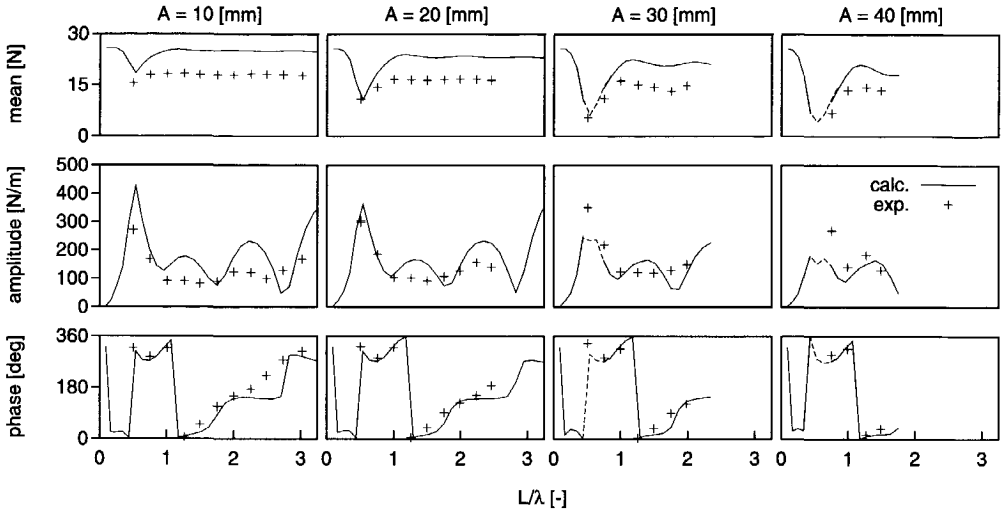
Figure 5.10: The mean value, amplitude response and phase of the longitudinal stern seal force (F_{s1}) in head waves (model free in heave and pitch)
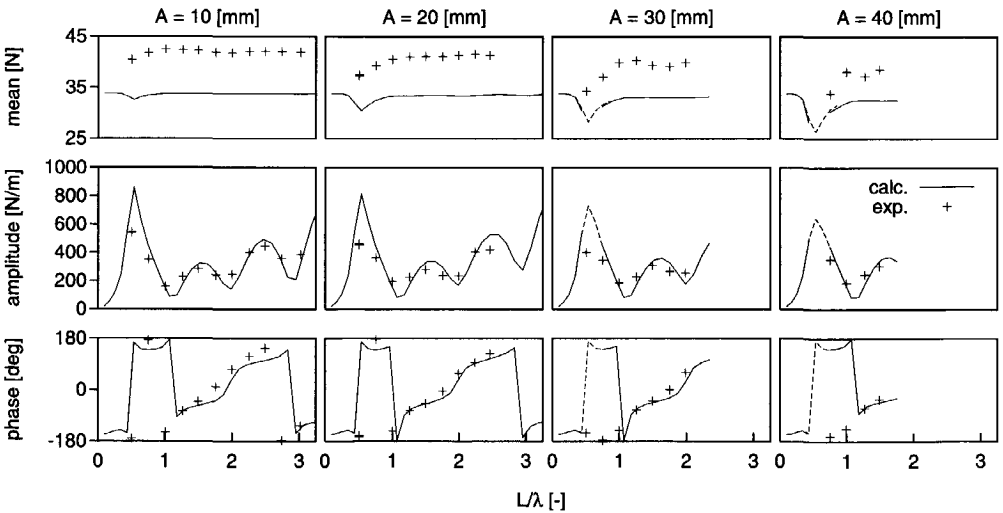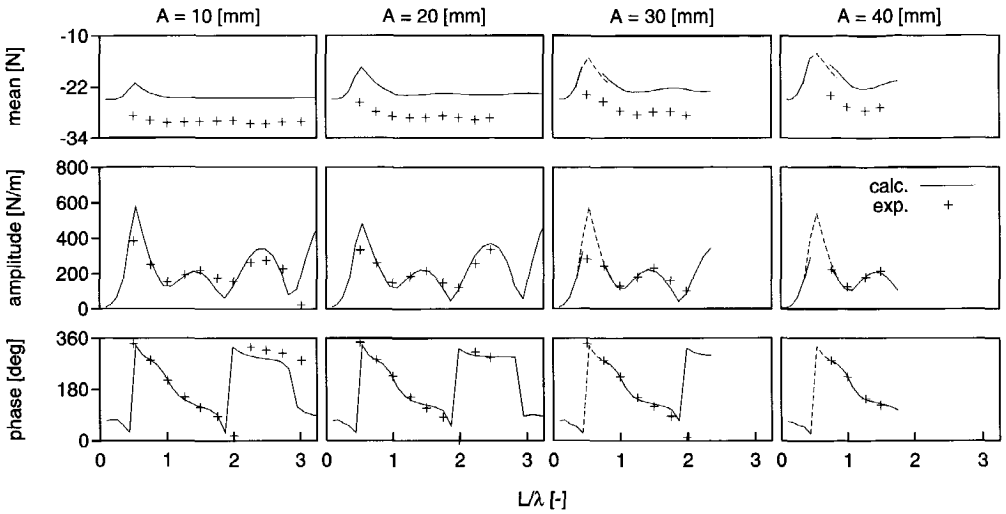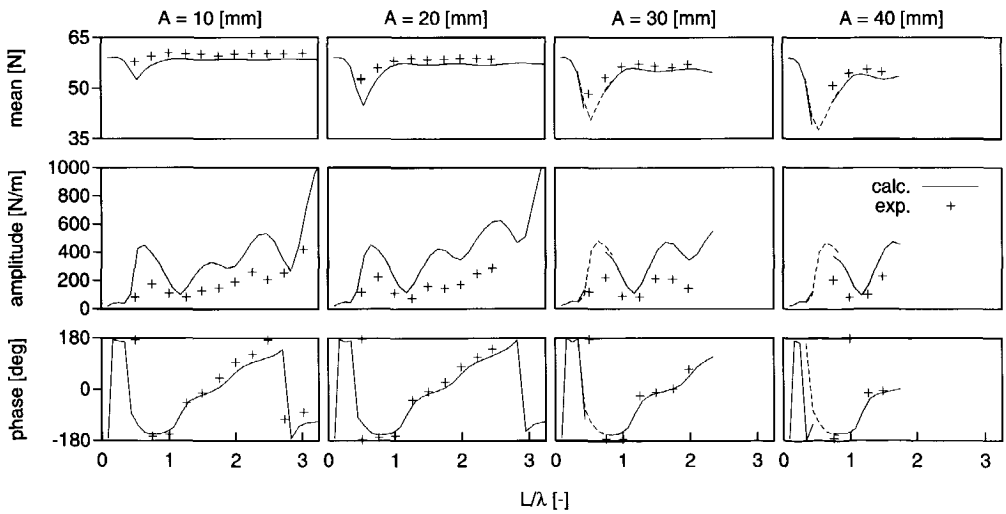

Figure 5.11: The mean value, amplitude response and phase of the vertical stern seal force (F_{s3}) in head waves (model free in heave and pitch)

even harder to compute, are excellent. The correlation for the phase characteristic of F_{s3} is good.

In general the correlation of the computational and the experimental seal forces is good. This indicates that the seal models are valid. Together with the good correlation of the pitch motions (Figure 5.3), this confirms the conclusion of Section 3.5.3 that the seal forces only have a small effect on the pitch motions.

5.5   The behavior of the fans

In the computational method the flow through the fans is approximated by means of the linearized static fan characteristic. Many authors show however that the fans respond in a dynamical way to pressure variations in the plenum that they pressurize (see Section 3.2.2). Furthermore Section 3.5.3 demonstrated that the fans have a very important damping effect on pressure variations and therewith on heave motions. Therefore this section presents results on the behavior of the fans.

Figure 5.12 shows the behavior of the fans during the experiments where the model was free in heave and pitch (i.e. heave and pitch motion experiments). It presents the amplitude of the volume flux through the cushion fan ($Q_{c,f}^{(in)}$) divided by the amplitude of the cushion excess pressure (p_c), and the amplitude of the volume flux through the stern seal fan ($Q_s^{(in)}$) divided by the amplitude of the stern seal excess pressure (p_s). It also presents the relative phases of the volume fluxes with respect the corresponding excess pressures. In the computational method the flow trough the fans is approximated by means of the linearized static fan characteristics. The slope of the static characteristic of the cushion and seal fans was estimated at -0.00029 [m^3/s/Pa]. Hence the computational results in Figure 5.12 are a constant amplitude relation of 0.00029 [m^3/s/Pa] and a phase relation of 180 [deg].

The experimental results are very much scattered. The reason for this scattering is not clear. Figure 5.13 shows the behavior of the fans during the wave force experiments. These results are not so much scattered. The results of the forced oscillation tests also show only a small amount of scatter.

Based on Figure 5.13 it can be concluded that the air flow trough the fans can be approximated by the linearized static fan characteristic with reasonable accuracy. In general the measured amplitude response is somewhat smaller than the slope of the static characteristic. The phase of the air flow with respect to the pressure is always
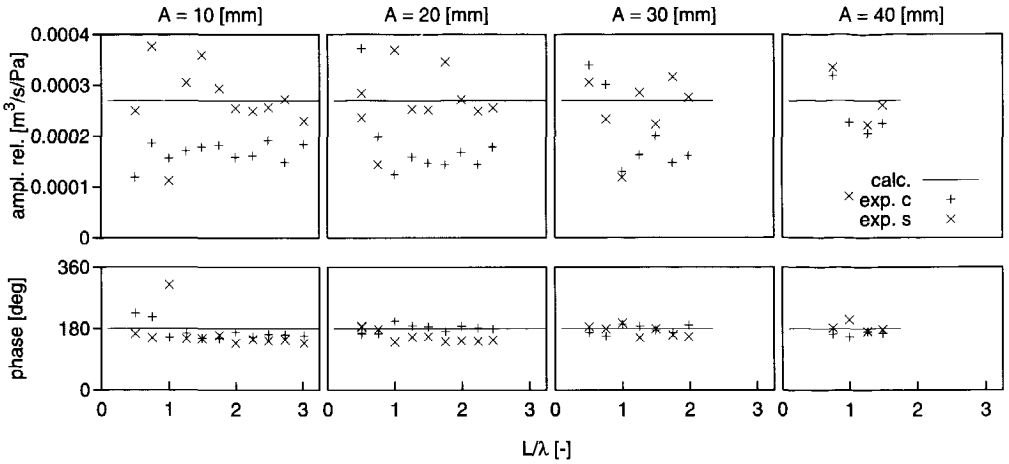
Figure 5.12: The behavior of the fans during the experiments where the DUTSES model was free in heave and pitch and the corresponding computations
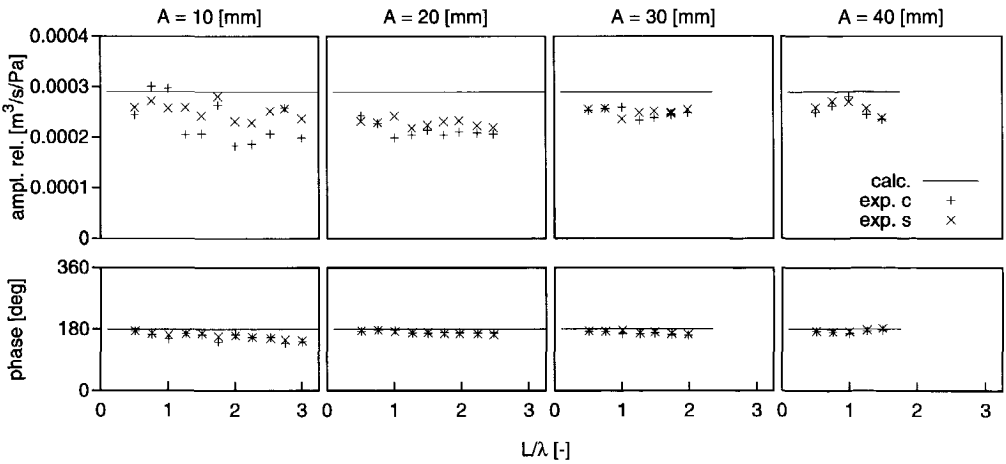

Figure 5.13: The behavior of the fans during the wave exiting force experiments and the corresponding computations
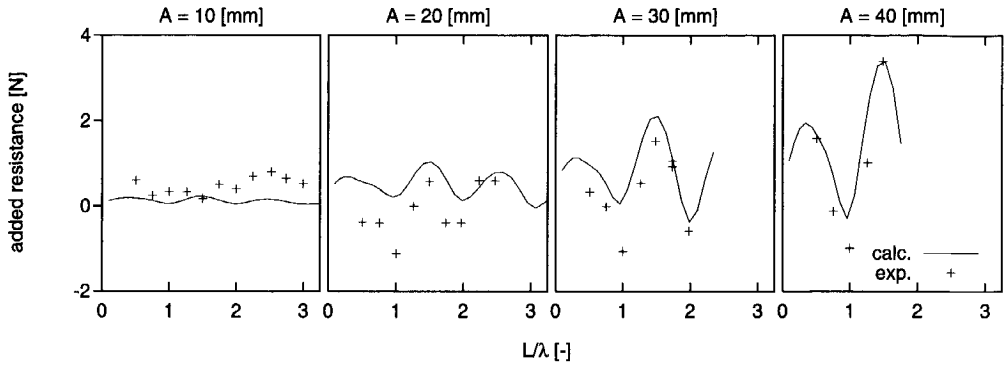
Figure 5.14: The added resistance of the air cushion ($R_{aw}^{(ac)}$) (restrained model)

close to 180 [deg], which means that the axial fans that were used in the present experiments do respond in reasonably static way. The knowledge of the behavior of real size air cushion lift fans is however still very limited.

5.6 Added resistance due to waves

This section presents a comparison of the computed and the measured added resistance of the DUTSES model. The computational method only calculates the added resistance of the air cushion. The experiments that were presented in Chapter 4 showed however that the contribution of the air cushion to the total added resistance is only of minor importance, and that the major contribution is due to the hulls. The experiments also showed that the large added resistance of the hulls is mainly caused by sinkage of the vessel while sailing in waves. Therefore this section also investigates to what extent the computational method can be applied for the prediction of the added resistance due to sinkage.

Figure 5.14 shows results for the added resistance of the air cushion. These results follow from experiments and computations where the DUTSES model was restrained in its mean position while it was towed in waves (i.e. wave force experiments). In this setup we measured the largest added resistance of the air cushion. The figure presents the added resistance of the air cushion as a function of L/λ, the air cushion length divided by the wave length. It presents results for several wave amplitudes.

The correlation of the computational and experimental results is very satisfactory. The actual values do differ significantly for the smaller wave amplitudes, but
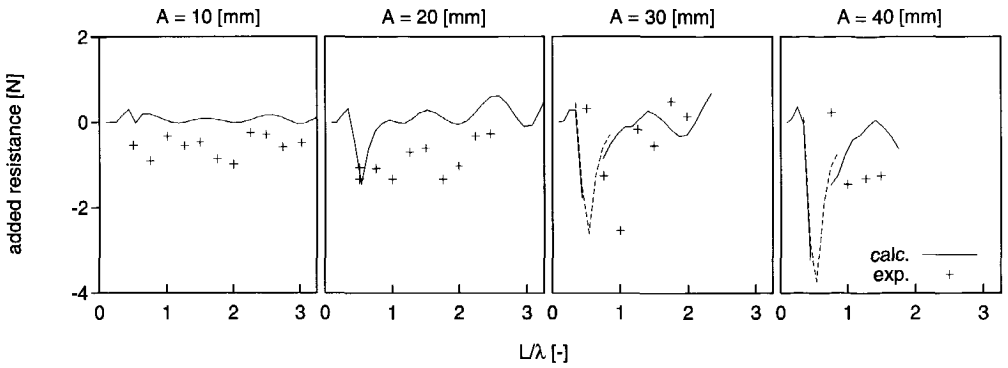
Figure 5.15: The added resistance of the air cushion $R_{aw}^{(ac)}$ (model free in heave and pitch)
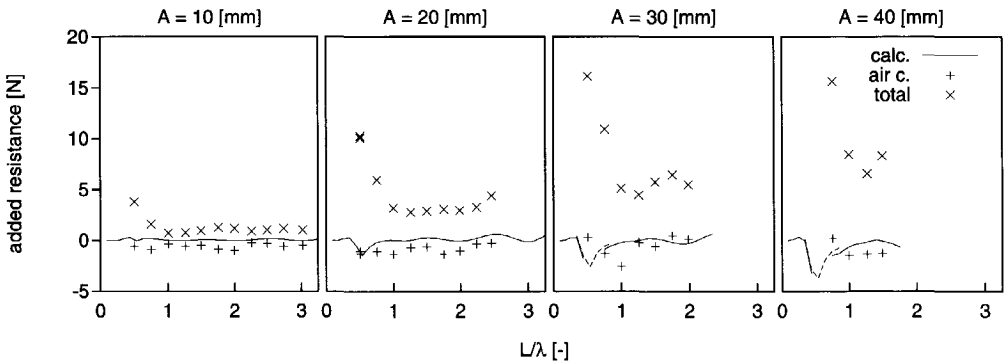
Figure 5.16: Comparison of the added resistance of the air cushion $R_{aw}^{(ac)}$ with the total added resistance R_{aw}

the trends of the added resistance of the air cushion with wave height and wave length are in good agreement. One should also realize that the measurement of the added resistance of the air cushion is very complex which leads to some scattering of the results. This scattering particularly emerges when wave amplitude is small.

Figure 5.15 also shows results for the added resistance of the air cushion. These results follow however from experiments and computations where the DUTSES model was free in heave and pitch (i.e. motion experiments). In this figure the dashed line again indicates that the stern seal linearization, which was discussed in Section 3.5.3, was applied.

The correlation is not as good as in Figure 5.14, where the DUTSES model was restrained. Both calculations and experiments lead to a small and in many cases even negative added resistance of the air cushion. The experiments do not show a clear trend. In Section 4.6.3 in Chapter 4 doubt was cast on the accuracy of the measurement of the added resistance of the air cushion in the heave and pitch motion experiments. The accuracy was affected by sticking of the soaked finger-type bow seal to the hulls, which resulted in a poor accuracy of the bow seal force measurement. This explains the scattering of the experimental results in Figure 5.15.

Figure 5.16 shows the measured total added resistance, next to the measured and computed added resistance of the air cushion. When compared to the total added resistance, the correlation of the computed and measured added resistance of the air cushion is good; both are small. This figure also shows that the goal of the research project that lies at the root of this thesis (the development and validation of a computational method for the added resistance of SESs) has not been accomplished yet. Therefore we will now investigate into the applicability of the computational method for the prediction of the added resistance due to sinkage.

The experiments that were presented in Chapter 4 showed that the added resistance of the hulls is the largest contribution to the added resistance of SESs. They also showed that the large added resistance of the hulls is mainly caused by sinkage of the vessel due to a drop of the cushion pressure. This pressure drop is caused by an increase of the air leakage flow out of the cushion when the vessel sails in waves. Section 5.2 and Section 5.3 showed that the computational method can compute the drop of the cushion pressure and the consequent sinkage and trim with good accuracy.

In Chapter 4 linear relations were derived for the resistance, the resistance of the air cushion and the resistance of the hulls as a function of the cushion excess pressure. These relations were used to determine the total added resistance due to sinkage, the added resistance of the air cushion due to sinkage and the added resistance of the hulls due to sinkage by substituting the measured mean cushion pressure.

These relations can also be used with the computed mean cushion pressure. Figure 5.17 presents a comparison of the thus semi-computed added resistance of the hulls due to sinkage with the measured added resistance of the hulls. The correlation of these data is excellent. This is not very surprising because the computational and experimental results for the mean cushion pressure were in good agreement too (see Figure 5.4). It shows however that the computational method can be very useful in the calculation of the added resistance of the hulls.
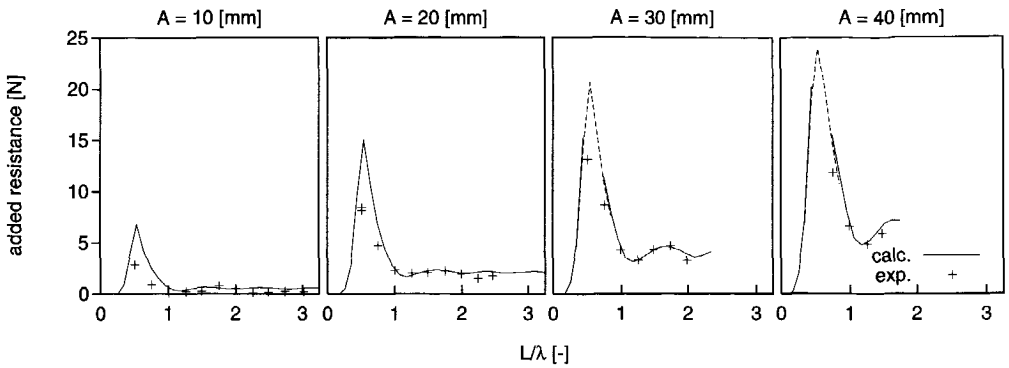
Figure 5.17: Comparison of the added resistance due to sinkage of the hulls $R_{aws}^{(h)}$
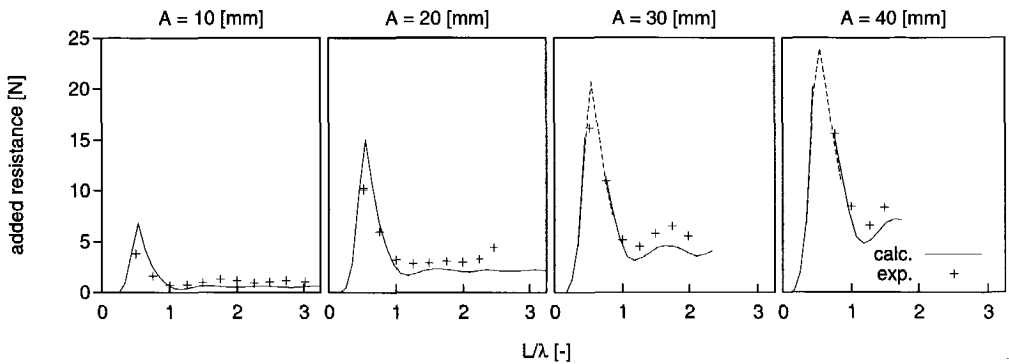
Figure 5.18: Comparison of the measured total added resistance (R_{aw}) with the sum of the computed added resistance of the air cushion and the semi-computed added resistance due to sinkage of the hulls ($R_{aw}^{(ac)} + R_{aws}^{(h)}$)

Figure 5.18 presents a comparison of the measured total added resistance with the sum of the computed added resistance of the air cushion and the semi-computed added resistance due to sinkage of the hulls. Please note that the thus computed added resistance does not include the added resistance due to wave radiation of the hulls. The data are in good agreement. It is therefore expected that inclusion of the added resistance due to sinkage of the hulls in the computational method will result in a method that gives a reasonably accurate prediction of the added resistance due to waves of Surface Effect Ships.

The added resistance of the hulls due to sinkage is basically an increase of the calm water resistance of the hulls which is caused by a larger draft of the vessel. The computational method can compute the drop of the cushion pressure and the consequent sinkage and trim with good accuracy. The work that still remains to be done is the development of an accurate method for the prediction of the calm water resistance of the hulls at different drafts.

5.7   Conclusions

This chapter presented a comparison of computational and experimental results. From this comparison the following conclusions can be drawn:

- The correlation of the computational and experimental results for heave and pitch motions, excess pressures, seal forces and behavior of the fans is generally good. The computed and measured mean values are also in satisfactory agreement. This subscribes the validity of the computational method.

- The computed and measured added resistance of the air cushion are also in good agreement.

- The computational method does *not* include the most important contribution to the added resistance; the added resistance of the hulls due to sinkage.

- The computational method can be very useful for the prediction of the added resistance of the hulls due to sinkage, because it can compute the drop of the cushion pressure and the consequent sinkage and trim with good accuracy.

Chapter 6

Conclusions

In the scope of the research question that was put in the introduction of this thesis (see Section 1.4) the following conclusions are drawn. One should however realize that these conclusion follow from a somewhat indirect analysis.

- The hulls give the major contribution to the added resistance of SESs. This follows from the experiments that are presented by Chapter 4. These experiments also show that the large added resistance of the hulls is mainly caused by the mechanism of sinkage[1].

- According to the experiments the added resistance of the air cushion and the added resistance of the hulls due to wave radiation (i.e. the added resistance that is experienced by conventional ships) are of minor importance. The hypothesis that the large added resistance of SESs is caused by the air cushion is therefore rejected.

- A computational method for the added resistance due to waves of Surface Effect Ships must at least compute the added resistance of the hulls due to sinkage. The computational method that is presented by Chapter 2 and Chapter 3 does *not* include the added resistance of the hulls due to sinkage. The goal of the research project that lies at the root of this thesis, the development

---

[1] Added resistance due to the mechanism of sinkage particularly occurs with Surface Effect Ships. When an SES sails in a seaway the amount of air leakage out of the air cushion increases because the motions of the vessel and the incident waves cause significant leakage gaps under the bow and stern seals. This results in a drop of the air cushion excess pressure. This subsequently leads to a larger draft of the hulls, because a larger part of the vessel's weight must be carried by buoyancy of these hulls. This sinkage results in an increase of the resistance of the hulls that is called the added resistance of the hulls due to sinkage. It is basically an increase of the calm water resistance of the hulls.

and validation of a computational method for added resistance of SESs, has therefore not been fully accomplished yet.

- The computational method can accurately compute the sinkage of an SES sailing in waves. This is the first important step towards the computation of the added resistance of the hulls due to sinkage. The second step, which is the calculation of the extra (calm water) resistance due to this sinkage, still needs to be implemented.

- The computational and the experimental results for the added resistance of the air cushion are in good agreement. The added resistance of the air cushion is however of minor importance.

- Air leakage is an important and highly non-linear phenomenon. It is crucial in the computation of the cushion pressure drop and the consequent sinkage due to waves.

Furthermore the computational method yields results for motions, excess pressures and seal forces that are generally in good agreement with experimental results. From these results the following conclusions, that are only of indirect relevance for the research question of Section 1.4, can be drawn:

- Air leakage has an important effect on the cushion pressure variations and heave motions. It appears to have a significant damping effect on the cushion pressure variation, particularly leakage under the stern seal. Furthermore air leakage also excites cushion pressure variations. It particularly excites higher harmonic components in the cushion excess pressure.

- The air supply system (fans) has an important damping effect on the cushion pressure.

- The effect of the interaction of the air cushion with the wave surface is significant, although it is not very large. The interaction causes a considerable shift of the Helmholtz resonant frequency. This resonance is however damped to a large extent by air leakage and the fans.

- The seals have an important effect on the cushion dynamics and thereby on the heave motions. The direct effect of the seals on the motions by means of the seal forces is only limited. The seals only have a small effect on pitch motions.

The following recommendations for further research are made:

- It is recommended to extend the computational method with a module that computes the added resistance of the hulls due to sinkage. The computational method can already compute the sinkage of an SES due to waves. The work that remains to be done is the development and validation of a method that computes the increase of the (calm water) resistance due to this sinkage. This requires further research into the calm water resistance of SESs.

- The fans have a very important damping effect on cushion dynamics. The axial fans that were used in the experiments of Chapter 4 could be modeled by a simple static fan model with reasonable accuracy. It remains however to be seen whether this also applies to full scale radial fans. Therefore further research into the behavior of air cushion lift fans is recommended.

Appendix A

The frequency domain and the time domain

This Appendix treats the interrelation of the frequency domain and the time domain with respect to ship motions. It presents theory that was developed in the early sixties by Cummins[56] and Ogilvie[57]. Furthermore it presents the actual implementation of the transformation of the frequency domain results of the panel method (Chapter 2) to the time domain. The time domain results are used in a non-linear time simulation method (Chapter 3).

A.1 Introduction

Naval architects are very much used to the frequency domain formulation of the equations of motion of a ship:

$$\sum_{k=1}^{6}\left\{(M_{jk}+A_{jk}(\omega))\ddot{\eta}_k(t) + B_{jk}(\omega)\dot{\eta}_k(t) + C_{jk}\eta_k(t)\right\} = X_j(t) \quad \text{for } j = 1,\ldots,6$$

$$(A.1)$$

In 1962 Cummins[56] presented an alternative formulation for the equations of motion of ships. He developed this formulation because of a dissatisfaction with the frequency domain formulation. A quotation:

> *In fact we appear to have forgotten that we are wearing a shoe which doesn't quite fit. The "shoe" to which I refer is our mathematical model, the forced representation of the ship response by a system of second order differential equations. The shoe is squeezed on, with no regard for the shape of the foot. The inadequacy of the shoe is evident*

in the distortions it must take if it is to be worn at all. I am referring, of course, to the frequency dependent coefficients [Equation A.1] which permit the mathematical model to fit the physical model.

Indeed Equation A.1 only holds when the forcing function $X_j(t)$ is purely sinusoidal with frequency ω. Furthermore the distribution of the in-phase hydrodynamic reaction force over the added mass and the restoring coefficient is quite arbitrary. Equation A.1 could for instance just as well be written as:

$$\sum_{k=1}^{6}\left\{M_{jk}\ddot{\eta}_k(t) + B_{jk}(\omega)\dot{\eta}_k(t) + (C_{jk} - \omega^2 A_{jk}(\omega)\eta_k(t)\right\} = X_j(t) \qquad \text{(A.2)}$$

The restoring coefficient C_{jk} is often defined in such a way that it only includes the hydrostatic part of the restoring force. When the velocity of the ship is non-zero, this causes $A_{jk}(\omega)$ to become infinite when ω tends to zero. When C_{jk} is defined in such a way that it also also includes the hydrodynamic part of the restoring force $A_{jk}(\omega)$ remains finite when ω tends to zero. Cummins developed a mathematical model which permits the representation of the response of a ship to an arbitrary forcing function. This model did not involve any frequency dependent parameters. Cummins made one major assumption: linearity of the system. This is also the most important underlying assumption of the frequency domain formulation.

In 1964 Ogilvie[57] presented relations between the equations of motion in the frequency domain and the equations of motion in the time domain. He showed that the frequency domain equations of motion and the equations of Cummins are fully equivalent. He also showed how to transform the frequency domain coefficients and the coefficients and impulse response function which occurs in the time domain expression into one another.

In 1976 van Oortmersen[58] used the equations of Cummins in computations of motions of moored ships in waves. This enabled the inclusion of non-linear mooring forces in the simulations, while the hydromechanical problem was solved in the frequency domain.

In the present study the motions and non-linear air cushion dynamics are solved in a time simulation procedure, while the linearized hydromechanical problem is solved in the frequency domain. The next section presents some theory on impulse response functions. This theory will be used in subsequent sections which present the theory of Cummins and the interrelation of the time domain and frequency domain expressions.

A.2   Impulse response functions

The response of a linear system to an arbitrarily shaped forcing function can be represented by means of an impulse response function. An Impulse response function gives the quantified response of a system to a unit impulsive input at $t = 0$. This unit impulsive input is also known as the δ-function (or δ-distribution as it is formally not a function). The δ-function $\delta(t)$ is defined as $\lim_{\Delta t \to 0} \delta_\Delta(t)$, where

$$\delta_\Delta(t) = 0 \quad \text{if} \quad t \notin [0, \Delta t] \quad , \text{and} \quad \delta_\Delta(t) = \frac{1}{\Delta t} \quad \text{if} \quad t \in [0, \Delta t] \qquad \text{(A.3)}$$

Because of the linearity of the system the response to several impulses (which act at different moments) can be superimposed. This means that the response (r) to a continuous input (x) can be expressed as a convolution of the impulse response function and input from the past:

$$r(t) \;=\; \int_{-\infty}^{t} h(t - t')\, x(t')\, dt' \qquad \text{(A.4)}$$

The convolution integral represents the *memory* of the system. When $t - t'$ is substituted by τ, Equation A.4 can also be written as:

$$r(t) \;=\; \int_{-\infty}^{\infty} h(\tau)\, x(t - \tau)\, d\tau \qquad \text{(A.5)}$$

where the integration boundaries could be changed to $-\infty$ and ∞ because $h(t) = 0$ when $t < 0$ due to causality.

An impulse response function is related to a corresponding complex harmonic response function by means of a Fourier transform. A complex harmonic response function $H(\omega)$ gives the (complex) harmonic response of a system to a (complex) harmonic input:

$$\hat{r} \;=\; H(\omega)\, \hat{x} \qquad \text{(A.6)}$$

where $r(t) \;=\; \Re\{\hat{r}\, e^{i\omega t}\}$ and $x(t) \;=\; \Re\{\hat{x}\, e^{i\omega t}\}$. The relation of $h(t)$ and $H(\omega)$ reveals itself when a harmonic input is substituted:

$$r(t) \;=\; \Re\{H(\omega)\, \hat{x}\, e^{i\omega t}\} \qquad \text{(A.7)}$$

or

$$r(t) \; = \; \int_{-\infty}^{\infty} h(\tau) \, \Re\{\hat{x} \, e^{i\omega(t-\tau)}\} \, d\tau = \Re\Big\{ \int_{-\infty}^{\infty} h(\tau) \, e^{-i\omega\tau} d\tau \cdot \hat{x} \, e^{i\omega t} \Big\} \qquad \text{(A.8)}$$

Apparently $h(t)$ and $H(\omega)$ are a Fourier transform pair:

$$H(\omega) \;\; = \;\; \int_{-\infty}^{\infty} h(t) e^{-i\omega t} dt$$

$$h(t) \;\; = \;\; \frac{1}{2\pi} \int_{-\infty}^{\infty} H(\omega) e^{i\omega t} d\omega \qquad \text{(A.9)}$$

The Fourier transform exists when when the following integral exists:

$$\int_{-\infty}^{\infty} |h(t)| \, dt \qquad \text{(A.10)}$$

For stable systems it generally does.

A.3 Cummins' Equation

This section presents the time domain equations of Cummins. Cummins derived his equations from a mathematical description of the hydromechanical problem of a ship sailing in waves.

From now on we will merely focus on the hydromechanic reaction force instead of on the full equations of motion. The hydromechanic reaction force is the force which acts on the wetted surface of a vessel due to it's motions. The frequency domain expression for the hydromechanic reaction force reads:

$$F_j \; = \; -\sum_{k=1}^{6}\Big\{ A_{jk}(\omega)\ddot{\eta}_k(t) \; + \; B_{jk}(\omega)\dot{\eta}_k(t) \; + \; C_{jk}\eta_k(t) \Big\} \qquad \text{(A.11)}$$

The equations of motion reappear when $F_j + X_j$ is set equal to $\sum_{k=1}^{6} M_{jk}\ddot{\eta}_k$, where X_j is the forcing function.

First the boundary value problem for a ship oscillating in otherwise calm water while sailing at a constant mean velocity U is recapitulated:

$$\Delta \varphi = 0$$

$$g \frac{\partial \varphi}{\partial z} + \frac{\partial^2 \varphi}{\partial t^2} - 2U \frac{\partial^2 \varphi}{\partial x \partial t} + U^2 \frac{\partial^2 \varphi}{\partial x^2} = 0 \qquad \text{on } z = 0$$

$$\nabla \varphi \cdot \vec{n} = \sum_{k=1}^{6} \left(\frac{\partial \eta_k}{\partial t} n_k + \eta_k m_k \right) \qquad \text{on } \bar{B}$$

$$\text{Radiation Condition} \tag{A.12}$$

Cummins proposes a solution of the following form:

$$\varphi(x, y, z, t) = \sum_{k=1}^{6} \Big\{ \theta_{nk}(x, y, z) \dot{\eta}_k(t) + \theta_{mk}(x, y, z) \eta_k(t) + \\ \int_{-\infty}^{t} \vartheta_{nk}(x, y, z, t - \tau) \dot{\eta}_k(\tau) \, d\tau + \\ \int_{-\infty}^{t} \vartheta_{mk}(x, y, z, t - \tau) \eta_k(\tau) \, d\tau \Big\} \tag{A.13}$$

The potentials $\theta_{nk}(x, y, z)$ and $\theta_{mk}(x, y, z)$ must fulfill the following boundary conditions:

$$\nabla \theta_{nk} \cdot \vec{n} = n_k \qquad \nabla \theta_{mk} \cdot \vec{n} = m_k \qquad \text{on } (\bar{B})$$

$$\theta_{nk} = 0 \qquad \theta_{mk} = 0 \qquad \text{on } z = 0$$

The potentials $\vartheta_{nk}(x, y, z, t)$ and $\vartheta_{mk}(x, y, z, t)$ have to fulfill these boundary conditions:

$$\nabla \vartheta_{nk} \cdot \vec{n} = 0 \qquad \nabla \vartheta_{mk} \cdot \vec{n} = 0 \qquad \text{on } (\bar{B})$$

$$g \frac{\partial \vartheta_{nk}}{\partial z} + \frac{\partial^2 \vartheta_{nk}}{\partial t^2} - 2U \frac{\partial^2 \vartheta_{nk}}{\partial x \partial t} + U^2 \frac{\partial^2 \vartheta_{nk}}{\partial x^2} = 0 \qquad \text{on } z = 0$$

$$g \frac{\partial \vartheta_{mk}}{\partial z} + \frac{\partial^2 \vartheta_{mk}}{\partial t^2} - 2U \frac{\partial^2 \vartheta_{mk}}{\partial x \partial t} + U^2 \frac{\partial^2 \vartheta_{mk}}{\partial x^2} = 0 \qquad \text{on } z = 0$$

Besides $\vartheta_{nk}(x, y, z, t)$ and $\vartheta_{mk}(x, y, z, t)$ must fulfill the initial conditions:

$$\vartheta_{nk} = 0 \qquad \vartheta_{mk} = 0 \qquad \text{for } t \leq 0$$

$$\frac{\partial \vartheta_{nk}}{\partial t} = -g \frac{\partial \theta_{nk}}{\partial z} \qquad \frac{\partial \vartheta_{mk}}{\partial t} = -g \frac{\partial \theta_{mk}}{\partial z} \qquad \text{for } t \downarrow 0$$

ϑ_{nk} and ϑ_{mk} must also fulfill the Radiation Condition. When these conditions are substituted in Equation A.13 it appears that φ fulfills it's boundary conditions.

This paragraph discusses the meaning of the potentials θ_{nk}, θ_{mk}, ϑ_{nk} and ϑ_{mk}. The potential θ_{nk} represents the direct response of the water to unit velocity of the ship in k^{th} direction without free surface effects. The potential θ_{mk} represents the direct response of the water to unit displacement in k^{th} direction without free surface effects. The boundary condition for θ_{nk} and θ_{mk} on $z = 0$ is fulfilled when $(\bar{B})$ is reflected in the surface $z = 0$, and the body boundary condition is taken negative on this reflection.

The potential ϑ_{nk} represents the decaying disturbance of the free surface after a unit impulsive velocity in k^{th} direction. The potential ϑ_{mk} represents the decaying disturbance of the free surface after a unit impulsive displacement in k^{th} direction. ϑ_{nk} and ϑ_{mk} are impulse response functions.

The potentials θ_{nk} and θ_{mk} ensure that the body boundary condition is fulfilled. The potentials ϑ_{nk} and ϑ_{mk} take care of the free surface boundary condition. The potentials that have a subscript m are associated with the *m-terms* of the body boundary condition for φ. They account for the interaction between the unsteady and the bases flow. If the ship has no forward speed the m-terms are zero. In that case these potentials vanish.

The expression for $\varphi(x, y, z, t)$ (Equation A.13) can be rewritten as:

$$
\begin{aligned}
\varphi(x, y, z, t) = \sum_{k=1}^{6} \Big\{ & \theta_{nk}(x, y, z) \dot{\eta}_k(t) + \\
& [\theta_{mk}(x, y, z) + \Theta_{mk}(x, y, z, 0)] \eta_k(t) + \\
& \int_{-\infty}^{t} [\vartheta_{nk}(x, y, z, t - \tau) - \Theta_{mk}(x, y, z, t - \tau)] \dot{\eta}_k(\tau) \, d\tau \Big\}
\end{aligned}
\tag{A.14}
$$

where

$$\Theta_{mk}(x, y, z, t - \tau) = \int_{-\infty}^{\tau} \vartheta_{mk}(x, y, z, t - \tau') \, d\tau'$$

The potentials $\theta_{mk}(x, y, z) + \Theta_{mk}(x, y, z, 0)$ in Equation A.14 are basically a correction to the steady potential due to a constant unit displacement of the vessel ($\eta_k = 1$).

The linearized pressure at the wetted hull surface can be expressed as:

$$p = -\rho\left(gz + \frac{\partial\varphi}{\partial t} - U\frac{\partial\varphi}{\partial x} + (\vec{a}\cdot\nabla)(gz)\right) \qquad \text{on } \bar{B} \qquad (A.15)$$

where $\vec{a}$ is the local displacement of the hull surface. The unsteady part of the pressure on the hull surface is now expressed in terms of the potentials θ_{nk}, θ_{mk}, ϑ_{nk} and ϑ_{mk}:

$$p = -\rho\sum_{k=1}^{6}\left\{\theta_{nk}(x, y, z)\ddot{\eta}_k(t) + \left(\theta_{mk}(x, y, z) - U\frac{\partial}{\partial x}\theta_{nk}(x, y, z)\right)\dot{\eta}_k(t) + \right.$$

$$-U\frac{\partial}{\partial x}\left(\theta_{mk}(x, y, z) + \Theta_{mk}(x, y, z, 0)\right)\eta_k(t) +$$

$$\int_{-\infty}^{t}\left[\frac{\partial}{\partial t}\left(\vartheta_{nk}(x, y, z, t - \tau) - \Theta_{mk}(x, y, z, t - \tau)\right) + \right.$$

$$\left. -U\frac{\partial}{\partial x}\left(\vartheta_{nk}(x, y, z, t - \tau) - \Theta_{mk}(x, y, z, t - \tau)\right)\right]\dot{\eta}_k(\tau)\,d\tau +$$

$$\left. (\vec{a}_k\cdot\nabla)(gz)\right\} \qquad (A.16)$$

The hydrodynamic reaction forces follow from pressure integration over the wetted part of the hull:

$$F_j = -\iint_{\bar{B}} p\,n_j\,dS \qquad j = 1, \ldots, 6 \qquad (A.17)$$

Now F_j can be written as:

$$F_j = -\sum_{k=1}^{6}\left\{a_{jk}\ddot{\eta}_k(t) + b_{jk}\dot{\eta}_k(t) + c_{jk}\eta_k(t) + \int_{-\infty}^{t} h_{jk}(t - \tau)\dot{\eta}_k(\tau)\,d\tau\right\}$$

$$j = 1, \ldots, 6 \qquad (A.18)$$

where

$$a_{jk} = -\rho\iint_{\bar{B}} \theta_{nk}(x, y, z)n_j\,dS$$

$$b_{jk} = -\rho \iint_{\bar{B}} \left(\theta_{mk}(x,y,z) - U\frac{\partial}{\partial x}\theta_{nk}(x,y,z) \right) n_j \, dS$$

$$c_{jk} = -\rho \iint_{\bar{B}} -U\frac{\partial}{\partial x}\left(\theta_{mk}(x,y,z) + \Theta_{mk}(x,y,z,0) \right) n_j \, dS + C_{jk}$$

$$h_{jk}(t) = -\rho \iint_{\bar{B}} \left[\frac{\partial}{\partial t}\left(\vartheta_{nk}(x,y,z,t) - \Theta_{mk}(x,y,z,t) \right) + \right.$$

$$\left. -U\frac{\partial}{\partial x}\left(\vartheta_{nk}(x,y,z,t) - \Theta_{mk}(x,y,z,t) \right) \right] n_j \, dS \quad \text{(A.19)}$$

and

$$(C_{j1}, C_{j2}, C_{j3})^T = \rho_h \iint_{\bar{B}} \nabla(gz) n_j \, dS$$

$$(C_{j4}, C_{j5}, C_{j6})^T = \rho_h \iint_{\bar{B}} (\vec{x} \otimes \nabla)(gz) n_j \, dS$$

The impulse response function $h_{jk}(t)$ is often called *retardation* function.

A.4 The interrelation of the domains

The previous section presented a frequency domain expression (Equation A.11) and a time domain expression (Equation A.18) for the hydromechanic reaction force. This section presents the interrelation of these expressions.

The interrelation of the time domain and frequency domain expressions becomes clear when a harmonic motion is assumed. Substitution of $\eta_{jk}(t) = \Re\{\hat{\eta}_{jk}e^{i\omega t}\}$ into the frequency domain expression leads after some rearranging to:

$$F_j = -\sum_{k=1}^{6} \Re\left\{ \left[-\omega^2 A_{jk}^*(\infty) + i\omega B_{jk}^*(\infty) + C_{jk}^* + i\omega H_{jk}^*(\omega) \right] \hat{\eta}_k e^{i\omega t} \right\} \quad \text{(A.20)}$$

where

$$H_{jk}^*(\omega) = i\omega\left(A_{jk}^*(\omega) - A_{jk}^*(\infty) \right) + \left(B_{jk}^*(\omega) - B_{jk}^*(\infty) \right) \quad \text{(A.21)}$$

Substitution of $\eta_{jk}(t) = \Re\{\hat{\eta}_{jk}e^{i\omega t}\}$ into the time domain expression results in:

$$F_j = -\sum_{k=1}^{6} \Re\left\{ \left[-\omega^2 a_{jk} + i\omega b_{jk} + c_{jk} + i\omega \int_{-\infty}^{\infty} h_{jk}(t)\,e^{-i\omega\tau}d\tau \right] \hat{\eta}_k e^{i\omega t} \right\} \quad \text{(A.22)}$$

Apparently:

$$a_{jk} = A_{jk}^*(\infty)$$
$$b_{jk} = B_{jk}^*(\infty)$$
$$c_{jk} = C_{jk}^*$$
$$H_{jk}^*(\omega) = \int_{-\infty}^{\infty} h_{jk}(t)e^{-i\omega t}dt$$

or

$$h_{jk}(t) = \frac{1}{2\pi} \int_{-\infty}^{\infty} H_{jk}^*(\omega)e^{i\omega t}d\omega$$

The complex harmonic response function $H_{jk}^*(\omega)$ has to be defined according to Equation A.21, otherwise the inverse Fourier transform does not exist. One can prove that a_{jk} and b_{jk} are indeed equal to the high frequency limit of A_{jk}^* and B_{jk}^*. In Section A.3 the coefficients a_{jk} and b_{jk} were expressed in terms of the potentials θ_{nk} and θ_{mk}. These potentials represent the water flow around the hull without free surface effects. The high frequency limit of the frequency domain solution ($\lim_{\omega \to \infty} \varphi_k(x, y, z, \omega)$) represents the same flow. The high frequency limit of the free surface boundary condition for $\varphi_k(x, y, z, \omega)$ reads: $\varphi = 0$. This is the same as the free surface boundary conditions for θ_{nk} and θ_{mk}. The hull surface boundary conditions for on the one hand φ_k, and on the other hand θ_{nk} and θ_{mk} are equivalent too.

It should also be noted that the modified coefficients (A_{jk}^*, B_{jk}^* and C_{jk}^*, defined in Chapter 2) are used. In these modified hydrodynamic coefficients the forward speed effect on the restoring force is incorporated in C_{jk} instead of in A_{jk}. When the usual definition of the coefficients is used $A_{jk}(\omega)$ tends to infinity when ω tends to zero. Then the inverse Fourier transform does not exist again. The difference of C_{jk} and C_{jk}^* also follows from the definition of c_{jk} that was presented by Equation A.19: the fact is that the potentials $\theta_{mk}(x, y, z) + \Theta_{mk}(x, y, z, 0)$ basically represent a correction to the steady potential due to a constant unit displacement of the vessel ($\eta_k = 1$). $\theta_{mk}(x, y, z) + \Theta_{mk}(x, y, z, 0)$ are just equal to $\varphi_k(x, y, x, 0)$.

This paragraph shows how the transformation of the frequency domain results of the panel method to the time domain is carried out in actual practice. Please note that in the present study k may also be equal to 7, since the air cushion excess pressure acts as an extra degree of freedom. Because the real part of $H_{jk}^*(\omega)$ is an even function of ω, while the imaginary part of $H_{jk}^*(\omega)$ is an odd function of ω, $h(t)$ can also be

expressed as:

$$h_{jk}(t) \; = \; \frac{2}{\pi} \int_0^\infty \Re\{H_{jk}^*(\omega)\} \cos \omega t \, d\omega \; = \; \frac{2}{\pi} \int_0^\infty \Im\{H_{jk}^*(\omega)\} \sin \omega t \, d\omega \qquad (A.23)$$

In the present method the cosine inverse Fourier transform of the real part of $H_{jk}^*(\omega)$ is used. For this transformation B_{jk}^* must be known on the entire frequency range. Although the panel method gives reasonably good results up to a relatively high frequency, the very high frequency tale of of the coefficients cannot be computed. Therefore the damping curve is extrapolated by an exponential curve: $ae^{-b\omega} + c$. The coefficients a, b and c are chosen in such a way that the damping curve is continuous and differentiable at the highest computed frequency, where b, which determines the rate at which the curve approaches it's asymptotic value, was fixed in advance. Then $B_{jk}^*(\infty)$ equals c, and $h_{jk}(t)$ follows from:

$$h_{jk}(t) \; = \; \frac{2}{\pi} \int_0^\infty \Re\{H_{jk}^*(\omega)\} \cos \omega t \, d\omega \; = \; \frac{2}{\pi} \int_0^\infty \Im\{H_{jk}^*(\omega)\} \sin \omega t \, d\omega \qquad (A.24)$$

Subsequently $A_{jk}^*(\infty)$ follows from the sine Fourier transform of $h_{jk}(t)$:

$$\omega\left(A_{jk}^*(\omega) - A_{jk}^*(\infty)\right) \; = \; \int_0^\infty h_{jk}(t) \, \sin \omega t \, dt \qquad (A.25)$$

where one should fill in the $A_{jk}^*(\omega)$ as it was computed by the panel method. If the extrapolation of the damping curve is accurate, the thus calculated $A_{jk}^*(\infty)$ is independent from ω. Fortunately $A_{jk}^*(\infty)$ does not appear to be very sensitive to the extrapolation of B_{jk}^*. Figure A.1 presentss an example of a thus calculated impulse response function. Figure A.2 shows the corresponding added mass and damping curves that were computed by means of the panel method. This figure also displays the added mass curve as it follows from Equation A.25, where $A_{jk}^*(\infty)$ was constant. The two added mass curves fit very well, thus demonstrating the validity of the extrapolation of B_{jk}^*.

Next to the hydromechanic reaction forces, the following quantities also need to be transformed to the time domain: the wave pumping volume, the wave height at the bow and stern seal, and the wave steepness at the bow and stern seal. The frequency domain expression of these quantities can be written in the following form:

$$\zeta \; = \; \sum_{k=1}^7 \Re\left\{D_k(\omega) \, \hat{\eta}_k \, e^{i\omega t}\right\} \qquad (A.26)$$
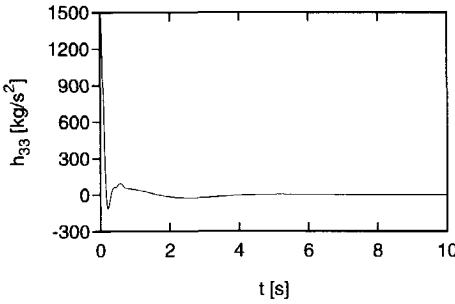
Figure A.1: Impulse response function for the heave force due to an impulsive heave velocity
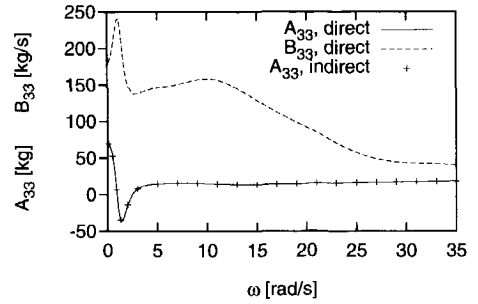

Figure A.2: Added mass and damping curves for the heave force due to harmonic heave motion

where ζ is one of the quantities mentioned above, and $D_k(\omega)$ is the complex harmonic response function for this quantity due to a harmonical oscillation in the kth degree of freedom. Analogous to the hydromechanic reaction force, the time domain expression for ζ reads:

$$\zeta = \sum_{k=1}^{7} \left(D_k(\infty)\eta_k + \int_{-\infty}^{t} d_k(t-\tau)\,\eta_k(\tau)\,d\tau \right) \tag{A.27}$$

where

$$d_k(t) = \frac{1}{2\pi} \int_{-\infty}^{\infty} \left(D_k(\omega) - D_K(\infty) \right) e^{i\omega t} d\omega$$

In Chapter 3 it appears that we also need derivatives with respect to time of the quantities represented by ζ. They follow from:

$$\dot{\zeta} = \sum_{k=1}^{7} \left(D_k(\infty)\dot{\eta}_k + \int_{-\infty}^{t} d_k(t-\tau)\,\dot{\eta}_k(\tau)\,d\tau \right) \tag{A.28}$$

The impulse response function $d_k(t)$ is computed from an inverse sine Fourier transform of the imaginary part of $D_k(\omega)$:

$$d_k(t) = -\frac{2}{\pi} \int_{0}^{\infty} \Im\{D_{jk}^*(\omega)\} \sin \omega t \, d\omega \tag{A.29}$$

This choice was made because the high frequency limit of the imaginary part of $D_k(\omega)$ is known, that is zero. The extrapolation of the curves in the high frequency
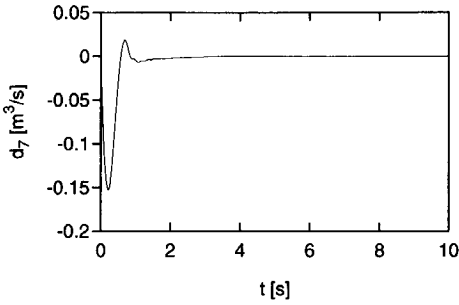
Figure A.3: Impulse response function for the wave pumping volume due an impulsive cushion pressure modulation
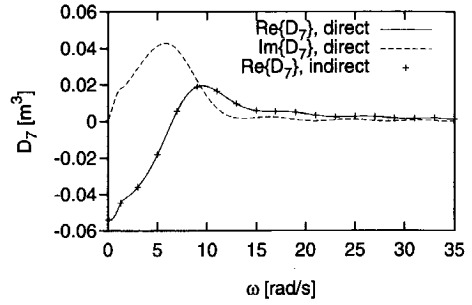
Figure A.4: Complex harmonic response function for the wave pumping volume due to a harmonic cushion pressure modulation

range is however difficult. The curves oscillate and do not approach their asymptotic value as rapidly as the damping curves did. Nevertheless satisfying results are obtained when $\Im D_k(\omega)$ is simply extrapolated by $ae^{-b\omega}$ in such a way that the function is continuous (but not differentiable) at the highest computed frequency. Again b is fixed in advance. Now $D_k(\infty)$, which is real, follows from:

$$\Re\{D_k(\omega) - D_k(\infty)\} = \int_0^\infty d_k(t) \cos\omega t \, dt \qquad (A.30)$$

where one should substitute $\Re D_k(\omega)$ as it was computed by the panel method. Figure A.3 presents an example of a thus calculated impulse response function. Figure A.4 shows the corresponding complex harmonic response function that was computed by means of the panel method. This figure also displays the real part of $D_k(\omega)$ as it follows from Equation A.30, where $D_k(\infty)$ was constant. The two $\Re D_k(\omega)$ curves fit very well thus demonstrating the validity of the rather crude extrapolation of $\Im D_k(\omega)$. Figure A.5 shows the same curves for a worst case: the wave steepness at the stern seal due to an oscillating cushion pressure. In this worst case a clear deviation of the directly computed curve and the curve that followed from the transformation of $d_k(t)$ can be observed. One should however realize that the convergence of these results of the panel method is also rather poor. Furthermore one might question whether the wave steepness at the stern seal is very important, especially if one realizes that the major contribution to the wave steepness is due to the incident waves.

This Appendix presented time domain expressions for the hydromechanic forces on the hulls of an SES due to motions and air cushion pressure oscillations. It also presented time domain expressions for the wave pumping volume of the air cushion, the wave height at the seals and the wave steepness at the seals due to motions and cushion pressure modulations. The time domain expressions involve constant (frequency independent) coefficients and a convolution of an impulse response function with the motions from the past. The appendix also explained how these coefficients and the impulse response function can be derived from the frequency domain results of the panel method which is presented by Chapter 2. The time domain expressions are applied in the non-linear time simulation method which is presented by Chapter 3.
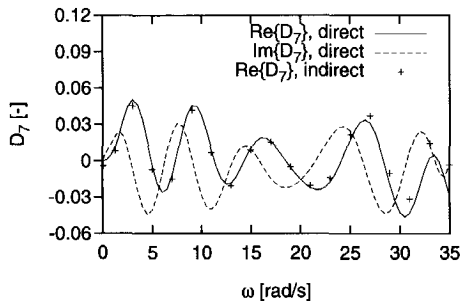

Figure A.5: Complex harmonic response function for the wave steepness due to a harmonic cushion pressure modulation

Appendix B

The bag-type stern seal geometry

This Appendix presents the method that is used to compute the geometry of the bag-type stern seal. Several seal models can be found in literature. For the present method Steen and Faltinsen[16] have largely been followed. For simplicity the method for a two-lobe seal is described. The extension of the two-lobe method to a three-lobe method is simple and straightforward. Figure B.1 shows a longitudinal cut of a two lobe bag seal.

B.1   Underlying assumptions

The stern seal model is a two-dimensional model (in a longitudinal plane). This implies that the wave height is assumed to be constant in transverse direction. This assumption is reasonable when head and following waves are considered, because the waves that are generated by the hulls and the air cushion are small compared to the incident waves. Therefore the mean wave height and wave slope at the seal are used. Furthermore the water surface is assumed to be rigid. This is assumption is valid because of the high speed of SES. The Froude number based on some characteristic seal length is of the order of 10! The wave curvature is also neglected, but the wave slope is taken into account. This assumption is reasonable for not too short waves. The air leakage flow under the seal is assumed to be stationary, inviscid and incompressible. A simple one-dimensional analysis of the leakage flow is used. The gravitational and inertial forces on the bag membrane are assumed to be small compared to forces due to the excess pressure. Therefore these forces can be neglected. Now the problem of computing the stern seal bag geometry does not depend on time any more. The only time dependency of the seal dynamics is through the seal and cushion excess pressures.
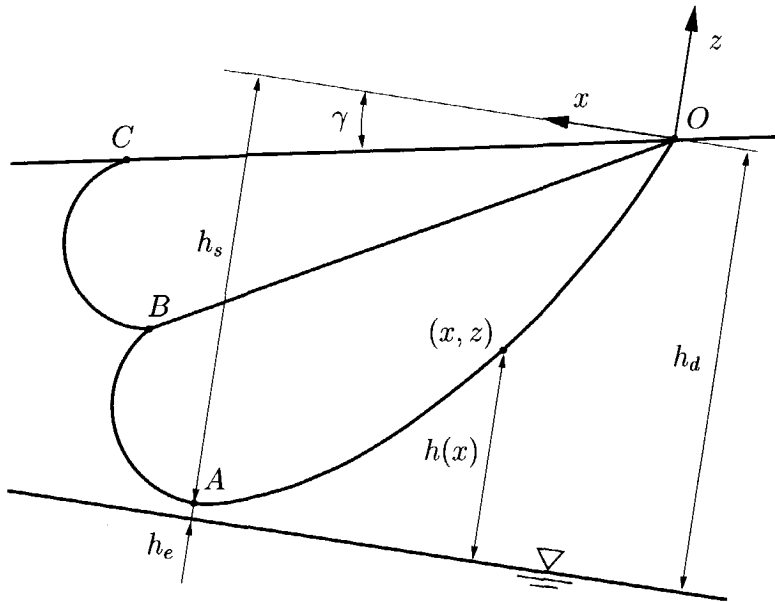
Figure B.1: Longitudinal cut of a two-lobe bag stern seal

The three-dimensional bag membrane is analyzed as a two-dimensional cable. The cable has no bending stiffness and only transmits tension. Force equilibrium for a cable segment yields the following relation:

$$\frac{T}{\Delta p} = R \tag{B.1}$$

where T is the tension in the cable, Δp is the pressure difference across the seal and R is the radius of curvature of the cable.

B.2   The dynamic pressure distribution under the seal

When the seal does not touch the water surface, air leakage from the cushion will occur. This air flow results in a spatially varying pressure distribution under the seal. This air flow has been studied elaborately by Ulstein[12]. He found that the following one-dimensional analysis yields good results compared to results obtained from a two-dimensional non-linear panel method.

The flow is assumed to be steady and inviscid, so Bernoulli's equation can be used. In the air cushion, at some distance from the stern seal, the velocity of the air equals

zero. The flow under the seal is assumed to separate at the lowest point A of the seal. At this point the pressure is atmospheric. The outflow velocity follows from Bernoulli's equation:

$$u_e = \sqrt{\frac{2p_c}{\rho}}$$

(B.2)

Where p_c is the cushion excess pressure which is small compared to the atmospheric pressure p_a. Therefore $\rho \approx \rho_a$. A mass balance gives the velocity upstream of the point a:

$$u(x) = \frac{h_e}{h(x)} \sqrt{\frac{2p_c}{\rho}}$$

(B.3)

where h_e is the leakage height under the seal, and $h(x)$ is the height of the seal above the water surface upstream of the point A (see Figure B.1). When the velocity distribution is known the pressure distribution follows from Bernoulli's equation:

$$p(x) = p_c \left[1 - \left(\frac{h_e}{h(x)} \right)^2 \right]$$

(B.4)

B.3   The cushion-facing part of the seal

The pressure jump across the segment OA of the seal is not constant because of the dynamic pressure distribution due to air leakage. The radius of curvature of the segment OA is therefore not constant (see equation B.1). This causes the analysis of this segment to be more difficult. Therefore this part of the bag is analyzed separately.

Figure B.2 shows the cushion-facing part of a bag seal. A local coordinate system with origin in O, z-axis pointing upwards and x-axis positive aft is shown. The pressure jump Δp across the seal in a point (x, z) can now be expressed as:

$$\Delta p(z) = p_s - p_c \left[1 - \left(\frac{h_d - h_s}{h_d + z} \right)^2 \right]$$

(B.5)

where h_d and h_s are defined by Figure B.1. The curvilinear coordinate s along the seal segment is defined as the distance along the seal from the point A to the point (x, z). The following relations follow from Figure B.2:

$$-\frac{dx}{ds} = \cos \theta$$

(B.6)

$$\frac{dz}{ds} = \sin \theta$$

(B.7)
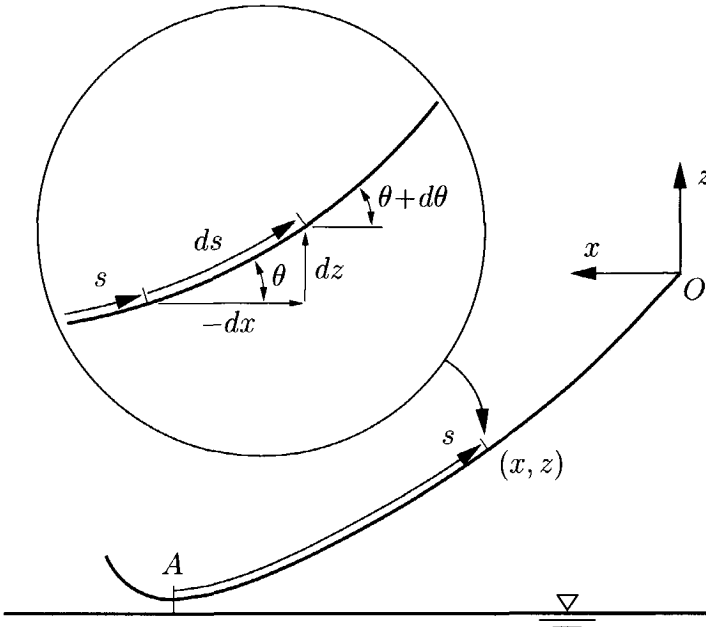
Figure B.2: Cushion-facing part of a bag seal

Force equilibrium for the infinitesimal segment ds leads to:

$$\Delta p\, ds \;=\; T\, d\theta \tag{B.8}$$

Combination of the equations (B.5), (B.7) and (B.8) results in:

$$\left\{ p_s \;-\; p_c \left[1 - \left(\frac{h_d - h_s}{h_d + z} \right)^2 \right] \right\} dz \;=\; T \sin\theta\, d\theta \tag{B.9}$$

Integration of the right hand side from $-h_s$ to z and integration of the left hand side from the corresponding 0 to θ yields the following relation:

$$\cos\theta(z) \;=\; 1 - \frac{1}{T} \left[(p_s - p_c)(h_s + z) + p_c(h_d - h_s)\frac{h_s + z}{h_d + z} \right] \tag{B.10}$$

Combination and integration of (B.6) and (B.7) leads to:

$$x \;=\; -\int_{\zeta=0}^{z} \frac{\cos\theta(\zeta)}{\sqrt{1 - \cos^2\theta(\zeta)}}\, d\zeta \tag{B.11}$$

The coordinates of the point A can now be expressed as:

$$x_A = -\int_{\zeta=0}^{-h_s} \frac{\cos\theta(\zeta)}{\sqrt{1-\cos^2\theta(\zeta)}}\, d\zeta \qquad \text{and} \qquad z_A = -h_s \qquad \text{(B.12)}$$

The length of the segment OA can be written as:

$$S_0 = -\int_{\zeta=0}^{-h_s} \frac{d\zeta}{\sqrt{1-\cos^2\theta(\zeta)}} \qquad \text{(B.13)}$$

Note that T and h_s are the only unknown parameters that occur in the expressions for x_A, z_A and S_0.

The integrals in (B.12) and (B.13) are evaluated by means of numerical integration. Because the integrand becomes singular at $\zeta = -h_s$, special care has to be taken at this integration boundary. Good results are obtained when a cosine distribution of integration steps and the mean value of θ are used, where the mean value of θ is $[\theta(z) + \theta(z + \Delta z)]$. The integrand at the mean value of θ is simply multiplied by the step size Δz.

B.4 The complete seal

All unknown parameters of a two lobe bag seal are shown in Figure B.3. For convenience all unknown parameters are drawn larger than zero. However, $|AA'|$ can only be larger than zero if $h_s = h_d$, and $|BB'|$ can only be larger than zero if $\varphi_1 = \varphi_2 = 0$, while $|CC'|$ can only be larger than zero when $\psi_2 = 0$. The unknown tension T in the segment OA that appeared in the previous section can be eliminated: force equilibrium in A combined with equation B.1 leads to $T = R_1 p_s$. When the friction on $|AA'|$ is taken into account this equation becomes:

$$T = R_1 p_s + C_f \frac{1}{2}\rho|AA'|U^2 \qquad \text{(B.14)}$$

where C_f is taken according to the ITTC plate friction line, ρ is the density of water, and U is the forward speed of the ship.

Now there are ten unknowns (R_1, R_2, h_s, β, ϕ_1, ϕ_2, ψ_2, $|AA'|$, $|BB'|$, $|CC'|$), so ten equations have to be formulated. First some shortcuts:

$$x_{B'} = x_A + |AA'| + R_1 \cdot \sin(\beta + \varphi_1) \qquad \text{(B.15)}$$

$$z_{B'} = z_A + R_1 \cdot [1 + \cos(\beta + \varphi_1)] \qquad \text{(B.16)}$$
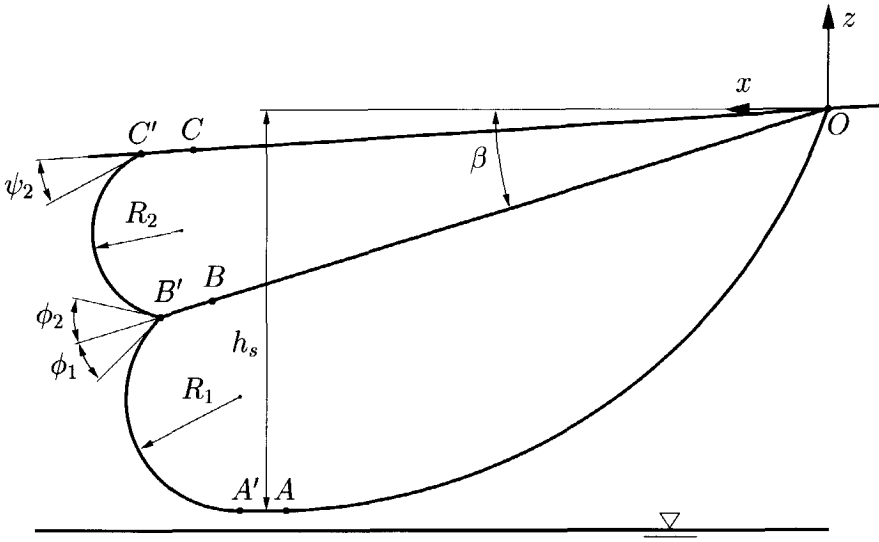
Figure B.3: Unknown parameters of a two lobe bag seal

where x_A and z_A follow from equation B.12.

The following six equations hold, irrespective of whether the bag flies or touches the water, and irrespective of overlapping of the lobes in the points B and C.

$$\beta = \arctan\left(\frac{-z_{B'}}{x_{B'}}\right) \tag{B.17}$$

$$x_{B'}^2 + z_{B'}^2 = (|OB| + |BB'|)^2 \tag{B.18}$$

$$x_{B'} + R_2 \cdot [\sin(\gamma + \psi_2) - \sin(\varphi_2 - \beta)] = \cos(\gamma) \cdot (|OC| + |CC'|) \tag{B.19}$$

$$z_{B'} + R_2 \cdot [\cos(\gamma + \psi_2) + \cos(\varphi_2 - \beta)] = -\sin(\gamma) \cdot (|OC| + |CC'|) \tag{B.20}$$

$$|BB'| + R_1 \cdot (\pi - \beta - \varphi_1) + |AA'| + S_0 = L_1 \tag{B.21}$$

$$|CC'| + R_2 \cdot (\pi + \beta - \varphi_2 - \gamma - \psi_2) + |BB'| = L_2 \tag{B.22}$$

The first two equations make the segment $OAA'B'$ connect to the straight line segment OBB'. The third and fourth equation make the segment $B'C'$ connect to the straight line segment OCC'. The angle of the deck (γ) is known on fore hand (see Figure B.1 for the definition of γ). It depends on the pitch displacement and the wave slope. The angle β of the segment OBB' is unknown. The fifth equation ensures the proper length L_1 of the lower lobe segment ($OAA'B'B$), and the sixth equation ensures the proper length L_2 of the upper lobe segment ($BB'C'C$).

If the bag touches the water surface ($|AA'| > 0$) the seventh equation can be written as:

$$h_s = h_d \qquad \text{(B.23)}$$

However, when the bag flies above the water surface ($h_s < h_d$) the seventh equation reads:

$$|AA'| = 0 \qquad \text{(B.24)}$$

When the upper and lower lobe overlap at the point B ($|BB'| > 0$) the eighth and ninth equation are:

$$\varphi_1 = 0 \qquad \text{(B.25)}$$

$$\varphi_2 = 0 \qquad \text{(B.26)}$$

But when the lobes do not overlap at B these equations become:

$$|BB'| = 0 \qquad \text{(B.27)}$$

$$R_1 \cdot \sin \varphi_1 = R_2 \cdot \sin \varphi_2 \qquad \text{(B.28)}$$

where the last equation represents force equilibrium in the point B in the direction which is perpendicular to the segment OB. If the upper lobe overlaps with the deck at the point C ($|CC'| > 0$) the tenth equation is:

$$\psi_2 = 0 \qquad \text{(B.29)}$$

When no overlapping occurs in C this equation becomes:

$$|CC'| = 0 \qquad \text{(B.30)}$$

Now the system of ten equations is complete.

This nonlinear system has to be solved in an iterative procedure. Newton-Raphson's method is used. The partial derivatives are calculated by means of finite differences. The method converges quite rapidly provided that a good initial guess is used. Otherwise no convergence will be obtained.

If the bag touches the water in the initial guess ($h_s = h_d$ and $|AA'| > 0$), and during the iterative process $|AA'|$ becomes smaller than zero, $|AA'|$ is set to zero, and h_s is set free to values smaller than h_d. When h_s becomes larger than h_d, h_s is set equal to h_d, and $|AA'|$ is set free to values larger than zero. For the overlapping at B and C a similar procedure is used. After every iteration an *overlapping test* is performed in order to select the four appropriate equations from equations B.23, B.24, B.25, B.26, B.27, B.28, B.29 and B.30 for the next iteration. In the case of a three-lobe bag seal, the third lope is treated in exactly the same way as the upper lobe of the two lobe seal.

B.5   Seal volume and seal forces

When the seal geometry is known, the seal volume (V_s), the volume of the part of the cushion plenum that is taken up by the stern seal (V_{sc}), and the seal force ($F_j^{(s)}$) can be computed easily. Figure B.4 shows definitions of V_s and V_{sc}. The definition of V_s is quite obvious, but the definition of V_{sc} requires more attention. The definition of V_{sc} depends on the definition of the deck area, which is used in the computation of the cushion volume. It also depends on the definition of the part of the free surface that is covered by the air cushion, which is used in the computation of the wave pumping volume (V_ζ). Figure B.4 also shows these areas. The cushion plenum is defined to end at the lowermost point A of the bag.

The seal force follows from the sum of the tension in all canvas segments plus the seal pressure multiplied by the area of $|OCC'|$. The tension in the segments $CC'B'B$ and $BB'A'$ follows from equation B.1. Force equilibrium in B leads to the tension in BO. The tension in the segment AO follows from equation B.14.
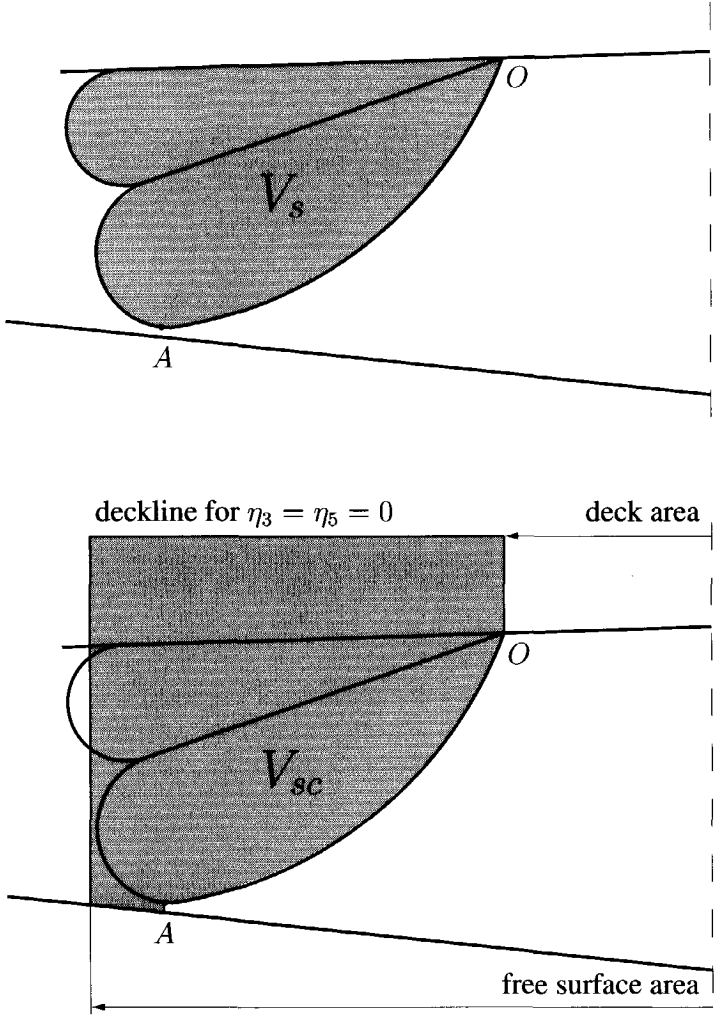
Figure B.4: Definition of V_s and V_{sc}

Appendix C

The diaphragm technique

A diaphragm is a device which is used to reduce the stiffness of the air cushion at model scale. It is a flexible membrane which is mounted on top of the air cushion. When the pressure in the air cushion increases, the diaphragm supplies extra volume which results in a much smaller increase of the pressure. The mass of the thin flexible membrane is very small. Therefore the inertial and gravitational forces on the membrane are negligible, so the diaphragm will not introduce new dynamical effects.

This appendix presents a method to compute the deformed geometry due to an excess pressure in the air cushion of a circular diaphragm. When this geometry is known the reduction of the cushion stiffness, dV/dp, can be calculated. Next to this the section presents an experimental method that can be used to determine dV/dp. The results of both methods are compared.

C.1   Computational method

A cylindrical coordinate system (x, r, θ) is used in the calculation of the deformed geometry of a circular diaphragm due to an excess pressure in the air cushion. The problem is angularly symmetrical. An axial ($\xi(r)$) and a radial ($\rho(r)$) displacement function are introduced (see Figure C.1). Because the membrane is very thin, it's bending stiffness can be neglected and stresses perpendicular to the membrane surface are zero. When the excess pressure equals zero both $\xi(r)$ and $\rho(r)$ are zero, and the stress in the membrane equals zero too. The radial and tangential strain (in the plane which is tangent to the deformed membrane surface) can be expressed in
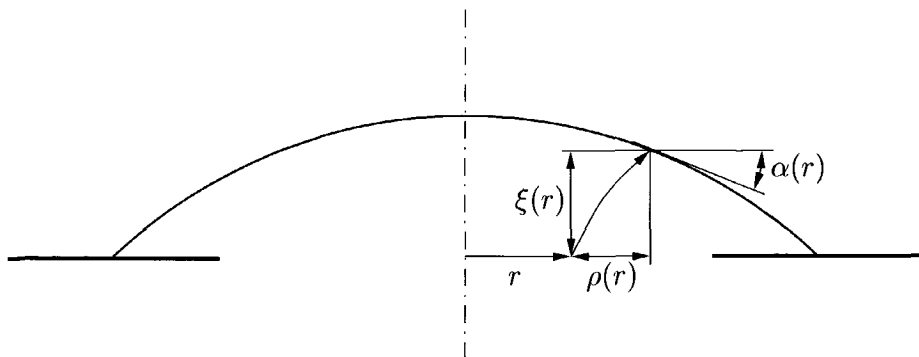
Figure C.1: Membrane displacement functions

the displacement functions:

$$\epsilon_r = \sqrt{\left(1 + \frac{d\rho}{dr}\right)^2 + \left(\frac{d\xi}{dr}\right)^2} - 1 \tag{C.1}$$

$$\epsilon_\theta = \frac{\rho}{r} \tag{C.2}$$

The radial and tangential stress (in the plane which is tangent to the deformed membrane surface) can be expressed in the radial and tangential strain:

$$\sigma_r = \frac{E}{1 - \nu^2}(\epsilon_r + \nu\epsilon_\theta) \tag{C.3}$$

$$\sigma_\theta = \frac{E}{1 - \nu^2}(\epsilon_\theta + \nu\epsilon_r) \tag{C.4}$$

where E is the modulus of elasticity and ν is Poisson's ratio of the membrane canvas. Radial and tangential force equilibrium for the element $dr \times r\, d\theta$ (see Figure C.2) leads to the following equations:

$$p(r + \rho)\left(1 + \frac{d\rho}{dr}\right) = t\frac{d}{dr}(r\,\sigma_r\,\sin\alpha) \tag{C.5}$$

$$p(r + \rho)\frac{d\xi}{dr} = t\left(\sigma_\theta - \frac{d}{dr}(r\,\sigma_r\,\cos\alpha)\right) \tag{C.6}$$

where p is the excess pressure in the air cushion, t is the thickness of the membrane canvas and $\alpha(r)$ is the angle of the slope of the (deformed) membrane canvas (see
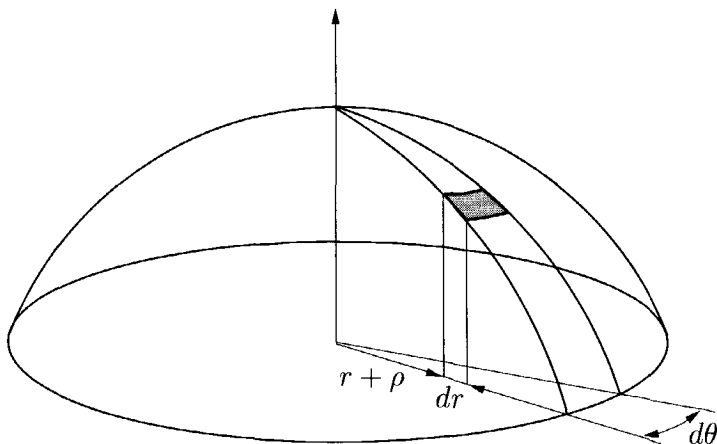
Figure C.2: A surface element of the membrane

Figure C.1). $\sin\alpha$ and $\cos\alpha$ are expressed in $\xi(r)$ and $\rho(r)$ directly:

$$\sin\alpha \;=\; \frac{-\frac{d\xi}{dr}}{1+\epsilon_r} \tag{C.7}$$

$$\cos\alpha \;=\; \frac{1+\frac{d\rho}{dr}}{1+\epsilon_r} \tag{C.8}$$

Their derivatives with respect to r simply follow from differentiation of these expressions. The displacement functions $\xi(r)$ and $\rho(r)$ are written as series of cosine and sine functions:

$$\xi(r) \;=\; \sum_{n=1}^{N} \xi_n \cos\!\Big(\pi\frac{2n-1}{2}\frac{r}{R}\Big) \tag{C.9}$$

$$\rho(r) \;=\; \sum_{n=1}^{N} \rho_n \sin\!\Big(\pi n\frac{r}{R}\Big) \tag{C.10}$$

where R is the radius of the circular diaphragm. Now N radii $r_1,\ldots,r_N$ are selected. Equations C.5 and C.6 are fulfilled at these radii. Subsequent substitution leads to $2N$ non-linear equations for $\xi_1,\ldots,\xi_N$ and $\rho_1,\ldots,\rho_N$. This system is solved by means of the method of Newton-Raphson which converges rapidly. The convergence in N is also very fast. Now the displacement functions (i.e.the deformed geometry of the diaphragm) are known. The volume of the diaphragm follows from:

$$V^{(d)} = \pi \int_0^R \Big(2r\xi - (2r\rho + \rho^2)\frac{d\xi}{dr}\Big)\,dr \tag{C.11}$$

The reduction of the air cushion stiffness ($dV^{(d)}/dp$) is calculated by means of finite differences using solutions for slightly different cushion excess pressures.

C.2 Experimental method

The reduction of the air cushion stiffness ($dV^{(d)}/dp$) by a diaphragm is also determined by means of experiments. A diaphragm is mounted on top of a floating open bottomed box. The excess pressure inside the box and the draft of the box are measured. Then the draft of the box is increased by putting some weights on the deck of the box. Because the air inside the box cannot escape, the excess pressure in the box increases. Then $dV^{(d)}/dp$ can be computed from:

$$\left(\frac{V^{(c)} + V^{(d)}}{\kappa(p + p_a)} + \frac{dV^{(d)}}{dp}\right) \cdot \Delta p = -\Delta V^{(c)} \tag{C.12}$$

This equation follows from equation 4.3. In the relevant scale range $dV^{(d)}/dp$ is much larger than $(V^{(c)} + V^{(d)})/(\kappa(p + p_a))$. Therefore there is no need for a very accurate estimation of this term. $\Delta V^{(c)}$ can be expressed as:

$$\Delta V^{(c)} = A_c \frac{\Delta p}{\rho g} - A_c \Delta T \tag{C.13}$$

where T is the draft of the box, A_c is the area of water surface that is covered by the air cushion, ρ is the density of water and g is the gravitational acceleration. Now $dV^{(d)}/dp$ follows from:

$$\frac{dV^{(d)}}{dp} = \frac{A_c \Delta T}{\Delta p} - \frac{A_c}{\rho g} - \frac{V^{(c)} + V^{(d)}}{\kappa(p + p_a)} \tag{C.14}$$

The air cushion area A_c should not be chosen too large. Otherwise a relevant Δp would result in an unmeasurably small ΔT.

C.3 Results

This section presents computational results for circular diaphragms (diameters are 775 mm and 895 mm) and experimental results for a rectangular diaphragm (745 × 845 mm). The development of a computational method for rectangular diaphragms was considered too complicated. On the other hand a rectangular diaphragm is much more easy to construct. Moreover, the actual space left for the diaphragm on

t	0.35 mm
E	$4.64 \cdot 10^6$ Pa
ν	0.49

Table C.1: Properties of membrane rubber

the final model is limited by the distance between the legs of the oscillator. The diameter of 775 mm was chosen because the computational results are in that case in excellent agreement with the experimental results. The diameter of 895 mm was chosen because the area of that circle is the same as the area of the rectangle that was used in the experiments. The membrane was constructed of artificial rubber. The properties of this rubber are shown in Table C.1. They were determined experimentally. These properties were also used in the calculations. The material appeared to have considerable creep. This is not included in the calculations. During the experiments a very small amount of air appeared to be leaking from the cushion. This resulted in a slowly decreasing excess pressure. Nevertheless we succeeded to obtain good and reproducible results.

Figure C.3 shows the computed volume of the circular diaphragms as a function of the excess pressure. Especially in the low pressure range the relation is highly non-linear. Figure C.4 shows the computed and the experimentally determined reductions of the cushion stiffness ($dV^{(d)}/dp$). Again the non-linear behavior of the diaphragms is clearly visible. The difference between the curves for the 775 mm circular diaphragm and the 895 mm circular diaphragm is very large. The reduction of the stiffness is very sensible to the size and probably also the form of the diaphragm. Therefore, a rectangular and a circular diaphragm are hard to compare. Keeping the area of the diaphragm constant does not seem to be a good idea, because the corners of the rectangular diaphragm will not supply much volume. This explains why the results of the 895 mm circular diaphragm are much larger than the experimental results for the 845*745mm rectangular diaphragm. In the case of a two-dimensional (infinitely long) diaphragm it can be shown that $dV^{(d)}/dp$ is proportional to the width cubed. The smallest side of the rectangle might therefore be the determining factor for the stiffness of a diaphragm. At least it can be concluded that the trend of the computational and experimental results agrees very well. This also supports the accuracy of the experiments.

For a correct scaling the reduction of the cushion stiffness ($dV^{(d)}/dp$) should be
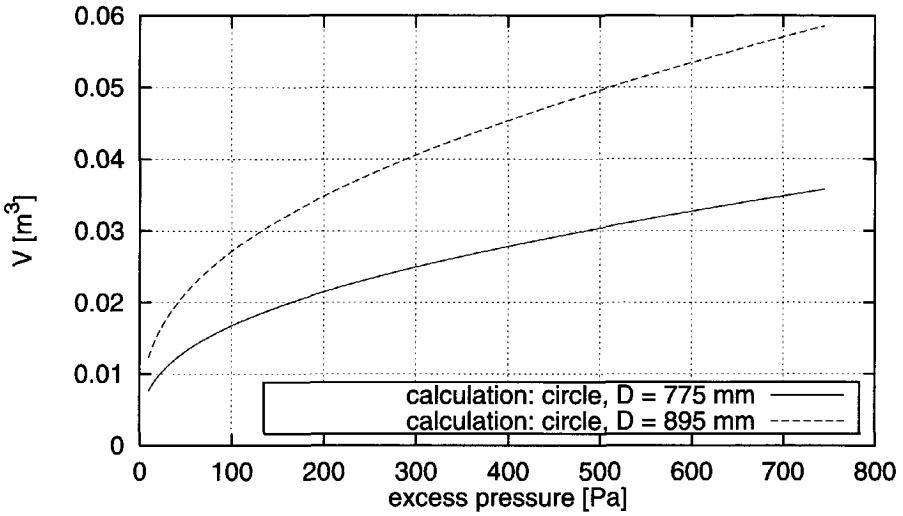
Figure C.3: Calculated volume of the circular diaphragm
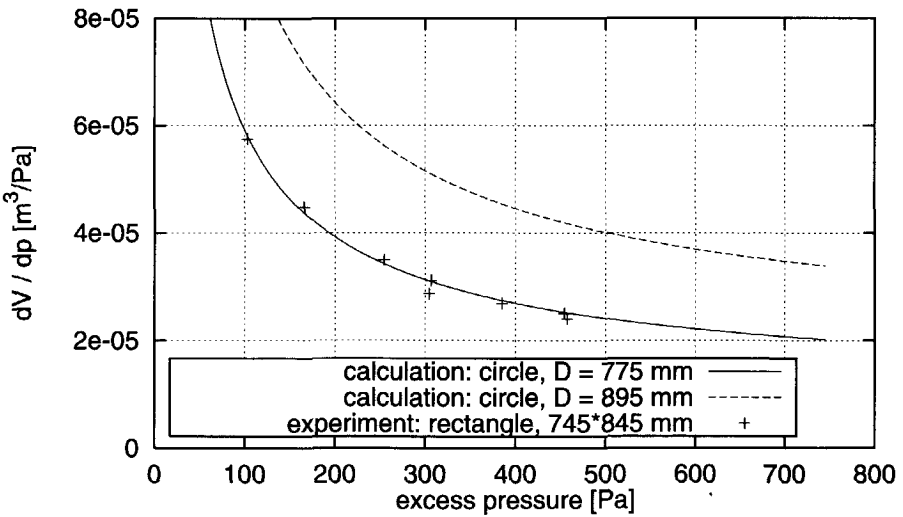
Figure C.4: Reduction of the cushion stiffness by the diaphragms

constant. Figure C.4 clearly shows that this is not the case. The diaphragm will introduce extra non-linear effects. For relatively small pressure oscillations (for instance between 250 and 350 Pa) the non-linear effect will be small. When the excess pressure becomes however very small, the stiffness is strongly reduced and the non-linear effect gets important.

References

[1] Ir. G.K. Kapsenberg, H. Bruder, and A.G. van Doeveren. Free running exper-
iments with a small scale model. Technical Report 212556-1-OE, MARIN,
Wageningen, 1995.

[2] W.J. Eggington and N. Kobitz. The domain of the surface-effect ship. In
Transactions of SNAME, volume 83, pages 268–298, 1975.

[3] G.D. McGhee. U. s. navy 3000-lt surface-effect ship (3kses) program. In
Transactions of SNAME, volume 85, pages 396–418, 1977.

[4] H. Ozawa, H. Yamaga, K. Kihara, and S. Horiba. The third stage of the tsl-
a program - tsl-a 'hisho' and high-speed cargo handling system. In *Proc.
Fourth International Conference on Fast Sea Transportation (FAST'97)*, Syd-
ney, Australia, 1997.

[5] G.K. Kapsenberg and P. Blume. Model tests for a large surface effect ship
at different scale ratios. In *Proc. Third International Conference on Fast Sea
Transportation (FAST'95)*, Lübeck-Travemünde, Germany, 1995.

[6] P. Kaplan and S. Davis. A simplified representation of the vertical plane dy-
namics of ses craft. In *AIAA/SNAME Advanced Marine Vehicles Conference,
AIAA Paper No.74-314*, 1974.

[7] P. Kaplan, J. Bentson, and S. Davis. Dynamics and hydrodynamics of surface
effect ships. In *Transactions of SNAME*, volume 89, pages 211–247, 1981.

[8] L.J. Doctors. The use of pressure distribution to model the hydrodynamics of
air cushion vehicles and surface effect ships. In *Intersociety High Performance
Marine Vehicle Conference and Exhibit (HPMV'92)*, Arlington, VA, 1992.

[9] D.E. Nakos, A. Nestegård, T. Ulstein, and P.D. Sclavounos. Seakeeping anal-
ysis of surface effect ships. In *Fast Conference, Trondheim*, 1991.

[10] A.J. Sørensen. *Modelling and Control of SES in the Vertical Plane.* PhD thesis, The Norwegian Institute of Technology, 1993.

[11] S. Steen. *Cobblestone Effect on SES.* PhD thesis, The Norwegian Institute of Technology, 1993.

[12] T. Ulstein. *Nonlinear effects of a flexible stern seal bag on cobblestone oscillations of an SES.* PhD thesis, The Norwegian Institute of Technology, 1995.

[13] G. McHenry, P. Kaplan, F. Korbijn, and A. Nestegård. Hydrodynamic analysis of surface effect ships: Experiences with a quasi-linear model. In *Fast Conference, Trondheim*, 1991.

[14] J.F. Masset, J.P. Morel, and G.K. Kapsenberg. Large surface effect ship (ses) air cushion dynamics: An innovative methodology for theoretical modelling validation. In *Proc. Third International Conference on Fast Sea Transportation (FAST'95)*, Lübeck-Travemünde, Germany, 1995.

[15] G.J. Lee. On the motions of high speed surface-effect-ships in waves. *Journal of Hydrospace Technology*, 1(2):13–35, 1995.

[16] S. Steen and O.M. Faltinsen. Cobblestone oscillations of an ses with flexible bag aft seal. *Journal of Ship Research*, 39(1):25–41, March 1995.

[17] J.F. Masset and J.P. Morel. A test rig for the analyses of a large surface effect ship seals dynamics: design, manufacturing and results. In *NAV'94 proceedings*, volume 1, 5-7 October 1994.

[18] J.M. Durkin and L. LUehr. Dynamic response of lift fans subject to varying backpressure. In *AIAA/SNAME Advanced Marine Vehicles Conference, AIAA Paper No.78-756*, 1978.

[19] P.A. Sullivan, F. Gosselin, and M.J. Hinchey. Dynamic responce of an air cushion lift fan. In *HPMV '92 Conference, Washington*, 1992.

[20] K.C. Witt. Lift fan stability for ses. In *Second International Conference on Fast Sea Transportation (FAST'93)*, Yokohama, Japan, 1993.

[21] P. Kaplan. The effects of motion-induced surface wave generation on ses vertical plane motions in incident waves. In *Intersociety Advanced Marine Vehicles Conference Washington*, 1989.

[22] L.J. Doctors. The effect of air compressibility on the nonlinear motion of an air cushion vehicle over waves. In *Proc. of the Eleventh Symposium on Naval Hydrodynamics*, London, 1976.

[23] C.H. Kim and S. Tsakonas. An analysis of heave added mass and damping of surface effect ship. *Journal of Ship Research*, 25(1), March 1981.

[24] D.D. Moran. The wave heigth under a high length-to-beal ratio surface effect ship in regular waves. Technical Report SPD-587-01, NSRDC, 1975.

[25] G.K. Kapsenberg. Seakeeping behaviour of a ses in different wave directions. In *Proc. Second International Conference on Fast Sea Transportation (FAST'93)*, Yokohama, Japan, 1993.

[26] D.R. Lavis, R.J. Bartholomew, and J.C. Jones. Response of air cushion vehicles to random seaways and the inherent distortion in scale models. *Journal of Hydronautics*, 8(3), 1974.

[27] G.K. Kapsenberg. Added mass and damping coefficients for a large ses including an appreciation of scale effects. In *Proc. NAV'94*, volume 1, 1994.

[28] O.M. Faltinsen, J.B. Helmers, K.J. Minsaas, and R. Zhao. Speed loss and operability of catamarans and ses in a seaway. In *First International Conference on Fast Sea Transportation (Fast'91)*, Trondheim, Norway, 1991.

[29] G.K. Kapsenberg, G.J. Feikema, and G. van Ballegoyen. Added resistance of a surface effect ship. Technical Report 212556-1-OE, MARIN, Wageningen, 1995.

[30] J. Gerritsma and W. Beukelman. Analysis of the resistance increase in waves of a fast cargo ship. *International Shipbuilding Progress*, 19(217), 1972.

[31] J.J. Blok. *The Resistance Increase of a Ship in Waves*. PhD thesis, Delft University of Technology, 1993.

[32] H. Maruo. The excess resistance of a ship in rough seas. *International Shipbuilding Progress*, 4(35):337–345, 1957.

[33] J.N. Newman. The exiting forces on fixed bodies in waves. *Journal of Ship Research*, 6(4):10–17, 1962.

[34] W.C. Lin and A.M. Reed. The second order steady force and moment on a ship moving in an oblique seaway. In *Proceedings of the 11th ONR Symposium on Naval Hydrodynamics*, London, 1976.

[35] T.H. Havelock. The driffting force of a ship among waves. *Philosofical Magazine*, 33:467–475, 1942.

[36] P. Boese. Eine einfache methode zur berechnungser widerstandserhohung eines schiffes im seegang. *Schiffstechnik*, 17(86), 1970.

[37] O.M. Faltinsen, K.J. Minsaas, N. Liapis, and S.O. Skjordal. Predictions of resistance and propulsion of a ship in a seaway. In *Proceedings of the 13th ONR Symposium on Naval Hydrodynamics*, Tokyo, 1980.

[38] J. A. Pinkster. *Low Frequency Second Order Wave Exiting Forces on Floating Structures*. PhD thesis, Delft Univerity of Technology, 1980.

[39] P.D. Sclavounos and D.E. Nakos. Seakeeping and added resistance of iacc yachts by a three-dimensional panel method. In *Proc. The Eleventh Chesapeake Sailing Yacht Symposium*, 1992.

[40] V. Bertram. A 3-d rankine panel method to compute added resistance of ships. Technical Report 566, Institut für Schifsbau ser Universität Hamburg, 1996.

[41] H.C. Raven. *A Solution Method for the Nonlinear Ship Wave Resistance Problem*. PhD thesis, Delft Univerity of Technology, 1996.

[42] T.H.J. Bunnik and A.J. Hermans. A time-domain algorithm for motions of high speed vessels using a new free surface condition. In *Proceedings of the 12th International Workshop on Water Waves and Floating Bodies*, Marseilles, France, 1997.

[43] C.W. Dawson. A practical computer method for solving ship-wave problems. In *Proc. of the 2nd International Conference on Numerical Ship Hydrodynamics*, Berkeley, USA, 1977.

[44] D. E. Nakos. *Ship Wave Patterns and Motions by a Three Dimensional Rankine Panel Method*. PhD thesis, M. I. T., 1990.

[45] A.P. van 't Veer. *Behaviour of Catamarans in Waves*. PhD thesis, Delft University of Technology, 1998.

[46] R. Timman and J.N. Newman. The coupled damping coefficients of a symmetric ship. *Journal of Ship Research*, 1962.

[47] T. F. Ogilvie and E. O. Tuck. A rational strip theory for ship motions -part i. Technical Report 013, Department of Naval Architecture and Marine Engineering, University of Michigan, USA, 1969.

[48] A.M. Reed, J.G. Telste, C.A Scragg, and D. Liepmann. Analysis of transom stern flows. In *18th Symposium on Naval Hydrodynamics, Ann Arbor, Mich*, 1990.

[49] M.P. Tulin and C.C. Hsu. Theory of high-speed displacement ships with transom sterns. *Journal of Ship Research*, 30-3, 1986.

[50] J.W. Sloof. Numerical methods in aircraft aerodynamics. Technical Report D-42, Delft University of Technology, Faculty of Aerospace Engineering, 1993.

[51] P.D. Sclavounos and D.E. Nakos. Stability analyses of panel methods for free-surface flows with forward speed. In *Proc. of the Seventeenth Symposium on Naval Hydrodynamics*, Den Haag, The Netherlands, 1988.

[52] D.E. Nakos and P.D. Sclavounos. Kelvin wakes and wave resistance of cruser- and transom-stern ships. *Journal of Ship Research*, 38(1):9–92, 1994.

[53] J.M.J Journée. Experiments and calculations on four wigley hullforms. Technical Report 909, Delft University of Technology, Ship Hydromechanics Laboratory, 1992.

[54] J.C. Moulijn. Non-linear motions of surface effect ships. In *International Conference on Air Cushion Vehicles (ACVs), RINA*, London, 1997.

[55] K.J.A. van den Berg. Het zeegangsgedrach van het surface effect ship (ses); modelproeven met een luchtkussen en verificatie van het simulatieprogramma seases. Technical Report 986-S, HYDRO, 1993.

[56] W. E. Cummins. The impulse-response function and ship motions. *Schiffstechnik*, 9(47):101–109, 1962.

[57] T. F. Ogilvie. Recent progress towards the understanding and prediction of ship motions. In *Proceedings of the 5th Symposium on Naval Hydrodynamics*, 1964.

[58] G. van Oortmessen. The motions of a moored ship in waves. Technical Report 510, Netherlands Ship Model Basin, Wageningen, 1976.

Samenvatting

Er is de laatste jaren steeds meer belangstelling voor grote zeegaande "Surface Effect Ships" (SESs). Voor het ontwerp van deze schepen is het noodzakelijk te beschikken over een methode die het gedrag van deze schepen in zeegang nauwkeurig kan voorspellen. Het blijkt dat SESs veel snelheid verliezen als ze in golven varen. Dit is bedreigend voor de economische haalbaarheid van SES. Het snelheidsverlies wordt veroorzaakt door een toename van de weerstand tengevolge van de golven. Deze weerstandstoename wordt toegevoegde weerstand door golven (of kortweg toegevoegde weerstand) genoemd. Het doel van het onderzoek dat ten grondslag ligt aan dit proefschrift is de ontwikkeling en de validatie van een rekenmethode voor de voorspelling van de toegevoegde weerstand van Surface Effect Ships.

De rekenmethode voor de bewegingen en toegevoegde weerstand is gebaseerd op de volgende aannames. Het hydromechanische probleem en de bewegingsvergelijkingen kunnen worden gelineariseerd. De overdruk in het luchtkussen is constant in de ruimte. Daarnaast berekent de rekenmethode alleen het deel van de toegevoegde weerstand dat wordt veroorzaakt door het luchtkussen, omdat verwacht werd dat dit deel de belangrijkste bijdrage aan de totale toegevoegde weerstand zou leveren.

Het hydromechanische probleem wordt opgelost met behulp van een driedimensionale "Rankine" panelenmethode. De randvoorwaarden op de romp en op het vrije vloeistofoppervlak zijn gelineariseerd rond de ongestoorde stroming. De panelenmethode berekent de hydromechanische krachten op de rompen, de golfhoogte in het luchtkussen, en de golfhoogte en golfhelling ter plaatse van het voor- en achterseal. Het probleem wordt opgelost in het frequentiedomein.

Daarna worden de bewegingen van de SESs en de overdrukken in het luchtkussen en het achterseal opgelost met behulp van een niet-lineaire tijdsimulatiemethode. De bewegingsvergelijkingen zijn gelineariseerd, maar de niet-lineaire vorm van de vergelijkingen die de kussen- en sealdynamica beschrijven is gehandhaafd. Vooral de lekkage van lucht onder de seals is een sterk niet-lineair fenomeen, dat niet kan worden gelineariseerd.

167

De toegevoegde weerstand van het luchtkussen volgt uit het verschil tussen de weerstand van het luchtkussen in golven en de weerstand van het luchtkussen in vlak water. De weerstand van het luchtkussen volgt in principe uit de overdruk in het luchtkussen vermenigvuldigd met het verschil in golfhoogte ter plaatse van het voor- en het achterseal keer met de kussenbreedte. Daarnaast is er nog een bijdrage tengevolge van de impuls van de lucht die het kussen in- en uitstroomt.

De resultaten van de rekenmethode worden vergeleken met experimentele resultaten van het MARIN. De overeenkomst is goed voor zover het de bewegingen en kussendruk betreft, maar er is een groot verschil tussen de berekende en de gemeten toegevoegde weerstand. De berekende toegevoegde weerstand van het luchtkussen is slechts klein en vaak zelfs negatief, terwijl de gemeten toegevoegde weerstand in het algemeen erg groot is.

Ten einde een verklaring te vinden voor het grote verschil tussen de berekende en de gemeten toegevoegde weerstand, is er een uitgebreide serie modelproeven uitgevoerd in het Laboratorium voor Scheepshydromechanica van de Technische Universiteit Delft. Het hoofddoel van deze proeven was om de oorsprong van de (grote) toegevoegde weerstand van SESs te achterhalen. Twee versies van een model zijn onderworpen aan drie soorten proeven: gedwongen oscillatie proeven, golfkracht metingen en proeven waarbij het model vrij kon dompen en stampen. De bijdrage van het luchtkussen aan de toegevoegde weerstand werd apart gemeten naast de totale toegevoegde weerstand. Het verschil levert dan de toegevoegde weerstand van de rompen op. Het resultaat van proeven is, dat de bijdrage van de rompen aan de toegevoegde weerstand groot is, terwijl de bijdrage van het luchtkussen slechts klein is. De grote toegevoegde weerstand van de rompen wordt vooral veroorzaakt door inzinking tengevolge van lagere kussendruk, die weer wordt veroorzaakt door een toename van de luchtlekkage als het schip in golven vaart.

Tenslotte wordt de rekenmethode gevalideerd door de resultaten van de proeven en de berekeningen met elkaar te vergelijken. De correlatie van de berekende en de gemeten resultaten is in het algemeen goed. Dit onderschrijft de validiteit van de rekenmethode. Voor de voorspelling van de totale toegevoegde weerstand is het echter noodzakelijk om de toegevoegde weerstand van de rompen te berekenen. De toegevoegde weerstand van de rompen wordt vooral veroorzaakt door inzinking tengevolge van een afname van de kussendruk. De reken methode geeft een goede voorspelling van de afname van de kussendruk en de daaruit voortvloeiende inzinking en trim. Het ligt daarom in de lijn der verwachting dat de rekenmethode nuttig gebruikt kan worden in de berekening van de toegevoegde weerstand van de rompen.

Curriculum vitae

Joost Moulijn werd geboren op 17 augustus 1969 te Leiden.

Hij volgde de opleiding V.W.O. aan de Openbare Scholengemeenschap Rooswijk te Zaandijk alwaar hij in 1987 het diploma behaalde.

Daarna heeft hij Maritieme Techniek gestudeerd aan de Technische Universiteit Delft. Hij is afgestudeerd bij de vakgroep Scheepshydromechanica onder begeleiding van Professor G. Kuiper. Zijn afstudeerproject betrof de ontwikkeling en toepassing van een model voor het afgaand wervelzog van scheepsschroeven. Dit afstudeerproject is beloond met de prijs voor de beste afstudeerder in de Maritieme Techniek van de N.V.T.S..

In 1995 is hij begonnen aan een promotie-onderzoek naar de toegevoegde weerstand van "Surface Effect Ships" bij het Laboratorium voor Scheepshydromechanica van de Technische Universiteit Delft. Dit proefschrift is het resultaat van dit onderzoek.

Momenteel is Joost werkzaam als Hydrodynamicus bij Lips B.V. te Drunen.

Dankwoord

Om te beginnen wil ik de Koninklijke Marine en het MARIN bedanken voor hun financiële ondersteuning van mijn promotie-onderzoek. Daarnaast wil ik het MARIN ook bedanken voor het terbeschikkingstellen van de meetinstrumenten en de fans plus besturing. Deze apparatuur is van grote waarde geweest tijdens de modelproeven. Ook wil ik het MARIN bedanken voor het terbeschikkingstellen van de resultaten van het HYDROSES project. Verder wil ik Geert Kapsenberg, Hoyte Raven en Rene Huijsmans, allen werkzaam bij het MARIN, en Marnix Krikke van de Koninklijke Marine bedanken voor de nuttige discussies.

Natuurlijk wil ik ook mijn collega's van de sectie Scheepshydromechanica heel erg bedanken voor al hun bijdragen aan het proces dat uiteindelijk tot dit proefschrift heeft geleid.

Ik wil mijn promotor professor Jo Pinkster en mijn toegevoegd promotor Lex Keuning bedanken voor het initiëren en begeleiden van het onderzoeksproject. Verder wil ik Riaan van 't Veer bedanken voor de goede samenwerking tijdens het ontwikkelen en programmeren van de panelenmethode. Daarnaast zijn de discussies met Henk de Koning-Gans, Arun Dev, Riaan van 't Veer, Wouter Pastoor en Johan Journée van onschatbare waarde geweest. Ik wil Alex van Gulik hartelijk bedanken voor zijn hulp bij het oplossen van alle computerproblemen, en Piet de Heer en Elly van Heek voor hun assistentie bij al die minder dankbare, maar niet minder belangrijke zaken.

Veel dank ben ik verschuldigd aan alle "collega's van beneden" voor hun hulp bij de modelproeven. Vooral Ruud Onnink wil ik bedanken voor zijn hulp tijdens het uitvoeren van de proeven. Daarnaast wil ik Peter Poot en Aad Versluis bedanken voor hun hulp bij het ontwerp van het model, Roel de Oude en Hans van de Hek voor het bouwen van het model, en Hans Ooms voor zijn hulp bij de signaalverwerking.

Daarnaast wil ik mijn familie heel erg bedanken voor alle belangstelling voor mijn onderzoek, en voor de steun die ik heb gekregen op die momenten dat het onder-

171

zoek minder soepel verliep. Ik wil pappa hartelijk bedanken voor het doorlezen en verbeteren van het manuscript. Ik vind het heel erg jammer dat mijn lieve mamma de promotie niet meer kan meemaken. Bij haar kon ik altijd mijn hart luchten, en ik kon altijd rekenen op steun en begrip. Tenslotte wil ik mijn lieve vriendin Josefine heel erg bedanken, onder andere voor het ontwerp van de omslag van dit boekje.